REDUCING SPECTRUM-DRIVEN UNCERTAINTIES WITH VARIANCE REDUCTION TECHNIQUES

JULIO 2023

Juan Antonio Monleón de la Lluvia Mazagatos

DIRECTORES DEL TRABAJO FIN DE MASTER:

Yurdunaz Çelik
Luca Fiorito
Nuria Garcia Herranz

INDUSTRIALES
ETSII | UPM

POLITÉCNICA

"If in the face of a problem you try to solve it, and your attempts are firm and solid, it's likely that along the way you end up finding something more valuable than the solution itself."

- Eduardo Saenz de Cabezón

ACKNOWLEDGMENTS

I would like to begin by expressing my profound gratitude to SCK CEN for affording me the incredible opportunity to undertake my master's thesis within their esteemed institution. I would also like to extend my heartfelt appreciation to Dr. Pablo Romojaro, who brought us this extraordinary opportunity, and Dr. Yurdunaz Çelik, who patiently mentored and guided me throughout this journey. Your unwavering support and assistance were invaluable to the successful completion of this thesis. To Luca Fiorito and the rest of the members of both SCK CEN and UPM who provided expert advice and invaluable insights, your assistance in addressing my queries was truly appreciated. The knowledge and wisdom I gained throughout this process is indescribable and I am deeply thankful for this enriching experience. It has solidified my resolve to continue pursuing a career in neutronics research.

Additionally, I am immensely grateful for the support system I found in Boeretang. The camaraderie and friendships that we developed, the bonds forged, and the memories created will stay with me forever. I would like to extend my special thanks to my colleagues from our master's program who have shared this unforgettable journey with me. Your presence made this challenging journey enjoyable and memorable. I wish each one of you immense success in your future endeavors. On a personal note, I would like to acknowledge the endless support and understanding provided by my mother throughout my academic journey. Her unwavering faith in my capabilities has been a source of constant inspiration and encouragement.

In conclusion, as Albert Einstein once said, "The important thing is not to stop questioning. Curiosity has its own reason for existing." May we all continue to ask, learn, and push the boundaries of knowledge for the betterment of our world. This thesis, while marking the end of one journey, is just the beginning of many more to come. Here's to lifelong learning and enduring curiosity.

RESUMEN EJECUTIVO

El creciente avance de las aplicaciones de reactores y aceleradores ha intensificado la demanda de cálculos precisos y eficientes en cuestiones de blindaje profundo. Este es un desafío complejo, debido a la naturaleza inherentemente incierta de los procesos físicos involucrados. A pesar de que los métodos tradicionales de simulación de Monte Carlo pueden ofrecer algunas soluciones, suelen ser intensivos computacionalmente y pueden resultar en alta incertidumbre estadística. Para superar estos desafíos, hemos explorado softwares de técnicas de reducción de varianza como ADVANTG, las cuales pueden aumentar la eficiencia de los cálculos de blindaje profundo. Estas técnicas están diseñadas para reducir la variabilidad de las simulaciones de Monte Carlo, ofreciendo estimaciones más precisas y confiables del espectro de partículas.

Un componente crítico de nuestra investigación ha sido el reactor MYRRHA, un reactor de investigación híbrido para aplicaciones de alta tecnología. Nuestro trabajo ha requerido la simulación de la penetración profunda de partículas a través de materiales de blindaje en varias partes del reactor, un proceso que ha llevado a incertidumbres en el cálculo del espectro de flujo. Para manejar esta incertidumbre, hemos optado por hacer uso de técnicas de reducción de varianza en lugar de simplemente aumentar el número de partículas de origen, lo cual solo habría incrementado el tiempo de cálculo. Estas técnicas están implementadas tanto en el código MCNP como en ADVANTG, proporcionando una vía prometedora para mejorar la precisión y eficiencia en este tipo de cálculos.

El propósito de esta tesis es examinar diversas técnicas de reducción de varianza aplicables a cálculos de blindaje profundo y evaluar su efectividad en el contexto del proyecto MYRRHA. Para lograr esto, realizaremos una revisión exhaustiva de la literatura con el fin de identificar las técnicas más prometedoras y comprender sus principios y supuestos fundamentales. A continuación, pondremos a prueba la eficiencia de estas técnicas seleccionadas en una serie de escenarios relevantes para el proyecto MYRRHA a través de simulaciones numéricas. Además, buscamos profundizar en la comprensión del software ADVANTG, el cual se utilizará para implementar las técnicas de reducción de varianza. Nuestro trabajo aspira a aclarar y facilitar el uso de ADVANTG, especialmente en la aplicación de ventanas de peso, para futuros usuarios. Un aspecto destacado de nuestra investigación es la exploración de fuentes de neutrones equivalentes en sistemas impulsados por protones, lo que puede simplificar considerablemente la modelización de estos sistemas, aumentando la eficiencia sin sacrificar la precisión de los resultados.

Esperamos que los hallazgos de esta tesis ofrezcan una visión valiosa sobre el uso de técnicas de reducción de varianza en cálculos de blindaje profundo, y que sean útiles para el diseño e implementación del proyecto MYRRHA. Además, nuestros descubrimientos podrían tener implicaciones más amplias en el campo de la protección radiológica y ser aplicables a otros proyectos y contextos similares. Por lo tanto, esperamos que esta tesis constituya una contribución relevante al proyecto MYRRHA y más allá, sirviendo tanto como ejemplo metodológico como guía práctica para implementar técnicas de reducción de varianza.

En vista de la complejidad del tema y con el objetivo de asegurar la máxima comprensión de todos los fenómenos implicados en el proceso, se adoptó una metodología de validación y verificación paso a paso antes de aplicarla a un sistema tan complejo como MYRRHA. La estrategia inicial implicó la investigación bibliográfica de experimentos más sencillos y relevantes para MYRRHA, que podrían ser utilizados para probar nuestra metodología en una escala más manejable. En este sentido, se decidió enfocarse en los experimentos de TIARA y KENS, ambos considerados experimentos de referencia que utilizan haces de protones disparados a blancos de espalación.

Sin embargo, nuestra meta principal era la aplicación del sistema de generación automática de varianzas denotado como ADVANTG para crear las ventanas de peso que posteriormente se utilizan en las simulaciones MCNP para mejorar la precisión estadística en las áreas de interés. Una limitación clave de ADVANTG es su incapacidad para utilizar fuentes de protones, lo que condujo a la necesidad de una adaptación metodológica. Como primer paso, convertimos los sistemas de TIARA y KENS que utilizan haces de protones en sistemas con una fuente equivalente de neutrones, replicando el mismo comportamiento en las zonas de interés que la fuente original de protones. Esta adaptación es relevante para MYRRHA, ya que nuestro objetivo es aplicar ADVANTG tanto en su operación subcrítica (como un sistema asistido por aceleradores, ADS) como en su operación crítica (como un reactor crítico).

Posteriormente, una vez obtenida la fuente equivalente de neutrones, la empleamos para ejecutar ADVANTG, generando un archivo con las ventanas de peso que se utilizan en la simulación posterior de MCNP. Un aspecto crucial a evaluar durante la investigación con TIARA fue la posibilidad de usar las ventanas de peso generadas con la fuente equivalente de neutrones en el input de MCNP que utiliza la fuente original de protones, y evaluar si los resultados obtenidos eran satisfactorios.

Adicionalmente a la metodología descrita, exploramos la opción de emplear lo que denominamos "fuentes no equivalentes de neutrones" en los sistemas de TIARA y KENS. Este enfoque implica simplemente cambiar las partículas utilizadas en la definición de la fuente en los inputs de MCNP, reemplazando los protones directamente por neutrones, sin considerar las implicaciones que ello conlleva. A pesar de que este procedimiento pueda parecer atípico o incluso extravagante, fue sugerido por los mismos desarrolladores de ADVANTG como una opción viable que podría producir resultados satisfactorios. Decidimos evaluar esta opción debido a su aparente simplicidad, que reduciría considerablemente el tiempo y esfuerzo necesarios en el desarrollo de la fuente equivalente de neutrones. Además, teníamos en cuenta que la creación de la fuente equivalente de neutrones puede ser una tarea intrincada dependiendo del tipo de fuente del sistema. Por lo tanto, si la aplicación de fuentes no equivalentes de neutrones resultara efectiva, se podría simplificar enormemente el proceso, optimizando así el tiempo y los recursos invertidos en futuros proyecto

Una parte fundamental de nuestra metodología fue investigar el impacto de la reducción de las incertidumbres en el espectro neutrónico en los cálculos de irradiación y en la determinación de la composición isotópica de los materiales tras un período de irradiación. Este aspecto es de suma importancia ya que tiene un efecto directo en el tiempo necesario para el decaimiento y el desmantelamiento de las instalaciones nucleares, así como en la dosis de radiación estimada recibida por los trabajadores. Para abordar esto, se incorporó en el experimento de KENS un apartado específico para realizar estos cálculos y evaluar el posible efecto de la reducción de las incertidumbres. La metodología fue diseñada para poder medir los cambios en las variables de interés y evaluar cómo estas modificaciones podrían influir en las estimaciones de decaimiento y dosis de radiación. Este enfoque no sólo nos permitió probar y ajustar nuestra metodología, sino que también nos proporcionó una visión crucial de cómo podría ser aplicada a los diversos componentes de MYRRHA en el futuro.

De modo que los estudios se llevaron a cabo en tres contextos principales: el experimento TIARA, el experimento de blindaje KENS y las simulaciones de MYRRHA. Cada uno de estos contextos proporcionó perspectivas valiosas y contribuyó a una comprensión más profunda del tema. A continuación, se presentan las resultados y conclusiones clave obtenidas de estos estudios, resaltando los hallazgos más importantes, las implicaciones, las limitaciones y las posibles direcciones para futuras investigaciones.

Durante el experimento TIARA, abordamos la viabilidad de la utilización de una fuente de neutrones equivalente para la reducción de la varianza en sistemas que utilizan fuentes de protones. En este proceso, descubrimos que la utilidad de esta técnica depende en gran medida de factores específicos, como la energía de las partículas y el espesor del blindaje. La precisión de los resultados se destacó como una función crucial de las librerías de datos nucleares, particularmente de los datos asociados a los protones como partículas incidentes. Además, reconocimos la optimización del mallado como un factor crítico para lograr una simulación computacionalmente eficiente y precisa.

Las simulaciones realizadas durante este experimento se resumen en la Tabla 0.1. Se analizaron dos casos: uno con un blindaje de hierro de 40 cm y otro con un blindaje de cemento de 100 cm. Los resultados de estas simulaciones, así como las diferencias entre los resultados obtenidos con y sin las ventanas de peso generadas por ADVANTG, se presentan en las Figuras 0.1 y 0.2. En ambas situaciones, la reducción de las incertidumbres en el espectro es notable. Además, es relevante mencionar que las simulaciones que emplearon las ventanas de peso fueron computacionalmente más rápidas en comparación con sus contrapartes analógicas.

Table 0.1: Comparación de rendimiento de simulación MCNP para el experimento TIARA con y sin ventanas de peso de ADVANTG.

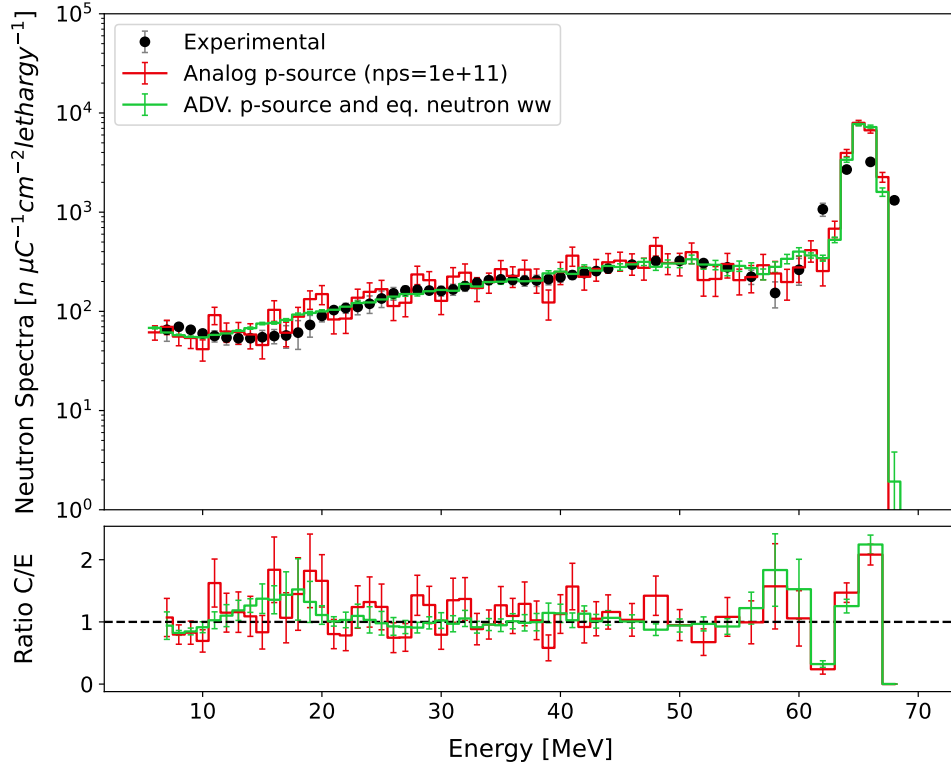| Shielding	Source	Weight Windows	Run time [hh:mm]	NPS
40 cm Iron	Eq. Neutron	None (analog)	00:20	2.00E+09
40 cm Iron	Non-Eq. Neutron	None (analog)	10:40	2.00E+09
40 cm Iron	Proton	None (analog)	00:10	2.00E+09
40 cm Iron	Proton	None (analog)	08:30	1.00E+11
40 cm Iron	Proton	Eq. Neutron	06:03	2.00E+09
40 cm Iron	Proton	Non-Eq.Neutron	Unfinished	-
100 cm Concrete	Eq. Neutron	None (analog)	00:23	2.00E+09
100 cm Concrete	Non-Eq. Neutron	None (analog)	01:29	2.00E+09
100 cm Concrete	Proton	None (analog)	00:10	2.00E+09
100 cm Concrete	Proton	None (analog)	07:30	1.00E+11
100 cm Concrete	Proton	Eq. Neutron	03:29	2.00E+09
100 cm Concrete	Proton	Non-Eq. Neutron	Unfinished	-

Figure 0.1: Comparación de resultados experimentales y calculados antes y después del uso de ADVANTG, con fuente de protones para el blindaje de hierro TIARA de 40 cm.
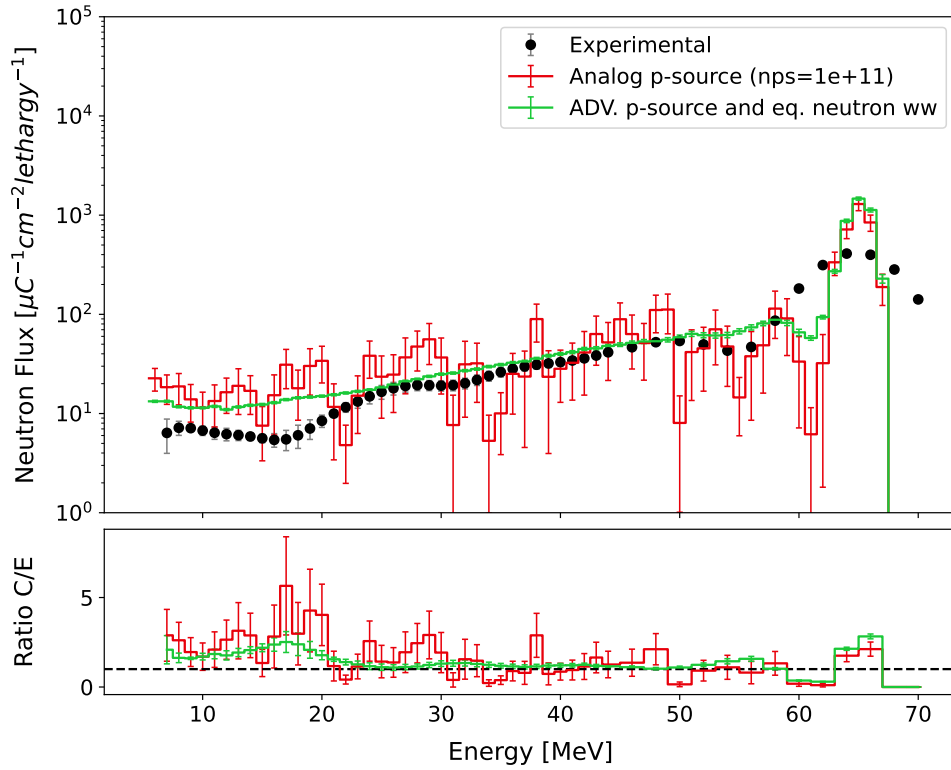

Figure 0.2: Comparación de resultados experimentales y calculados antes y después del uso de ADVANTG con fuente de protones para el blindaje de concreto TIARA de 100 cm.

Profundizando en las ideas obtenidas del experimento TIARA, el experimento de blindaje KENS nos proporcionó una comprensión más profunda de los aspectos claves. Nos enfocamos en particular en cómo los resultados podían cambiar en función de la zona que decidiéramos optimizar. Llevamos a cabo diversas simulaciones en ADVANTG, ajustando los mallados y las tallies a optimizar para evaluar su impacto. En algunos casos, centramos nuestros esfuerzos en optimizar solo la ranura 8, mientras que en otros, la optimización se aplicó a todas las ranuras. A su vez, nos interesaba investigar cómo estas variaciones afectaban la eficiencia computacional del sistema. Puede consultar el resumen de las simulaciones realizadas para este experimento en la Tabla 0.2.

Table 0.2: Comparación de rendimiento de simulación MCNP para el experimento de blindaje KENS con y sin ventanas de peso de ADVANTG.

Source	Weight Windows	Optimization	Run time [hh:mm]	NPS
Proton	None	None	77:33	2.00E+09
Non-Eq. Neutron	None	None	77:09	5.00E+08
Eq. Neutron	None	None	13:03	2.00E+09
Proton	Eq. Neutron	All-Slots	22:55	1.00E+06
Proton	Eq. Neutron	Slot-8	04:30	1.00E+06
Proton	Non-Eq. Neutron	Slot-8	00:30	1.00E+06
Proton	Non-Eq. Neutron	All-Slots	03:57	1.00E+06

En cuanto al uso de una fuente no equivalente de neutrones, los resultados fueron diversos. Aunque este método no funcionó en TIARA, en KENS se obtuvieron resultados satisfactorios y se logró una mayor rapidez computacional en comparación con el uso de una fuente equivalente de neutrones. Abordamos las posibles razones de estas discrepancias a lo largo del trabajo. Las Figuras 0.3 y 0.4 muestran los resultados del espectro neutrónico en las ranuras 8 y 1, respectivamente, para simulaciones en las que se optimizaron distintos parámetros y las comparamos con las simulaciones analógicas. En este caso puede observarse como la fuente no equivalente de neutrones proporciona resultados de precisión equivalente a los obtenidos con la fuente equivalente, pero de manera más eficiente.

Las Figuras 0.3 y 0.4 muestran los resultados del espectro neutrónico en la ranura 8 y 1 respectivamente para simulaciones en las que se optimizaron distintos parámetros y comparandolas con las simulaciones analógicas. Cabe destacar que en este ocasión y a diferencia de del caso anterior (TIARA) la fuente no equivalente de neutrones obtiene unos resultados equivalentes en cuanto a nivel de precisión a los obtenidos mediante la fuente equivalente y de manera más eficiente.
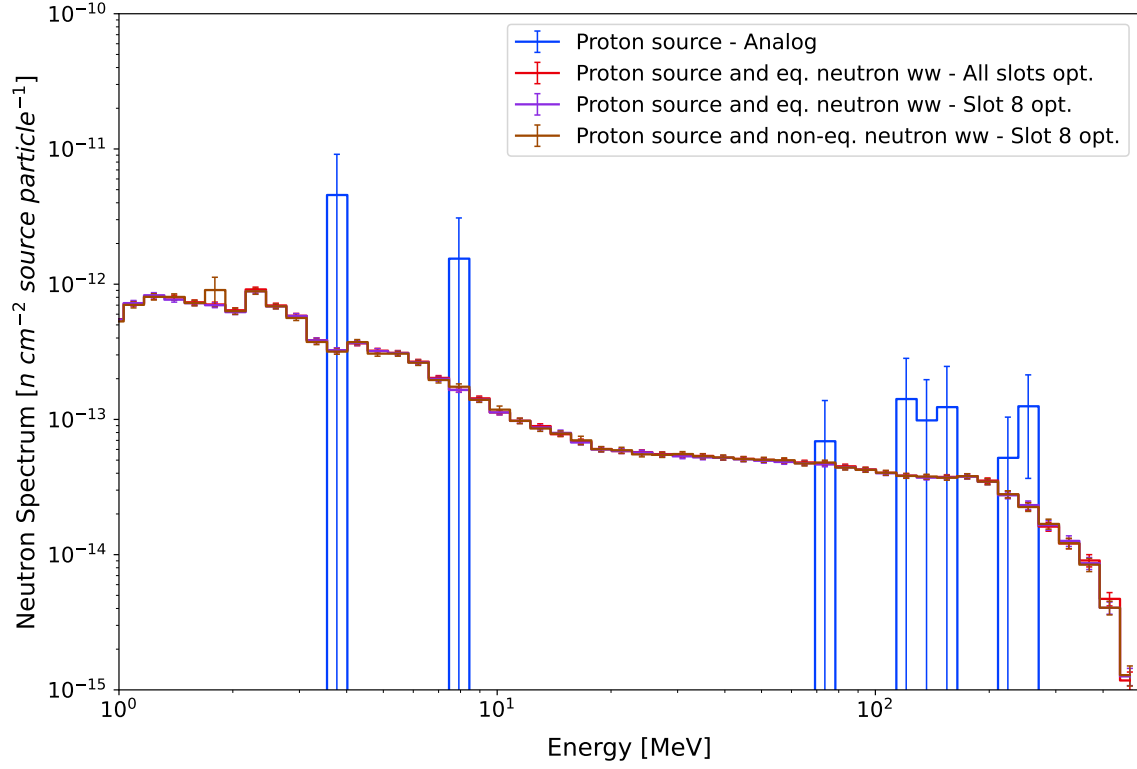
Figure 0.3: Espectros de neutrones obtenidos a partir de simulaciones de MCNP utilizando una fuente de protones para la Ranura 8 del experimento de blindaje KENS.
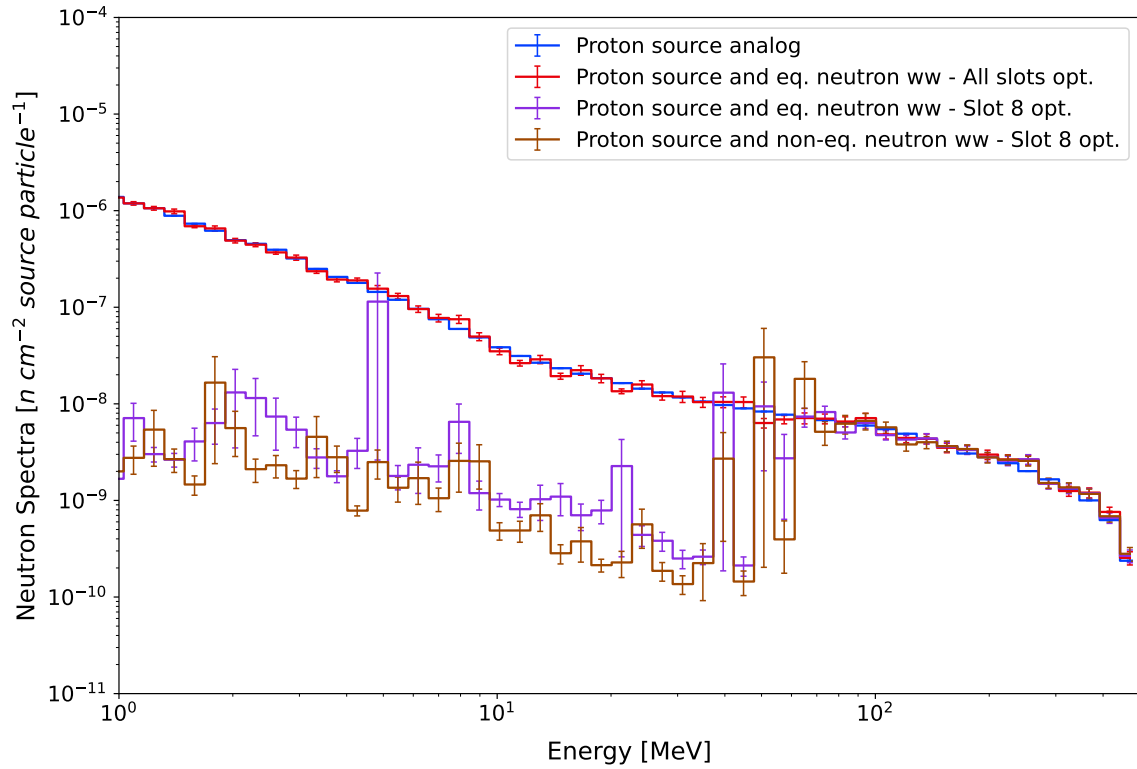

Figure 0.4: Espectros de neutrones obtenidos a partir de simulaciones de MCNP utilizando una fuente de protones para la Ranura 1 del experimento de blindaje KENS.

La Figura 0.5 presenta una comparativa de las tasas de reacción para los distintos detectores y ranuras del experimento. Se observó una mejora general en la precisión de los resultados al utilizar las ventanas de peso para optimizar todas las ranuras, todo ello con un tiempo de simulación considerablemente más corto que en el caso de las simulaciones analógicas. Estos hallazgos subrayan la eficacia de nuestras técnicas de optimización y prometen mejoras significativas en eficiencia para futuras investigaciones.
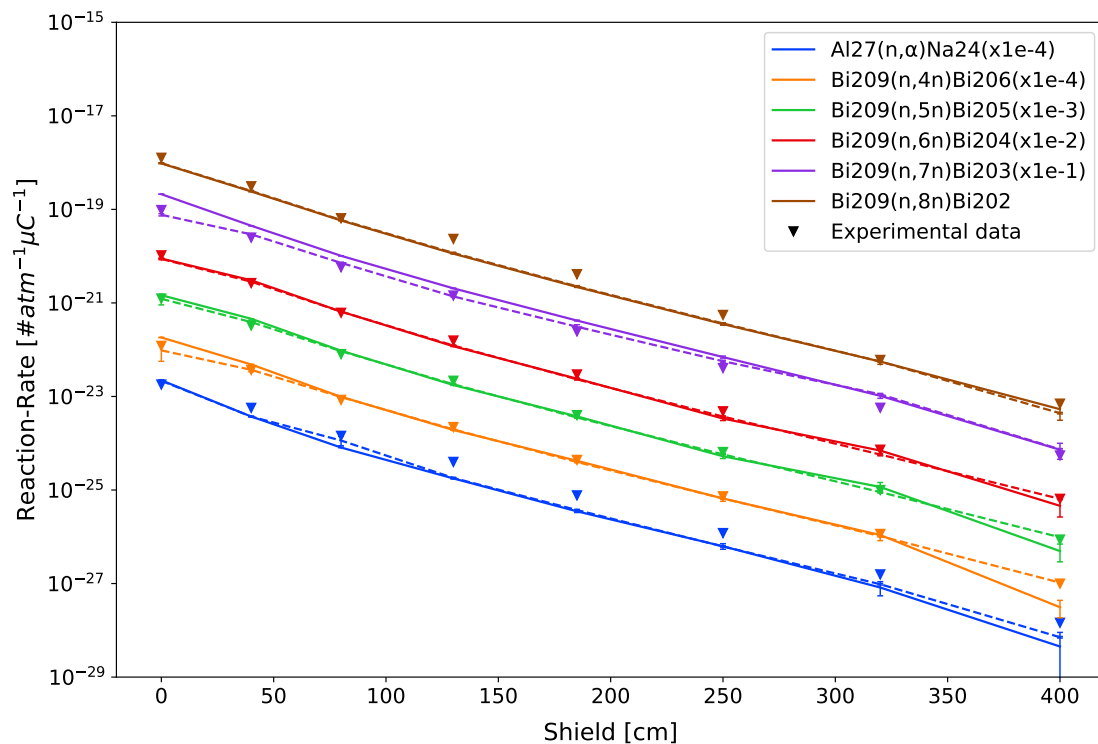
Figure 0.5: Comparación de resultados experimentales y calculados antes (línea sólida) y después (línea punteada) del uso de ADVANTG con fuente de protones para el experimento de blindaje KENS.

En cuanto a los cálculos de irradiación, la investigación demostró que las mejoras en la convergencia del espectro pueden resultar en reducciones sustanciales en las tasas de producción isotópica. Esto fue evidente en el caso de una muestra de acero inoxidable con la misma composición prevista que la vasija del reactor MYRRHA. Al examinar la actividad total de la muestra, se encontró que los isótopos principales representan aproximadamente el 85.5% de la misma (ver Figura 0.6). En este escenario, las contribuciones individuales de actividad de los radionúclidos dominantes a la activación total de la muestra de acero permanecen constantes. Se observó una reducción en la actividad del 3.86% y del 5.29% cuando el error de flujo se redujo de alrededor del 5% al 1.5% y al 0.5% respectivamente. Como conclusión, se demostró que mejorar la convergencia del espectro, que también se refleja en el error relativo del flujo promedio, conduce a reducciones sustanciales en las tasas de producción isotópica.
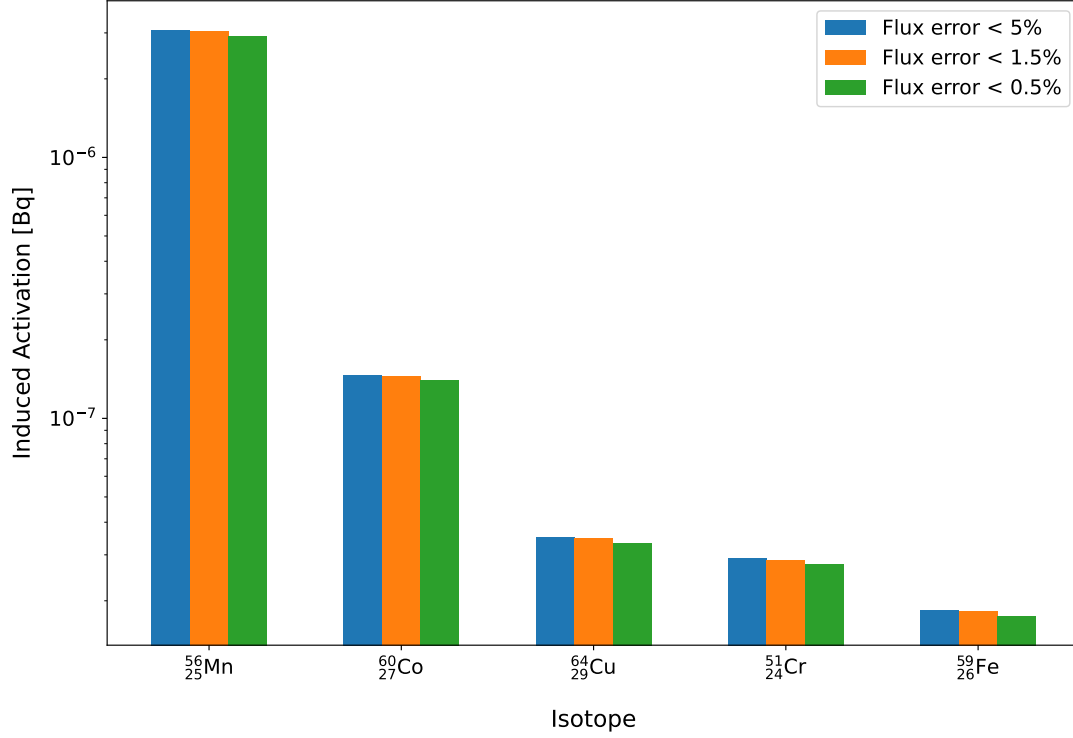
Figure 0.6: Actividades inducidas de los principales emisores gamma en la muestra de acero activado después de 1 año de irradiación.

En el transcurso de esta tesis, se llevaron a cabo simulaciones de MYRRHA para investigar la aplicabilidad de una fuente fija en simulaciones ADVANTG para problemas de criticidad. Este sistema representa un desafío notablemente mayor que los experimentos de validación (TIARA y KENS) debido a su complejidad y al volumen de la fuente, que involucra todas las reacciones de fisión. A pesar de ello, logramos establecer una fuente fija de neutrones tanto para el modo subcrítico como para el modo crítico, lo que supone un avance significativo.

Aunque originalmente se concibió la fuente fija para ser utilizada exclusivamente por ADVANTG en el cálculo de las ventanas de peso, las simulaciones demostraron que su aplicación directa en simulaciones con MCNP constituye una técnica de reducción de varianza muy efectiva. Los resultados obtenidos presentaron una precisión y exactitud equivalentes a las de las fuentes originales, con una mejora del 10% en términos de velocidad.

Para confirmar la efectividad de la fuente creada, se realizó un análisis detallado de las distribuciones radial, axial y angular de neutrones a lo largo del reactor. Consideramos que el comportamiento de la fuente era equivalente si estas distribuciones mostraban patrones similares. Las Figuras 0.7 a la 0.10 ilustran estas distribuciones, comparando los resultados obtenidos utilizando la fuente original, en este caso el haz de protones para la configuración subcrítica, y la fuente fija de neutrones creada.
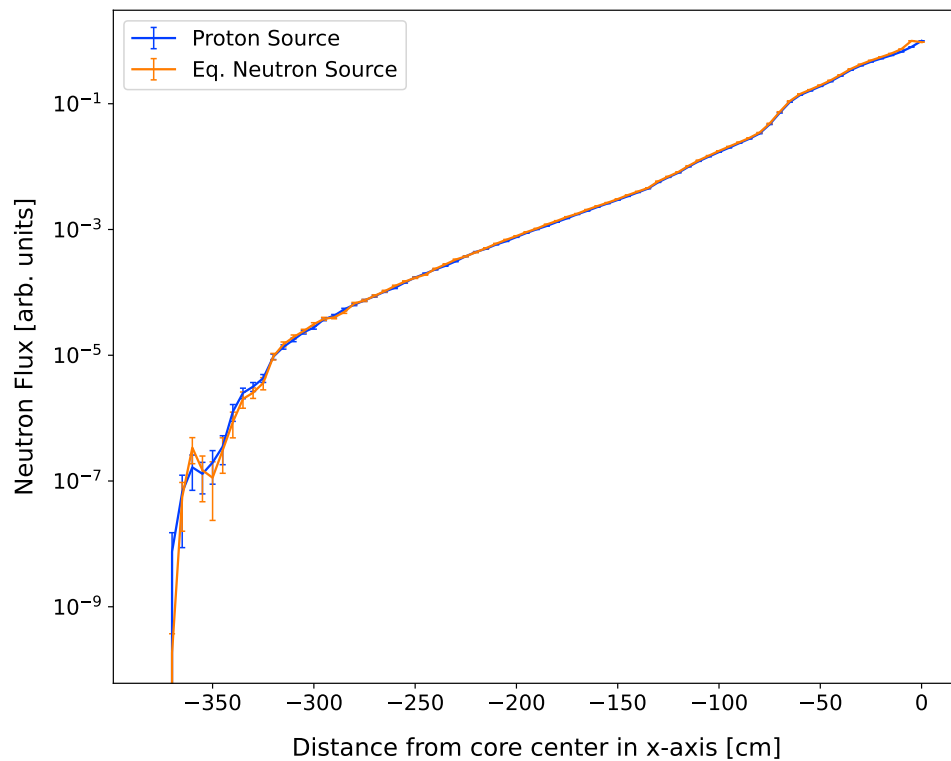
Figure 0.7: Comparación del flujo radial de neutrones a lo largo del eje x para $(y, z) = (0, 0)$: Fuente de protones vs. Fuente equivalente de neutrones.
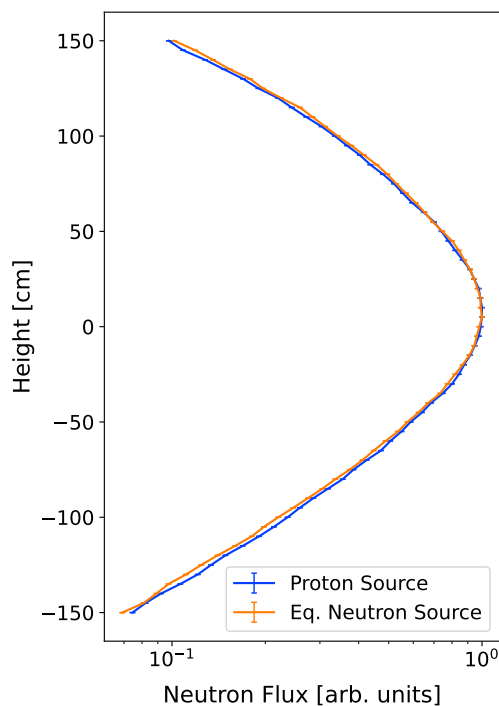

Figure 0.8: Comparación del flujo axial de neutrones en x=150 cm: Fuente de protones vs. Fuente equivalente de neutrones.
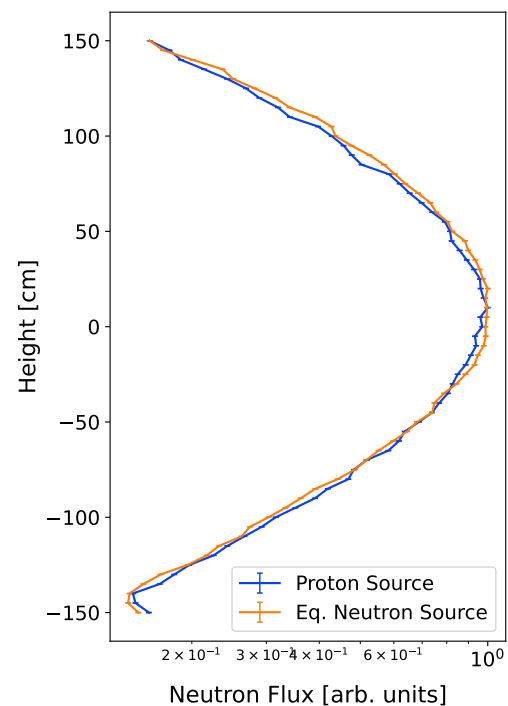

Figure 0.9: Comparación del flujo axial de neutrones en x=200 cm: Fuente de protones vs. Fuente equivalente de neutrones.
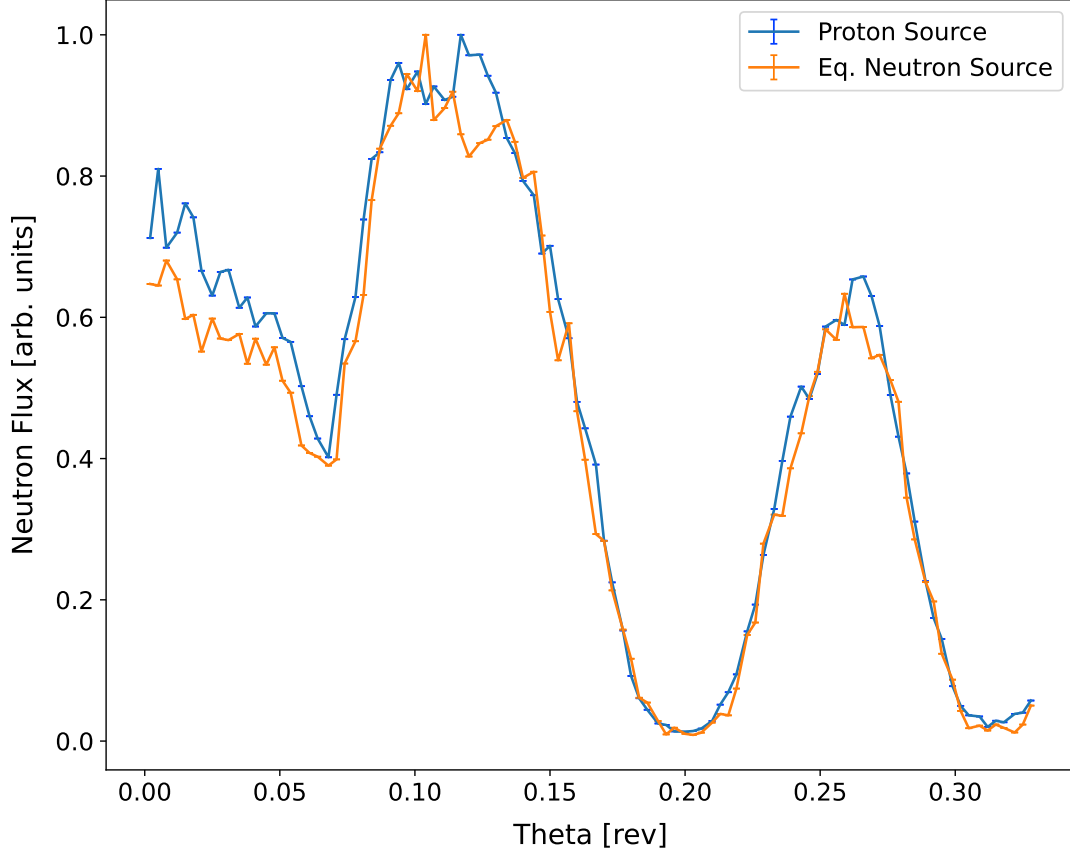
Figure 0.10: Flujo angular de neutrones en $(x, z) = (300, 0)$ cm: Fuente de protones vs. Fuente equivalente de neutrones.

El procedimiento empleado para crear la fuente fija de neutrones para el modo subcrítico fue luego aplicado al modo crítico del reactor, logrando resultados igualmente satisfactorios.

A pesar de estos avances, aún no hemos sido capaces de obtener un mallado de ADVANTG que permita mejorar los resultados en la simulación final de MCNP. Este desafío sigue siendo una tarea pendiente, pero estamos seguros de que el trabajo realizado hasta ahora ha establecido una sólida base para futuras investigaciones. Además, hemos adquirido una mayor comprensión de cómo funcionan las ventanas de peso y cómo se pueden utilizar de manera efectiva.

Como broche final a este trabajo de investigación, merece la pena destacar varios puntos clave. En primer lugar, la optimización del mallado en ADVANTG es esencial para obtener correctamente los valores de la ventana de peso y, por lo tanto, para utilizar eficazmente este método de reducción de varianza. Sin embargo, el camino hacia el éxito no está claramente marcado y requiere de una gran experiencia o de un enfoque exhaustivo de prueba y error. Este trabajo busca arrojar luz sobre este complejo procedimiento, con la esperanza de allanar el camino y facilitar futuras aplicaciones que necesiten técnicas de reducción de varianza, particularmente técnicas de ventana de peso a través de ADVANTG.

Igualmente crucial es la necesidad de una fuente equivalente de neutrones al aplicar ADVANTG en un sistema crítico o con fuente de protones. La creación de una fuente equivalente de neutrones fiable que refleje el comportamiento del sistema puede ser una técnica de reducción de varianza por sí misma. Esta estrategia podría acelerar las simulaciones, proporcionando resultados estadísticos más precisos. Si se necesita más refinamiento, este paso sigue siendo esencial.

Para mejoras adicionales, podemos recurrir a ADVANTG para los cálculos de ventana de peso, o incluso considerar las ventanas de peso de MCNP como una alternativa.

Además de los conceptos mencionados, el aspecto de la reducción de incertidumbres impulsadas por el espectro tiene un peso significativo en el contexto de los cálculos de irradiación. Esto se ha demostrado incluso en el escenario relativamente simple de los experimentos de blindaje KENS, donde la producción de todos los radionúclidos pertinentes resultó de la captura radiativa de neutrones. Podemos anticipar que estas incertidumbres tendrán un efecto más pronunciado cuando entran en juego reacciones adicionales, especialmente reacciones de resonancia o umbrales.

Por último, me gustaría señalar y dejar claro que el enfoque principal de esta tesis ha sido mitigar las incertidumbres derivadas de las simulaciones de Monte Carlo. Esto se debe principalmente a que, en el ámbito de los cálculos de blindaje profundo, estas incertidumbres influyen significativamente en los resultados. Aún así, es importante reconocer la existencia de otras fuentes de incertidumbres, particularmente aquellas relacionadas con los datos nucleares, que pueden requerir más atención para lograr resultados más precisos y concluyentes.

Códigos UNESCO

- Campo:
  - 33 - Ciencias de la Tecnología
  - 12 - Ciencias de la Computación e Información

- Disciplina:
  - 3307 - Tecnología de los reactores nucleares
  - 3320 - Ingeniería y Tecnología Nuclear
  - 1203 - Ciencias de la Computación
  - 1208 - Estadística

- Subdisciplina:
  - 330708 - Ingeniería de reactores
  - 120326 - Simulación
  - 332099 - Otras
  - 120808 - Procesos Estocásticos
  - 332004 - Reactores de Fisión Nuclear

Palabras Clave

- MCNP
- ADVANTG
- Técncias de reducción de varianza
- Ventanas de peso
- Fuente de protones
- Física nuclear
- Simulaciones
- Reactores Nucleares
- MYRRHA
- SCK CEN
- TIARA
- KENS

ABSTRACT

This master's thesis investigates the use of variance reduction techniques to mitigate spectrum-driven uncertainties in nuclear simulations, focusing on three primary contexts: the TIARA experiment, the KENS shielding experiment, and MYRRHA simulations.

In the TIARA experiment, the study explores the potential of an equivalent neutron source for variance reduction in proton-based systems. The accuracy of results was found to be significantly influenced by nuclear data libraries, especially those associated with protons as incident particles. The study also underscores the importance of mesh optimization for efficient and precise simulation. The KENS shielding experiment offered insights into how results could vary based on the selected optimization area. The study conducted several simulations in ADVANTG, adjusting meshes and tallies to assess their impact. The unconventional approach of using non-equivalent neutron sources, as suggested by ADVANTG developers, was also examined and found to be a potentially viable option. In the MYRRHA simulations, the research examined the feasibility of a fixed source in ADVANTG simulations for criticality issues. Despite the source's complexity and size, significant progress was made by establishing a fixed neutron source for both sub-critical and critical modes. The thesis also delves into the effects of reducing uncertainties in the neutron spectrum on irradiation calculations and the determination of isotopic composition post-irradiation. This aspect is crucial as it directly influences the decay time and dismantling of nuclear facilities, as well as the estimated radiation dose received by workers.

In summary, this thesis offers valuable insights into the application of variance reduction techniques in nuclear simulations, particularly the use of ADVANTG generated weight windows in proton-driven systems, paving the way for future research in this field.

TABLE OF CONTENTS

1 INTRODUCTION

1.1 Background and Motivation

In recent years, there has been a growing need for accurate and efficient methods for deep shielding calculations in the context of complex reactor and accelerator application projects. Deep shielding calculations are required to estimate the amount of radiation that is attenuated by various target, structural and shielding materials that surround the radiation source and to determine the effectiveness of different shielding configurations in protecting the radiation workers and public residence, and also the structural equipment from harmful radiation. The materials are activated by the incoming beam or by indirect interactions of secondary particles in the reactor and accelerator components. To evaluate radionuclide concentrations of activated materials is important to assign a certain waste level and to determine the final disposal options, additionally to the protection of the radiation workers from the delayed gamma dose rates. All those required calculations rely on the spectrum and total average flux of the particles at the investigated locations.

However, the calculation of deep shielding can be challenging due to the inherent complexity and uncertainty of the underlying physical processes. In particular, the use of traditional Monte Carlo simulation methods for deep shielding calculations can be computationally intensive and can produce results with high statistical uncertainty. To overcome these challenges, a number of variance reduction techniques have been developed, such as the use of ADVANTG [1], a software specifically developed to apply these techniques, that can improve the efficiency of the results in terms of statistics and computational time, of deep shielding calculations. These techniques exploit various statistical and physical principles to reduce the variance of the Monte Carlo simulations, and to provide more precise and reliable estimates of the particle spectra.

The MCNP code is a reference Monte Carlo code for the neutronic calculations of the MYRRHA reactor, which is multi purpose hybrid research reactor for high-tech applications. MYRRHA-related calculations such as determining particle fields/doses on reactor components not located in the proximity of the core – e.g., reactor vessel, primary pumps, primary heat exchangers – or even outside the reactor vessel – e.g., reactor hall – require simulating the deep penetration of particles through shielding material. Being the MYRRHA pool filled for its majority by LBE and steel a large number of photons/neutrons is absorbed before reaching the periphery of the system, where the particle flux is generally several orders of magnitude lower compared to inside the core. Calculation uncertainty in the flux spectrum far from the reactor core have an impact not only on the dose rate results but also on isotopic production predictions. As the safety margin parameters of the MYRRHA reactor is based on the calculated parameters obtained with the MCNP, it is important to ensure that obtained results are reliable.

Due to the statistical nature of any Monte Carlo code, to increase the calculation uncertainty, the simple way is to increase the number of source particles or to apply variance reduction techniques. As the former solution will increase the computational time, it is required to use variance reduction techniques either implemented in the MCNP code or to use ADVANTG code, which is an automated tool for generating variance reduction parameters for fixed-source continuous energy Monte Carlo simulations with MCNP based on approximate 3-D multigroup discrete ordinates adjoint transport solutions generated by Denovo.

1.2   Objectives

The objective of this thesis is to explore the different variance reduction techniques that can be applied to deep shielding calculations and to evaluate their effectiveness in the context of the MYRRHA project. To achieve this aim, a comprehensive literature review will be conducted to identify the most promising techniques and to understand their underlying principles and assumptions. Next, a series of numerical simulations will be carried out to test the performance of the selected techniques in a range of scenarios relevant to the MYRRHA project. These simulations will allow us to assess the accuracy and computational efficiency of the techniques, and to identify any potential limitations or challenges that may arise in their application.

With these objectives in place, we also aim to contribute to a wider understanding of the ADVANTG software [1]. which will be used for the implementation of the variance reduction techniques. This thesis seeks to make the workings of ADVANTG, especially in the application of weight windows, clearer and more accessible for its future users. The insights and experiences derived from this thesis may assist future users in optimally leveraging this powerful tool.

Moreover, we aim to provide valuable information on source biasing in proton-driven systems. An interesting aspect of our research is the exploration of equivalent neutron sources within these systems. Equivalent neutron sources are valuable in this context as they can significantly simplify the modeling of such systems, reducing computational demands and increasing efficiency, without sacrificing the accuracy of the results.

This thesis's findings will provide valuable insights into the use of variance reduction techniques for deep shielding calculations and will inform the design and implementation of the MYRRHA project. Additionally, the findings of this study may have wider implications for the field of radiation protection and may be applicable to other similar projects and contexts. Therefore, this thesis is expected to be a valuable contribution to the MYRRHA project and beyond, serving as both a methodology exemplar and a practical guide for implementing variance reduction techniques.

1.3   Thesis Structure

The structure of this thesis is delineated across several chapters, each with its own dedicated focus and purpose:

- **Computer Codes:** This chapter delves into the computational tools and codes employed throughout the thesis, addressing their characteristics, advantages, and limitations.

- **Theory:** The theoretical foundations relevant to this study are comprehensively discussed in this chapter. It elucidates the theories that underpin the methodologies used in this research.

- **Methodology:** Here, the research design is expounded, detailing the methods and strategies that guided the study. An in-depth exploration of the variance reduction techniques used is also presented.

- **Results:** This chapter offers a presentation of the research findings obtained from the numerical simulations. It clearly, concisely, and comprehensively articulates the research outcomes.

- **Conclusions:** This chapter consolidates the key findings of the thesis, discusses their implications, and proposes potential avenues for future research within this domain.

- **Social and Professional Responsibility:** This section examines the ethical, social, and professional responsibilities linked with the study and its findings, showcasing how these responsibilities have been addressed throughout the project.

- **Project Management:** The management aspects of the thesis project are detailed in this chapter, including planning, resource allocation, time management, risk assessment, and mitigation strategies.

The final sections, 'Glossary' and 'Annexes', serve as useful resources for the reader. The Glossary provides definitions for crucial terms and concepts, and the Annexes include supplementary materials and data relevant to the research.

2 COMPUTER CODES

In this fast-paced era of technological advancement, sophisticated software tools are vital for pushing the boundaries of scientific research. They serve as powerful instruments, allowing us to tackle and explore complex phenomena that can be nearly impossible to comprehend otherwise. The focus of this chapter will be to present the key computational tools that have been the backbone of the research journey in this thesis.

2.1 MCNP 6.2

MCNP, [2] is a general-purpose Monte Carlo N-Particle transport code developed and maintained by Los Alamos National Laboratory. It was initially developed in the 1950s for simulating radiation transport in nuclear reactors, but it has since been extended and used for a wide range of applications, including radiation protection, medical physics, space exploration, and national security.

A wide variety of particles, up to 1TeV/nucleon, including neutrons, photons, electrons, ions, and many other elementary particles can be used for transport calculations. These particles are transported using a three-dimensional representation of the materials enclosed by first-, second-, and fourth-degree user-specified surfaces and described in constructive solid geometry. Additionally, by embedding a mesh within a constructive solid geometry cell, external structured and unstructured meshes may be used to generate the problem geometry in a hybrid mode, offering a different method of constructing complicated geometry, [3]. This allows it to simulate a wide range of systems, including nuclear reactors, medical imaging devices, and spacecraft. Additionally, MCNP can simulate the effects of radiation on materials, such as the damage caused by high-energy particles.

Some of the main limitations of MCNP include the fact that it is a probabilistic code, meaning that it uses random numbers to simulate particle transport. As a result, the results of an MCNP simulation can vary from run to run. Additionally, MCNP is a computationally intensive code, so it can take a long time to run complex simulations. Finally, MCNP is not well suited to simulating some types of problems, such as those involving fluids or gases.

Also, compared to other particle transport codes, some strengths and weaknesses can be mentioned. On the one hand, it is widely used and has a strong track record of reliability and accuracy. It also has a large user community, which can provide support and resources for those using the code. On the other hand, it can be difficult to use and may not have some of the advanced features and capabilities that are available in other codes, such as SERPENT or OpenMC.

Overall, MCNP is a powerful and versatile tool for simulating the transport of particles through matter. It has been widely used in a variety of fields and has been a valuable tool for understanding the behavior of radiation and other particles.

2.2 ADVANTG 3.2.0

ADVANTG, [1] stands for Automated Variance Reduction Generator. It is a software tool developed by Oak Ridge National Laboratory (ORNL), being ADVANTG 3.2.0 the latest version available at RSICC and NEA. This software tool is used to improve the accuracy of continuous-

energy Monte Carlo simulations of neutron, photon, and coupled neutron-photon transport problems using MCNP through the use of variance reduction techniques. It generates space- and energy-dependent weight-window bounds and biased source distributions using 3D discrete ordinates solutions of the adjoint transport equation and creates an output compatible with MCNP. It can also perform discrete ordinates calculations and construct discretized representations of transport problems on a user-provided spatial grid and can be used to visualize these models and solutions. ADVANTG aims to reduce both user effort and computational time in order to obtain accurate and precise tally estimates and has been applied to simulations in radiation shielding, detection, and neutron activation. It provides a more efficient and automated alternative to traditional methods for generating variance reduction parameters.

As mentioned previously, variance reduction is a statistical technique that is used to reduce uncertainty or variability in simulation results. This is achieved by performing a large number of simulations with different sets of input parameters and then averaging the results.

ADVANTG is implemented as a preprocessor to MCNP, which means that it processes the input file for MCNP and generates a modified version of the input file with the appropriate variance reduction parameters. This modified input file is then used as input to MCNP to perform the actual simulation. ADVANTG includes a number of different variance reduction techniques that can be used to improve the accuracy of MCNP simulations. These techniques include importance sampling, stratified sampling, Russian roulette, and variance reduction by decomposition. Also includes a number of advanced features that can be used to customize and optimize the variance reduction process. These features include the ability to specify different variance reduction techniques for different regions of the simulation domain, the ability to adjust the parameters of the variance reduction techniques, and the ability to monitor and control the variance reduction process.

ADVANTG is primarily used in the field of nuclear engineering and has been used in applications such as nuclear reactor design, simulation of nuclear accidents, and evaluation of the safety of nuclear devices. Some examples of real-world applications in which ADVANTG was demonstrated to significantly increase the tally figure of merit (FOM) compared to analog MCNP simulations are [1]:

- Shielding applications including radiation shielding, detection, rate analyses of the ORNL Spallation Neutron Source and High Flux Isotope Reactor and the ITER Tokamak.

- Radiation detection, safeguards and special nuclear material movement detection test problems.

- Prediction of activation rates within light water reactor facilities.

As a whole, ADVANTG provides a powerful and efficient alternative to traditional methods, such as analog MCNP simulations, for generating variance reduction parameters and manages to reduce effort and computational time, while obtaining accurate and precise tally estimates.

2.3   ALEPH 2.0

ALEPH2.0 is a Monte Carlo burn-up code, developed at SCK-CEN since 2004. Its central purpose is to bridge the gap between steady-state Monte Carlo transport and time-dependent depletion calculations, providing essential consistency for our project. What makes ALEPH2.0 stand out among other depletion codes are its unique features that directly address several

limitations of previous versions. It incorporates the most recent nuclear data libraries such as JEFF-3.1.1, ENDF/B-VII and JENDL-4. These libraries provide a rich source of activation data, spontaneous fission information, fission product yield data, and radioactive decay data. By integrating this wealth of data, ALEPH2.0 offers a more precise and reliable framework for our simulations. Furthermore, ALEPH2.0's built-in depletion algorithm provides a more accurate understanding of time-dependent nuclide concentrations, effectively reducing uncertainties. It also includes additional features such as a predictor-corrector mechanism, and the capability to calculate nuclear and decay heat, as well as decay neutron sources [4].

In the context of our project, ALEPH2.0 is used to perform depletion calculations using an external neutron spectrum file, which is generated through MCNP. This coupling of software enriches our research process and allows us to delve deeper into the realm of spectrum-driven uncertainties.

Finally, it is noteworthy that ALEPH2.0 has undergone rigorous validation against the results of the REBUS experimental program [4], with it demonstrating a superior agreement with the measured data compared to other depletion codes. This further emphasizes its reliability and relevance to our research.

2.4 Cluster

In this study, simulations were run on the Newton calculation cluster, a high-performance computing system built at SCK CEN. The cluster consists of 45 computing nodes, providing 1476 non-hyperthreaded computing cores or 2952 hyperthreaded computing cores. The hardware specifications of the nodes include the use of Intel Xeon Gold 6154 CPUs, a total of 8.7 TB of RAM, and dedicated 10 Gbps inter-node and storage connections. The cluster also has dedicated storage options with capacities of 10+10 TB and 21 TB, connected via 40Gbps network. The operating system used on the cluster is CentOS 7.x.

2.5 Python

Python is an open-source, high-level programming language developed by Guido van Rossum in 1991. It has since become one of the most popular and versatile languages in the world of programming due to its simplicity, readability, and broad library support. Python's straightforward syntax and semantics make it a go-to language for beginners and experienced programmers alike, and its extensive range of libraries and modules make it exceptionally useful for a multitude of applications ranging from web development to data analysis and machine learning [5].

In this project, Python has been extensively used to automate tasks and analyze data. Its extensive suite of scientific libraries, such as NumPy for numerical computing and Matplotlib for data visualization, made it an ideal tool for handling and processing the large datasets generated by our simulations. Its powerful scripting capabilities facilitated the automation of repetitive tasks, thereby increasing the efficiency of our research process.

2.6 SANDY

Another significant tool utilized in this thesis is SANDY, a nuclear data sampling code compatible with nuclear data files in the ENDF-6 format. Developed by Luca Fiorito and his team

at SCK CEN, SANDY employs the fundamental theory of stochastic sampling to generate random nuclear data samples. These samples accurately reflect the covariance information from the ENDF-6 files, and they can be used as inputs to produce perturbed responses in nuclear codes. A key capability of SANDY lies in its capacity to perform a variance-based decomposition method to estimate global sensitivity indices for both correlated and uncorrelated input parameters. This enables the determination of parameters with the largest impact, thus aiding in the identification of crucial variables [6].

In the context of our project, SANDY has been employed in a more specific role - as a tool for reading output files from MCNP and ALEPH. This targeted use of SANDY complements our other software tools and contributes to the overall efficiency and effectiveness of our research process.

3 THEORY

3.1 Relative Error

Accompanying each tally in the MCNP6.2 standard output is a fundamental quantity of statistical significance known as the relative error, denoted by R. This value is derived from the ratio of the standard deviation of the mean ($S_{\bar{x}}$) to the mean ($\bar{x}$) itself. The relative error quantifies the uncertainty tied to the mean, and thus can be interpreted as a measure of the reliability of the simulation results. To construct confidence intervals around the estimated mean, the relative error plays an indispensable role [2].

For simulations displaying normal behavior, the relative error, R, is inversely proportional to the square root of N, where N signifies the number of particle histories. As articulated by the Central Limit Theorem, as N approaches infinity, there exists a 68% probability that the true result lies within the range $\bar{x}(1 \pm R)$, and a 95% probability it is within $\bar{x}(1 \pm 2R)$. However, it is crucial to note that these confidence intervals primarily relate to the precision of the computation, not its accuracy. To make assertions regarding the accuracy of a simulation, a comprehensive analysis involving factors such as the uncertainties in the physical data, the modelling, the sampling technique etc., is mandatory.

The MCNP manual [2] offers valuable guidelines for interpreting the quality of the confidence interval based on the value of R, as outlined in Table 3.1. It is worth emphasizing the significance of these ranges, as they provide critical insights into the quality of the tally and consequently, the reliability of the simulation results.

Table 3.1: Guidelines for interpreting the relative error R [2].

Range of R	Quality of the tally
0.5 to 1.0	Not meaningful
0.2 to 0.5	Factor of a few
0.1 to 0.2	Questionable
<0.10	Generally reliable
<0.05	Generally reliable for point detectors

Further, as discussed, the estimated relative error R scales as $\frac{1}{\sqrt{N}}$, with N signifying the number of particle histories. Given that the computational time, T, for any MCNP run scales with N, we may represent the relative error in terms of computational time as follows:

$$R \sim \frac{C}{\sqrt{T}} \tag{3.1}$$

where C is a positive constant contingent upon the tally choice and the sampling techniques employed. If the aim is to reduce the estimated relative error R, strategies may involve either increasing the computational time T (i.e., augmenting the number of particle histories) or decreasing the constant C via appropriate variance reduction techniques (as detailed in Section 3.2). However, merely increasing the number of particle histories is generally an inefficient method for reducing R given the significant computational resources required to generate a large number of histories. Therefore, implementing advanced variance reduction techniques often presents a more practical approach for enhancing the reliability of the simulation results.

3.2   Variance Reduction

Variance is a measure of how much a random variable deviates from its expected value. In the context of Monte Carlo simulations, variance reduction techniques are utilized to enhance the precision of estimates within a fixed computational effort. These methods allow for either decreased computer time while maintaining adequate precision or increased precision without additional computational resources [2].

However, it is important to distinguish between accuracy and precision. A reduced variance does not necessarily imply a more accurate calculation. Accuracy refers to how close the tally estimate is to the true physical quantity being estimated [2]. It is influenced by factors such as geometry and physics approximations, cross-section data, and material definitions. On the other hand, the relative error reflects the precision of a result in the presence of statistical fluctuations inherent to probabilistic methods.

Several factors can affect the accuracy of Monte Carlo calculations [7]:

1. Code factors

   - Physics and models
   - Data uncertainties
   - Cross-section representations
   - Errors in coding

2. Problem-modeling factors

   - Source model and data
   - Geometrical configuration
   - Material composition

3. User factors

   - User-supplied subroutine errors
   - Input errors
   - Variance reduction abuse
   - Checking the output
   - Understanding the physical measurements

Despite its advantages, the Monte Carlo method has a significant drawback: it is often too computationally expensive for a large number of calculations. This is not due to the procedure's slowness but rather the extensive computational time required to follow trivial or statistically insignificant occurrences to reach the desired outcome. Therefore, the key to making the Monte Carlo approach efficient is to focus on relevant features of a problem while avoiding minor ones. This is where "variance reduction methods" come into play, as they reduce the statistical variance for the same amount of computing time [8].

MCNP, a tool used in these simulations, measures the efficiency of calculations in several ways, one of which is the figure of merit (FOM). The FOM is defined as:

$$FOM = \frac{1}{\sigma_{mr}^2 T} \tag{3.2}$$

where σ_{mr}^2 is the relative standard deviation of the mean and T is the computational time for the calculation in minutes. The FOM should be roughly constant for a well-sampled problem because while σ_{mr}^2 is on average inversely proportional to the number of histories (N), T is on average directly proportional to N. Therefore, the product remains fairly constant.

MCNP has the following mathematical form for tallies to be estimated:

$$\langle T \rangle = \int d\vec{r} \int d\vec{v} \int dt N(\vec{r}, \vec{v}, t) T(\vec{r}, \vec{v}, t) \tag{3.3}$$

The method involves sampling particle histories that generate the appropriate particle density $N(\vec{r}, \vec{v}, t)$ statistically. In cases where a tally is not required, the tally function $T(\vec{r}, \vec{v}, t)$ is zero. By employing MCNP variance reduction techniques, improved statistical estimates of N can be obtained in regions where T is large, at the cost of less accurate estimates where T is zero or small.

Non-analog techniques in MCNP do not directly emulate nature but can be utilized as long as both N and $\langle T \rangle$ are conserved. To maintain this conservation, the weight of particles can be altered, which can be interpreted as the number of particles that an MCNP particle represents [2]. The concept of particle weight is vital to the practice of variance reduction. It is not necessary to track each physical particle to simulate the movement of a large number of them. Instead, a statistically significant sample of particle 'histories' must be followed, with each history assigned a weight that corresponds to the number of actual particles being modeled.

Several variance reduction techniques are employed in MCNP, including importance sampling, weight windows, geometry splitting, and Russian roulette.

- **Importance sampling** is a technique that biases the sampling process to give more weight to the more significant outcomes, thereby reducing the variance of the estimated quantities and leading to more accurate results.

- **Weight windows** set upper and lower weight bounds for each spatial region in the problem. Particles that fall below the lower weight bound are terminated, while those that exceed the upper bound are split into multiple particles. This technique is further explained in Section 3.3.

- **Geometry splitting and Russian roulette** are two complementary techniques used to control the weight of the particles. When a particle crosses a boundary between two regions with different importances, its weight is adjusted according to the ratio of the importances of the two regions. If the weight of the particle increases (i.e., it moves to a region of higher importance), the particle is split into multiple particles, each with a fraction of the original weight. This process is known as geometry splitting.

  Conversely, if the weight of the particle decreases (i.e., it moves to a region of lower importance), the particle is subjected to a game of Russian roulette. In this game, the particle has a certain probability of being terminated and a certain probability of surviving with an increased weight. This process helps maintain the computational efficiency of the simulation by eliminating particles that contribute little to the estimated quantities.

3.3 Weight Windows

Weight windows are a crucial component in variance reduction techniques, specifically used to reduce spectrum-driven uncertainties in Monte Carlo simulations. They function by controlling

the weight of particles in a simulation, ensuring that they fall within a specific range. This control over particle weight reduces the fluctuations that can introduce uncertainty.

Unlike geometry splitting, which is based on the ratio of importances across a surface, the weight window operates with absolute weight bounds. It can be applied at surfaces, collision sites, or both, offering more flexibility than geometry splitting, which is only applied at surfaces. This flexibility allows the weight window to control weight fluctuations introduced by other biasing techniques.

A weight window requires all particles in a cell to have a weight within the range $W_L < W < W_u$. This range is always adjusted to be at least a factor of 2 wide, that is $W_u/W_L \geq 2$. This ensures that the weight window can effectively control the weight of particles and reduce fluctuations [7].
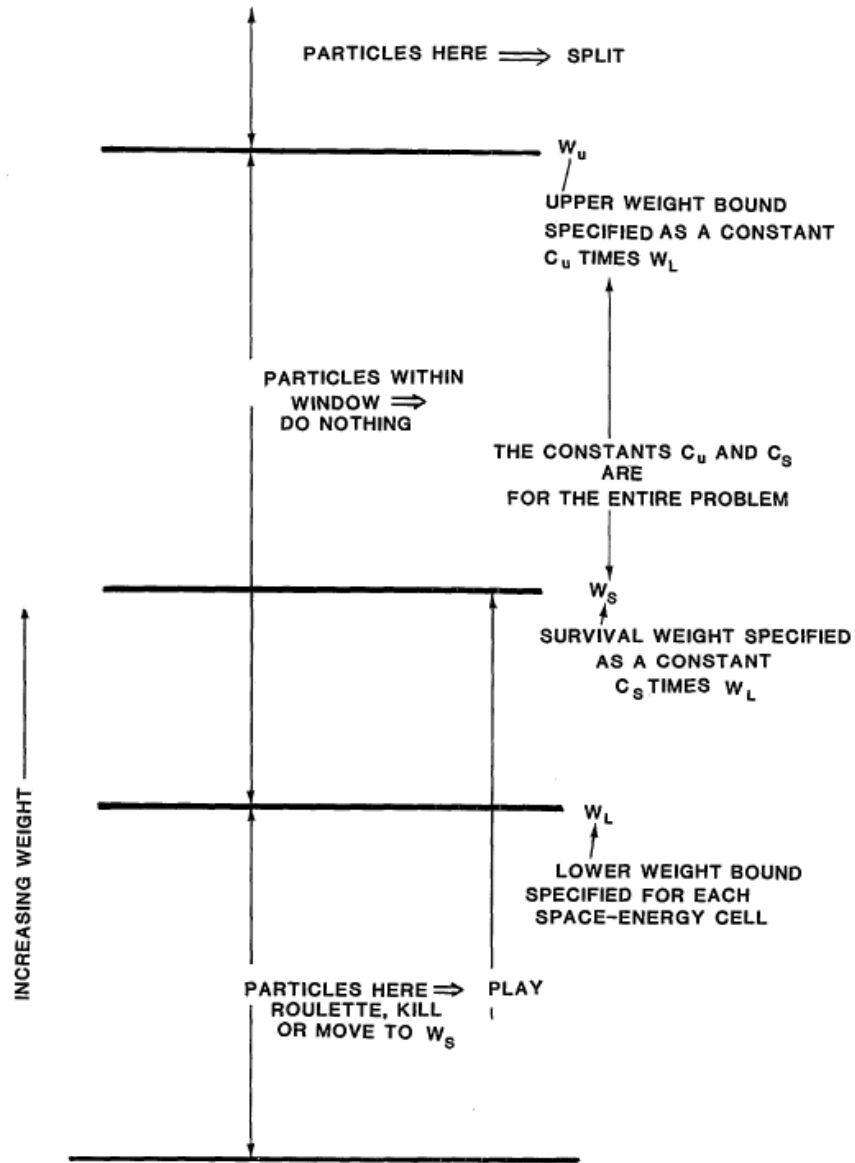
Figure 3.1: Detail of the weight window [7].

Weight windows have special features that enhance their effectiveness. For instance, there is a maximum split/roulette feature that limits the amount of splitting/rouletting that can occur at any particular weight window game. In the context of a specific problem, the weight window parameters should be such that the weight windows are inversely proportional to the space-energy importance. This requires either a guess of what the importance function looks like or use of information from experience.

In MCNP simulations, weight and importance have distinct meanings. The weight of a particle represents its statistical contribution to the estimated quantities. It is a measure of the number of 'real' particles that the simulated particle represents. On the other hand, importance is a user-defined quantity that indicates the relative significance of different spatial regions in the problem. It is used in conjunction with weight windows to control the statistical weight of the particles and reduce the variance of the simulation.
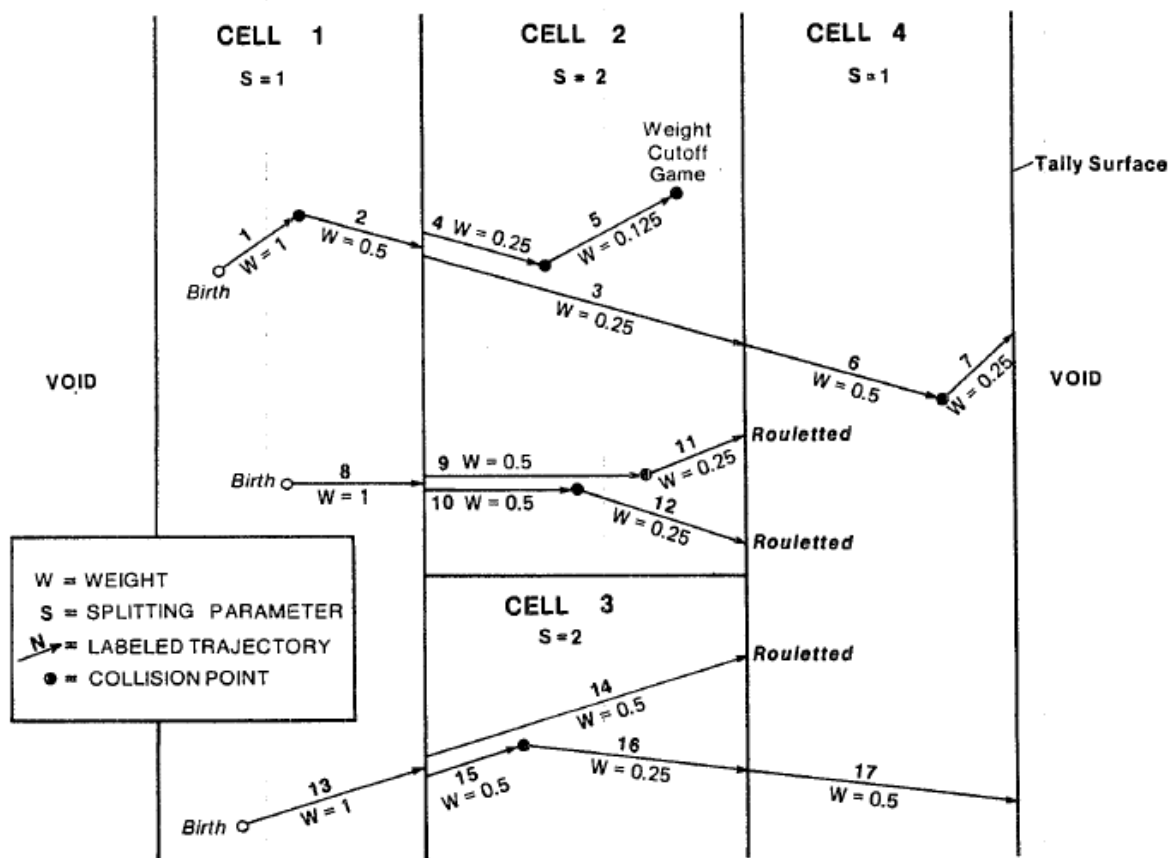

Figure 3.2: Generic Monte Carlo problem of four cells with three particle histories, illustrating how importances can be estimated [7].

Row	Description	Cell 1	Cell 2	Cell 3	Cell 4
	Weight				
1	Trajectories entering	1, 8, 13	3, 4, 9, 10	14, 15	6, 17
2	Weight entering associated with above trajectories	1, 1, 1	0.25, 0.25, 0.5, 0.5	0.5, 0.5	0.5, 0.5
3	Total weight entering	3	1.5	1	1
	Score				
4	Trajectories entering that resulted in score	7, 17	7	17	7, 17
5	Scores associated with above trajectories	0.25, 0.5	0.25	0.5	0.25, 0.5
6	Total score	0.75	0.25	0.5	0.75
	Estimate				
7	Estimated importance Row 6/Row 3	0.25	0.167	0.5	0.75

Figure 3.3: Importance estimation process for particle histories in Figure 3.2 [7].

The weight windows are chosen according to available cell importances. The lower weight bound (W_l) is calculated as 0.5 divided by the cell importances, the survival weight (W_s) is 3.0 times W_l, and the upper weight bound (W_u) is 5.0 times W_l. In any given game, no particle will be split more than five for one, nor rouletted harsher than one in five. The weight window game can be turned off in certain cells if that part of the problem is too angle-dependent for the weight window to be effective. The weight window can be applied both at collisions and surface crossings [7].

In conclusion, weight windows are a powerful tool in variance reduction techniques. They provide a means to control the weight of particles, thereby reducing the uncertainties in a simulation. Their flexibility and special features, such as the maximum split/roulette feature, make them a valuable component in the reduction of spectrum-driven uncertainties.

3.4 Denovo

Denovo is an essential component of ADVANTG, offering 3-D solutions to radiation transport problems. This powerful and user-friendly software is built to handle complex transport issues involving neutrons and gamma rays. Simply put, Denovo breaks down the problem's structure, source, and data points into a grid format, making it easier to calculate particle movements and interactions in the system [1]. It utilizes state-of-the-art mathematical tools from the Trilinos library and uses the Generalized Minimum RESidual (GMRES) method to reach a solution step by step.

One of the key strengths of Denovo is its ability to handle big problems by dividing work among multiple computer processors. This division of labor makes the calculations faster and more efficient, especially when dealing with complicated systems with many spatial cells [1]. Furthermore, Denovo supports various methods to break down space and angles, including both triangular and product quadratures. These choices can affect how accurate and efficient the calculations are, depending on the specifics of the problem [1].

Denovo is widely applicable in the field of nuclear engineering and radiation transport. It is useful for solving problems involving neutron and gamma-ray movements such as designing shields, planning reactors, and planning radiation therapy. By providing accurate and efficient solutions, Denovo helps us to better understand and optimize radiation movement processes in various systems [1].

To summarize, Denovo is a multi-purpose, 3-D software package within ADVANTG, designed

to calculate deterministic radiation transport. By breaking down the problem and using modern mathematical tools and division of labor among processors, Denovo offers an effective and efficient solution to radiation transport problems. Its wide range of applications illustrates its importance in the field of nuclear engineering and radiation transport.

3.5 CADIS Method

The Consistent Adjoint Driven Importance Sampling (CADIS) method is a variance reduction technique that was developed to expedite the estimation of a single scalar quantity in transport problems. It is implemented in the ADVANTG software and works by calculating an adjoint solution, which is representative of the importance of different regions and energies in contributing to the desired tally. This adjoint solution is then utilized to generate variance reduction parameters, such as weight-window targets and biased source distributions [1].

The CADIS method guides the Monte Carlo simulation to concentrate on the most significant regions and energies by using these variance reduction parameters. This focus reduces statistical uncertainties and enhances simulation efficiency. In essence, the CADIS method uses an adjoint solution to ascertain the importance of different regions and energies, and then applies variance reduction parameters to steer the simulation towards these crucial areas. This results in quicker and more precise estimations of the desired tally [1]. Figure 3.4 depicts a diagram showing the differences between forward and adjoint transport.
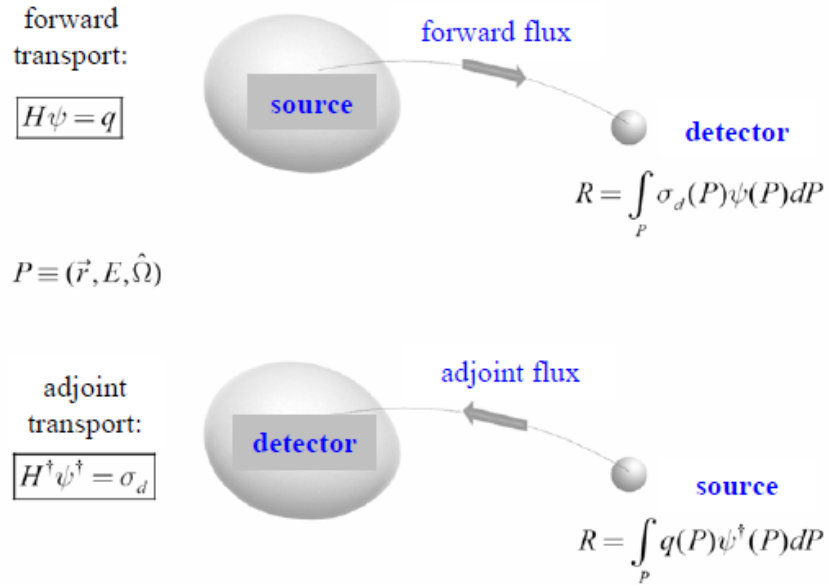

Figure 3.4: Layout illustrating the differences between forward and adjoint transport [9].

To implement the CADIS method, an importance map is generated by solving the adjoint transport equation, with the appropriate boundary conditions:

$$H^+ \psi^+ = \sigma_d \tag{3.4}$$

In this equation, H^+ is the adjoint transport operator, ψ^+ is the adjoint flux density, and σ_d is an

arbitrary response function such as a detector cross-section. This importance map, also known as the importance function, is instrumental for MCNP calculations as it aids in determining whether a particle's trajectory will lead it towards a region where it is more or less likely to contribute to a specific tally [1].

However, the CADIS method is primarily designed for problems where a single scalar quantity needs to be estimated, which means it is focused on accelerating individual tallies. When multiple quantities need to be calculated, one approach would be to calculate N different adjoint solutions, generate N different sets of variance reduction parameters, and execute N different Monte Carlo simulations for the N different tallies. While this solution may work for small N, it becomes impractical as the number increases. There are other potential approaches for calculating multiple tallies with CADIS, such as the Cooper and Larsen method, but these are beyond the scope of this work.

3.6   FW-CADIS Method

The Forward-Weighted CADIS (FW-CADIS) method is a variance reduction technique that is implemented in the ADVANTG software. It was developed to generate variance reduction parameters for multiple tallies with approximately uniform statistical precision [1]. This method is designed to span the range from a few localized tallies to space- and energy-dependent mesh tallies that encompass the entire domain.

The FW-CADIS method involves constructing an adjoint source that consists of appropriately weighted contributions from all tallies of interest. The weights are the inverses of the individual responses, and the total response is a sum of equal-weight terms [1]. This adjoint source includes all tallies of interest and is used to generate variance reduction parameters, such as weight-window targets and biased source distributions. By using these variance reduction parameters, the FW-CADIS method guides the Monte Carlo simulation to focus on the most important regions and energies for all tallies of interest. This focus reduces statistical uncertainties and enhances simulation efficiency, thereby improving the accuracy of the simulation [1].

The FW-CADIS method can be applied to both localized detectors and spectra, as well as global distributions. It aims to optimize Monte Carlo calculations for various types of responses, including flux, dose rate distributions (e.g., mesh tallies), and responses at multiple localized detectors and spectra [10]. This method provides a novel use of the adjoint methodology for biasing Monte Carlo simulations, allowing for more accurate and efficient calculations of responses in both global and localized scenarios [10].

The FW-CADIS method involves several steps:

1. Estimate the forward flux

$$\phi(\vec{r}, E) \tag{3.5}$$

2. Define the adjoint source

$$q^+(\vec{r}, E) = \frac{\sigma_d(\vec{r}, E)}{\iint \sigma_d(\vec{r}, E)\phi(\vec{r}, E) \ d\vec{r}dE} \tag{3.6}$$

The response function $\sigma_d(\vec{r}, E)$ can represent any type of response function, such as dose rate, cross section or spectrum as used in our case.

3. Create the adjoint flux from the adjoint source and solve for the adjoint flux

$$\phi^+(\vec{r}, E) \tag{3.7}$$

4. Estimate "detector" response

$$c = \iint q^+(\vec{r}, E)\phi^+(\vec{r}, E) \ d\vec{r}dE \tag{3.8}$$

5. Construct weight windows

$$\bar{w}(\vec{r}, E) = \frac{c}{\phi^+(\vec{r}, E)} \tag{3.9}$$

6. Construct the biased source

$$\hat{q}(\vec{r}, E) = \frac{1}{c}q(\vec{r}, E)\phi^+(\vec{r}, E) \tag{3.10}$$

In summary, the FW-CADIS method is a powerful tool for achieving effective global variance reduction in Monte Carlo simulations for a wide range of applications and objectives. By constructing an adjoint source that includes all tallies of interest and using the adjoint solution to generate variance reduction parameters, the FW-CADIS method guides the simulation towards the most important regions and energies for all tallies, thereby improving simulation efficiency and accuracy.

3.7 Multigroup libraries

Multigroup libraries in ADVANTG serve as reservoirs of multigroup cross-section data, embodying essential information on neutron and gamma-ray interactions with various materials across diverse energy levels. This data is instrumental in facilitating the discrete ordinates computations performed by Denovo, a component of ADVANTG.

Discrete ordinates methodology is a numerical strategy used to resolve the transport equation for neutrons and gamma rays within a system. The essence of multigroup libraries in ADVANTG lies in their provision of requisite data for these discrete ordinates computations, effectively serving as a knowledge hub for these calculations.

Within ADVANTG's toolset, several ANISN-format coupled neutron-gamma cross-section libraries are incorporated. These libraries are accessible through the "anisn_library" input option. ADVANTG's ability to read and interpret the cross-section data from these libraries, mix cross sections when required, and generate a working library for Denovo, is instrumental in enabling precise and efficient simulations. It supplies the necessary inputs for the transport calculations, thereby promoting accuracy in ADVANTG simulations [1].

As detailed in Table 3.2, several ANISN-format coupled neutron-gamma cross-section libraries are included in the ADVANTG distribution. These libraries are tailored for use with Denovo and require no auxiliary codes for their application. Furthermore, the characteristics and attributes of these libraries vary, offering different numbers of groups, isotopes of elements, and evaluations.

Table 3.2: Multigroup libraries used in Denovo calculations, [1]

Library	Anisn_library option	# of groups (N/G)	# of isotopes of elements	Evaluation
27n19g	27n19g	27/19	393	ENDF/B-VII.0
200n47g	200n47g	200/47	393	ENDF/B-VII.0
BUGLE-96	bugle96	47/20	120	ENDF/B-VI.3
BPLUS	bplus	47/20	393	ENDF/B-VII.0
DABL69	dabl69	46/23	80	ENDF/B-V
DPLUS	dplus	46/23	393	ENDF/B-VII.0
FENDL67	fendl67	46/21	71	FENDL-2.1
HILO2K	hilo2k	83/42	32	ENDF/Bertini INC model

The recent release of ADVANTG (3.2.0) added HILO2K to the multigroup library, which includes data for incident particles up to 2GeV. This expansion significantly facilitates simulations for reactors like MYRRHA with an Accelerator Driven System (ADS) configuration, where protons are accelerated up to 600 MeV. Nevertheless, a notable limitation of the HILO2K library is that it only includes 32 isotopes. This necessitates that only the isotopes featured in the library should be used in the ADVANTG simulation input. Any other isotopes need to be either omitted or substituted with one from the library.

An important caveat with using HILO2K in ADVANTG 3.2 is the discrepancy in energy group definitions. While HILO2K defines energy groups in eV, MCNP uses MeV, leading to an incompatibility that needs to be resolved for a seamless operation. Therefore, always ensure this discrepancy is addressed before proceeding with simulations. Seek assistance from the software developers if any difficulties arise in resolving this issue.

3.8 MYRRHA

The MYRRHA [11, 12] (Multi-purpose hYbrid Research Reactor for High-tech Applications) project, led by the Belgian Nuclear Research Centre, has been in development since 1998. It is intended to replace the BR2 material testing reactor and enable research in numerous fields, such as irradiation of materials for fusion reactors and transmutation of spent fuel. The MYRRHA reactor is an example of an accelerator-driven system that combines a particle accelerator, a spallation target, and a subcritical reactor. The project originated from research conducted by physicist Carlo Rubbia at CERN, focusing on the experimental determination of the energy generated in nuclear cascades by high-energy beams [13]. This work led to the idea of using the concept of spallation targets to create neutron sources for subcritical reactors.

As a multi-purpose project, there are many objectives to be achieved, some of the most prominent of which are, [11]:

- To demonstrate the feasibility of the accelerator, spallation target, and subcritical reactor assembly for industrial-scale ADS operation.

- To enable the study of the transmutation of high-level waste, in particular the minority actinides that cause the long lifetimes of radioactive waste.

- Demonstrate the ability to operate in a wide range of high energies to carry out experiments focused on materials for Generation IV and fusion reactors.
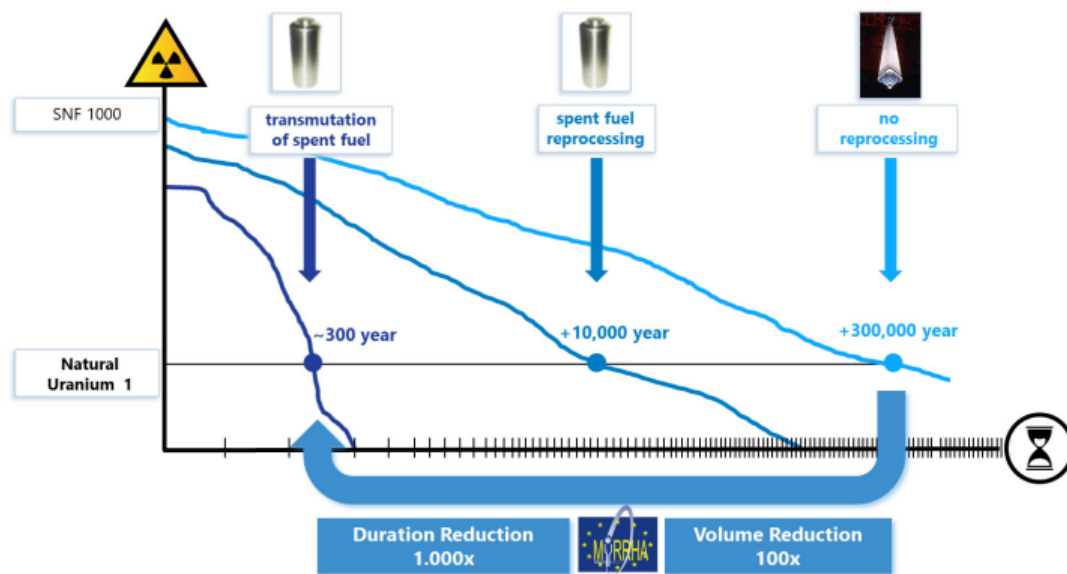
Figure 3.5: Scheme of the waste problem with radiotoxicity over the years [12].

- Production of medical radioisotopes.

Accelerator-Driven Systems (ADS) involve a particle accelerator coupled to a nuclear reactor operating under sub-critical conditions. A reactor is in sub-critical conditions when $k_{eff} < 1$, meaning that fewer neutrons are generated in the current generation than in the previous one. It is impossible, therefore, to achieve a chain reaction under these conditions. To compensate for the lack of neutrons and to keep the reactor running, an external neutron source is used, typically from a nuclear spallation target.

One of the main problems facing the nuclear industry is the management of radioactive waste, especially those with a longer half-life. In this respect, ADS can play a key role in developing the nuclear industry over the coming decades thanks to their potential for transmutation. Transmutation is a process in which long-lived radioactive isotopes are converted into shorter-lived or stable isotopes through neutron-induced reactions. There are two major concerns, [14]:

1. The intensity and longevity of the radioactivity of some radioactive waste complicate management in geological disposal.

2. Disposal without spent fuel reprocessing means larger storage space and a loss of the energy still stored inside the spent fuel.

By reducing the intensity and longevity of the radioactivity of some radioactive waste (see Figure 3.5), transmutation can help address the challenges of geological disposal and spent fuel reprocessing, leading to more sustainable and efficient nuclear waste management.

The initial idea of the SCK CEN was to use the designs of the FP6 EUROTRANS project as a basis for the MYRRHA/XT-ADS (eXperimental facility demonstrating the technical feasibility of Transmutation in an Accelerator-Driven System) so that the work already done could be reused. The MYRRHA/XT-ADS is a pool-type lead-bismuth eutectic-cooled (LBE) reactor design. The main features of this design can be found in Table 3.3.

The current design being worked on in the Belgian research center is the MYRRHA-FASTEF,

Table 3.3: MYRRHA/XT-ADS main parameters [11].

Nominal reactor power	57 MW
Primary circuit cooling power	70 MW
Core inlet temperature	300 ºC
Core outlet temperature	400 ºC
Coolante velocity in core	2 m/s
Primary coolant	LBE
Secondary coolant	Saturated water/steam
Teriary coolant	Air

Table 3.4: MYRRHA-FASTEF main parameters [11].

FA length	2000 mm
Nominal power	100 MW
Core inlet temperature	270 ºC
Core outlet temperature	410 ºC
Coolante velocity in core	2 m/s
Coolant pressure drop	2.5 bar
Primary coolant	LBE
Secondary coolant	Saturated water/steam
Teriary coolant	Air

which is approximately the same as the MYRRHA/XT-ADS but with an increase in size. Its main features can be found in Table 3.4.

The design works by means of a mixture of oxides (MOX) commonly used in fast reactors. The design of the spallation target has changed between the two models. The FASTEF has a window unlike the XT-ADS, which allows for simplification of the design and greater flexibility in the In-Pile test Sections (IPS).

The reactor can operate in either ADS or critical mode. In ADS mode the central position of the core is occupied by the spallation target assembly and is easily removable and replaceable. When the operating mode is critical, the target assembly is removed from the core and control rods are inserted. There are 3 objectives for the spallation target assembly, [11]:

1. It guides the proton beam into the core where conditions are optimal for spallation.

2. To support the irradiation from the protons and neutrons and to allow the evacuation of heat through the coolant, produced by the energy deposition that occurs due to the spallation.

3. To act as a protective barrier between the coolant and the reactor hall.

Concerning the challenges ahead, two main areas require further research: the development of enhanced instrumentation for more accurate measurement of parameters such as pressure, temperature, or neutron flux, and the improvement of deep shielding calculations. These advancements are crucial for the MYRRHA project, as they enable the assessment of various shielding configurations' efficacy, ensuring the safety of both individuals and equipment involved [11]. Given the MYRRHA reactor's complexity and its multiple applications, including waste transmutation, refining deep shielding calculations can assist in optimizing the reactor's design and
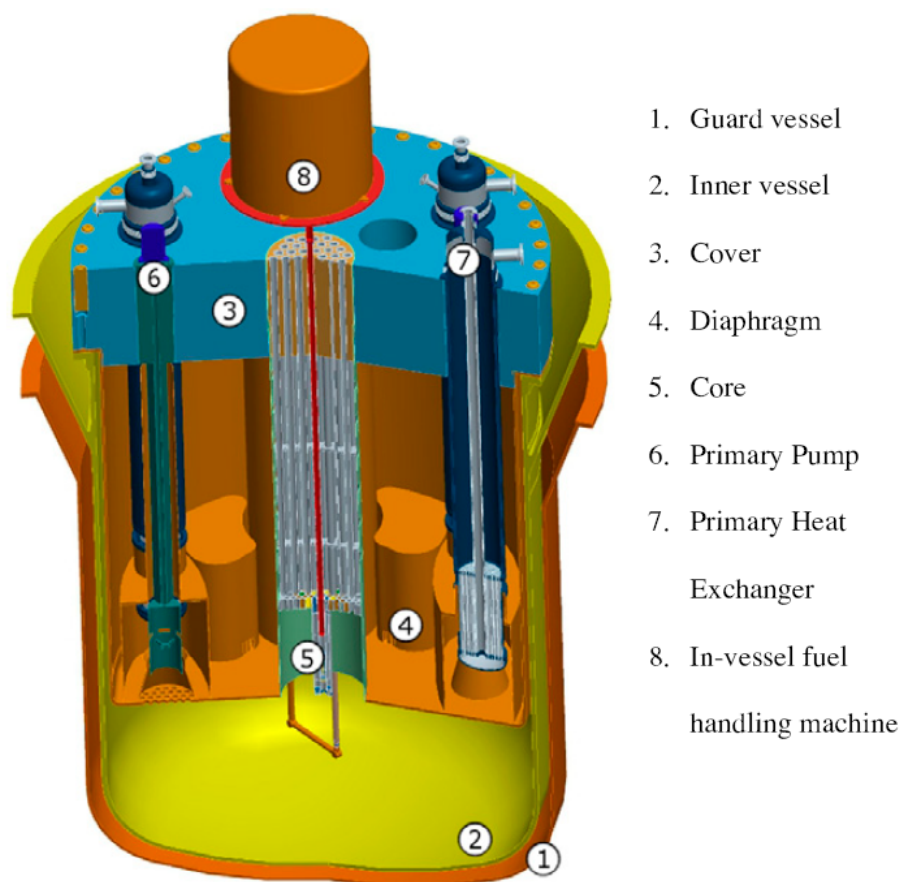
1. Guard vessel

2. Inner vessel

3. Cover

4. Diaphragm

5. Core

6. Primary Pump

7. Primary Heat

   Exchanger

8. In-vessel fuel

   handling machine

Figure 3.6: MYRRHA-FASTEF main components [11].

operational aspects. The use of variance reduction techniques is particularly important, as these methods can significantly improve the accuracy and efficiency of calculations, ultimately contributing to the project's safe and successful completion. The ADVANTG software, specifically designed for implementing variance reduction techniques, will play a key role in achieving the thesis objectives by enhancing the accuracy and reliability of deep shielding calculations for the MYRRHA reactor.

4 METHODOLOGY

Our main aim with this methodology is to establish a solid process to apply variance reduction techniques to complex nuclear systems, with a focus on the MYRRHA reactor. Recognizing the complexity of MYRRHA, we will first apply our approach to simpler, but still relevant, cases to ensure it works effectively. This means that, the starting point is to explore similar experiments that can offer a benchmark for our work. For this purpose, we have selected the TIARA and KENS shielding experiments. By replicating these experiments, we can test the effectiveness of our proposed methodology.

In this part of the thesis, an overview of the TIARA and KENS experiments will be presented, detailing their setup and geometrical design. This will help us gain a firm understanding of these reference cases. Following this, the focus will shift to the application of our methodology to MYRRHA. To facilitate this, we will describe the key aspects of MYRRHA that are important for our MCNP simulations and their inputs. By doing this, we can make sure that our methodology is fully adapted to MYRRHA, taking into account its specific characteristics and the challenges it presents.

In order to properly understand the methodology and the ensuing results, it is essential to clarify the differences between the sources used and the notation employed to identify them. The 'proton source' refers to the actual proton source of the problem, wherein a proton source is utilized with a neutron production target to generate neutrons. The 'non-equivalent neutron source' denotes the same input and source definition, with the sole alteration being the type of particle from proton ('h' or '9' in MCNP) to neutron ('n' or '1' in MCNP). This approach was recommended by developers as a proven and easy solution for obtaining weight windows without having to create a proper equivalent neutron source. That said, the term 'equivalent neutron source' is used to identify the source created to mirror the behavior of neutron particles in the area of interest as precisely as possible. For this approach, the input, and especially the source definition, may change to achieve the same spectrum in the area of interest

Upon implementing our methodology, we will present and analyze the results in Section 5. This includes the application of the methodology to the TIARA and KENS experiments and, to the extent possible, its application to MYRRHA. The analysis will allow us to gauge the performance of our variance reduction techniques and identify areas for potential improvement. Ultimately, the intention is to refine our methodology to be effective in handling the complexities of the MYRRHA reactor.

4.1 TIARA Experiment

The TIARA [15, 16] (Takasaki Ion Accelerator for Advanced Radiation Application) experiment is one of the high-quality experiments that is part of SINBAD [17] (Shielding Integral Benchmark Archive and Database) database. All the benchmark experiments inside this project have been proved to be of a high order of quality in order to be suitable for the validations and evaluation processes of nuclear data libraries. In particular, TIARA experiment is of great interest due to the high-energy neutron spectra and deep penetration (see Figure 4.1), which is closely related to the subject of this master's thesis. It includes experimental results with three shielding materials, iron, concrete, and polyethylene. As a neutron source, a 99.9% ^{7}Li target is bombarded with a high-energy proton beam from a cyclotron, with proton incident energies of 43 MeV and 68 MeV, producing two quasi-monoenergetic neutron sources of 40 MeV and 65 MeV, respectively [16]. In this context, it is interesting to evaluate the usage of ADVANTG code in a more straight

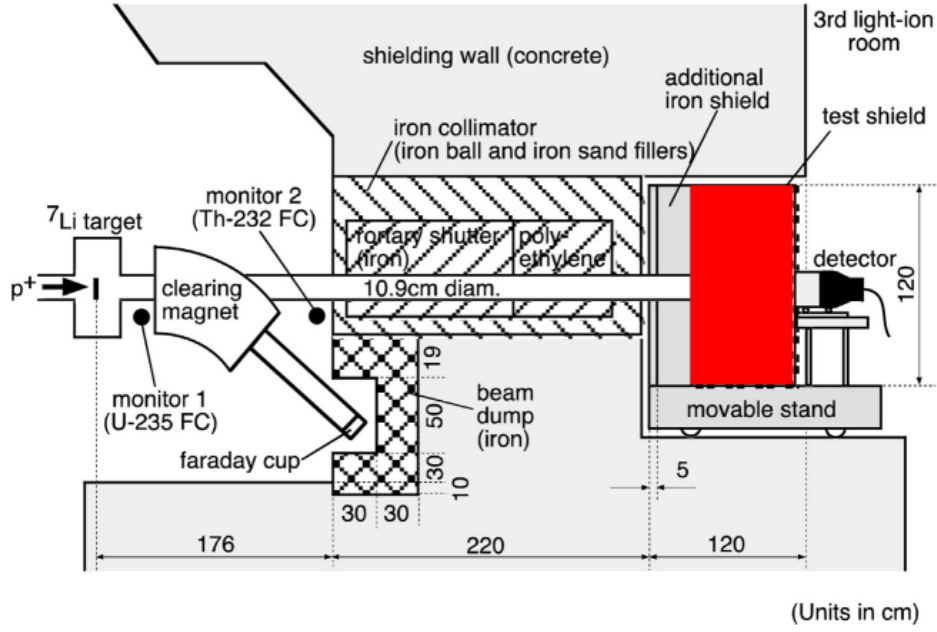forward problem as it is TIARA, compared to MYRRHA reactor.

Figure 4.1: Experimental configuration of TIARA shielding experiment [16].

In the technical report titled "MCNP modelling of TIARA SINBAD shielding benchmark" by Bor Kos and Ivan A. Kodeli [15], ADVANTG was employed to enhance calculations through thick layers of shielding. Since the original source was a proton source, an equivalent neutron source had to be created to run ADVANTG and obtain the weight windows. The MCNP geometry model was developed from scratch using CAD (see Figures 4.2a and 4.2b), the neutron source inputs and weight windows can be downloaded from the IAEA nuclear database [18].
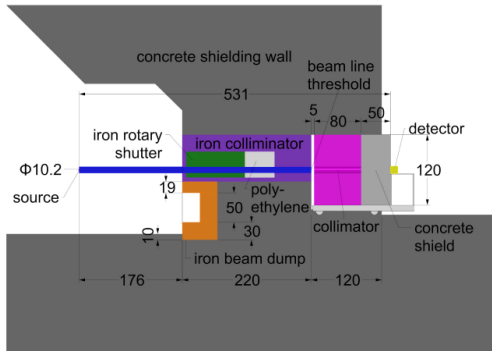
(a) Side view. y=0, 50 cm concrete shield, 80 cm collimator.
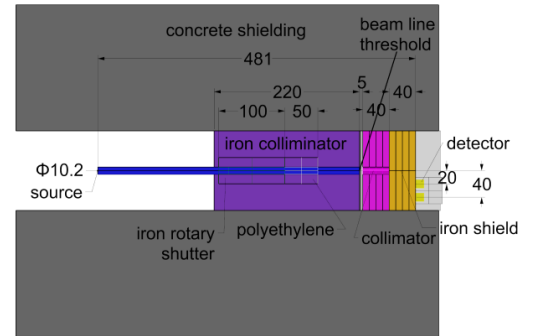
(b) Top view. y=0, 40 cm iron shield, 40 cm collimator.

Figure 4.2: CAD model of TIARA geometry [15]. (a) Side view; (b) Top view.

The equivalent neutron source was modeled as a point source at the system's origin, precisely at the same location as the ^{7}Li target in the experiment, situated 396 cm away from the beginning of the shielding. To avoid interactions along the beam line, it was modeled as a vacuum. The source was confined to a conical shape, with its base directly corresponding to the beam line's opening at $x = 396$ cm and a diameter of $\Phi = 10.2$ cm. This source definition already serves as

an effective variance reduction technique, as it reduces the time needed for the code to simulate neutrons traveling from the point source to locations away from the detector [15].

Regarding the detectors, three different detectors were modeled in the original input:

1. BC 501A liquid scintillator.

2. Bonner sphere counters of various sizes.

3. Two different fission counters (^{238}U and ^{232}Th fission cells).

For the purpose of this thesis, only the BC 501 liquid scintillator located on the same axis as the beam will be used as an F4 volume tally. The model consists of a cylinder with a height and diameter of 12.7 cm, filled with the material defined in the detector manufacturers' technical documentation.

For a more comprehensive understanding of the input specifications, such as geometry, materials, source, and tally definitions, readers are encouraged to refer to [15].

4.2 KENS Shielding Experiment

In the KENS experiment at KEK Spallation Neutron Source Facility [19, 20], a 500 MeV - 5μA synchrotron proton source is directed onto a tungsten target, creating a neutron source through spallation. Positioned 2.5 meters from the spallation target's center is a 4-meter-thick ordinary concrete shield. Eight detectors, placed at distinct locations (see Figure 4.3), measure the neutron flux and energy distribution. Six of these detectors (slots 2-7) are encased within acrylic capsules at the base of insertion plugs comprised of the same material as the shield. The other two detectors are located in a rectangular slot (slot 1) on the shield's front surface, and at the shielding's terminus (slot 8) (see Figure 4.4).

(a) Side view.

(b) Top view.

Figure 4.3: KENS Shielding experiment set up [21]. (a) Side view; (b) Top view.

Figure 4.4: Shielding geometry for KENS shielding experiment [21].

In terms of the neutron source definition in MCNP, we define a point isotropic neutron source that is collimated into a cone shape along the positive z-axis. This means that the neutrons are emitted from a single point and are directed into a cone shape. The half-angle of the cone is specified according to the geometry of the experiment, confining the emitted neutrons to a specific direction. This setup is often used to simulate specific experimental conditions where the neutron source is directional.
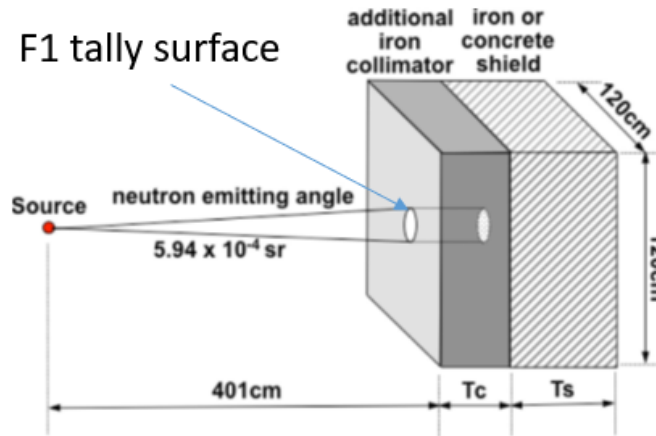
Figure 4.5: Schematic representation of creating an equivalent neutron source from a proton source[1].

The neutron yield, which represents the number of neutrons produced per proton [n/p], is an

---

[1]Note that the depicted geometry does not match the KENS shielding setup; it is a generalized example to facilitate understanding of the procedure.

essential parameter in our study. This yield is not constant but varies depending on the energy of the protons. These values can be calculated using the F1 tally function in MCNP. The neutron flux, a measure of the intensity of neutron radiation, is then calculated behind a shielding. The results from the MCNP code are normalized per source particle. This normalization can be in 4π steradians, encompassing all directions, or it can be per source particle. The choice of normalization depends on whether the study is interested in the total neutron flux (in which case 4π steradians is used) or the flux per source particle. To convert the results to a more standard form, they are multiplied by the total [n/p.sr] or [n/p] value and 4π, depending on the normalization used.

This study emphasizes a detailed reproduction of the neutron energy spectrum, particularly in the high-energy region (E >1 MeV). At these higher energies, certain types of nuclear reactions, which significantly influence the isotopic composition post-irradiation, can occur. Specifically, reactions such as (n, p), (n, α), and $(n, 2n)$ become possible, as they have threshold energies typically exceeding 1 MeV. Therefore, ensuring an accurate representation of the neutron spectrum in this energy range is crucial for evaluating the changes in isotopic composition following these neutron-induced reactions.

Irradiation calculations will be performed for a continuous period of one year at slot-8, both with and without the application of variance reduction techniques. This will facilitate an analysis of the resulting neutron spectra, allowing for a comparison that demonstrates the impact of variance reduction techniques on the spectral uncertainties. By conducting this comparative analysis, we hope to better understand the potential benefits and limitations of variance reduction techniques within the scope of this complex nuclear shielding experiment.

4.3 MYRRHA

MYRRHA (Multi-purpose Hybrid Research Reactor for High-tech Applications), is an intricate system, for which the Belgian Nuclear Research Centre (SCK CEN) has developed a comprehensive model in MCNP. Spanning tens of thousands of lines, the MCNP input file accurately represents all components expected to exist within the reactor, some of them illustrated in Figure 3.6 of Section 3.8. This model is equipped to simulate both critical and subcritical (Accelerator Driven System - ADS) modes of operation, necessitating certain portions of the input to be alternately commented or uncommented to accurately select the mode of interest.

For the scope of this project, the base model will largely be retained, with modifications limited to implementing specific tallies required to generate results pertinent to the simulations performed. Figure 4.6 provides a radial view of the heterogeneous core of MYRRHA, as modeled in the MCNP input. The overarching goal of our project is to apply variance reduction techniques to both working modes. Figure 4.7 compares the neutron spectra when simulated in both the subcritical and critical mode.
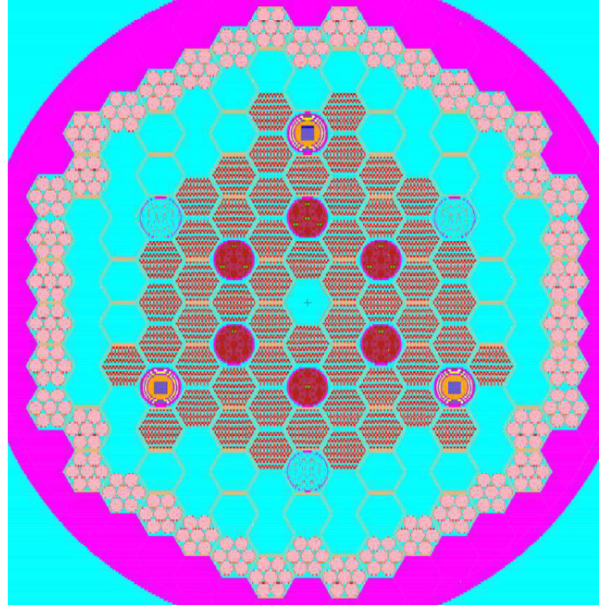
Figure 4.6: Radial view of the MYRRHA heterogeneous core as modelled with MCNP [22].
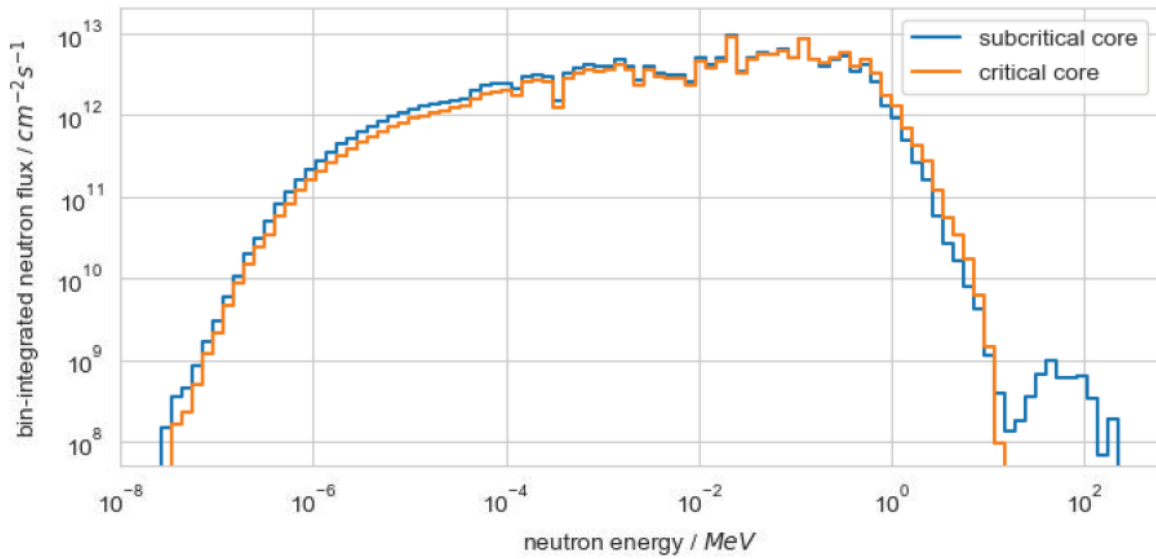
Figure 4.7: Neutron fluxes in the core barrel for the critical and subcritical mode [22].

Given MYRRHA's complexity, and the fact that it is a larger system which undergoes fission, it remains unclear whether the methodology used in the TIARA and KENS experiments is directly transferable. Furthermore, the unique feature of MYRRHA being capable of operating both as a proton-driven system, akin to the aforementioned experiments, and in a critical mode without a proton source, adds to the uncertainty. Another important aspect that will be scrutinized is the potential applicability of the methodology used for irradiation calculations in the KENS experiment. Further considerations will need to be addressed such as threshold reactions and the resonance region of reactions pertaining to the neutron spectra, as these could induce reactions affecting the isotopic composition.

Addressing these uncertainties will entail a rigorous and systematic evaluation of the impact of

variance reduction techniques on the precision of the neutron spectra in both modes. Ultimately, this study aims to enrich our understanding of MYRRHA's unique characteristics, and, in turn, to leverage this knowledge to optimize the use of variance reduction techniques in simulating complex nuclear systems.

5 RESULTS

The aim of this chapter is to establish the validity and reliability of our research methodology, which revolves around the application of the ADVANTG code and the generation of equivalent and non-equivalent neutron sources. These sources are used to simulate radiation transport in a proton-driven system and are crucial for achieving accurate results. To ensure the effectiveness of our methodology, it is essential to assess the impact of these generated neutron sources on the efficiency of the calculations in terms of both calculation time and statistical accuracy. By determining their influence, we can optimize the overall performance of the final MCNP code simulations, particularly in the context of MYRRHA applications with the proton accelerator.

To validate and verify the methodology investigated in this study, we rely on two critical benchmarks as part of our validation process. These benchmarks are the TIARA and KENS shielding experiments, which were introduced in Chapter 4. These experiments provide valuable reference data that enables us to evaluate the precision and robustness of our methodology. By comparing our simulation results with the experimental data from these benchmarks, we can establish the reliability of our methodology and demonstrate its suitability for proton-driven systems.

In particular, the KENS experiment allows us to further delve into the spectrum-driven uncertainties impacting isotopic composition of an activated material after a certain time of irradiation. This analysis forms a critical part of the validation process. The specific steps involved in the validation and verification process within our research are as follows:

1. Validating the created equivalent neutron sources to ensure ensure that it accurately represent the neutron field created by the proton interactions with the target material, which has a thickness in the range of the proton.

2. Verifying the proper implementation of the ADVANTG code and assessing its compatibility with the generated neutron sources.

3. Testing the ADVANTG weight windows generated with generated neutron source against the original proton source and the experimental data to confirm the effectiveness of the conversion.

4. Studying the effect of spectrum-driven uncertainties on the isotope composition of a specific material after irradiation using ALEPH 2.0.

5. Evaluating the efficiency, accuracy, and precision of the methodology in various scenarios and shielding designs.

In Sections 5.1 and 5.2, a detailed overview of the simulation design will be first provided to define all key simulation parameters as comprehensively as possible. Following this, we will present the results from the simulations, briefly discussing their primary attributes. Subsequently, an analysis of the performance metrics will be undertaken to evaluate the precision and efficiency of the simulation. To conclude these sections, a discussion of the results will be presented, wherein the primary conclusions will be emphasized, and any necessary additional explanations concerning the results will be provided. Additionally, for the KENS experiment, irradiation calculations will be included alongside a corresponding analysis of the results. This analysis will not only provide insightful information about the impact of spectrum-driven uncertainties on isotopic composition but also equip us with the specific knowledge and tools that will be instrumental in addressing the complexities of the MYRRHA reactor in our final section, thus enhancing our prospects of success.

Section 5.3 of this chapter is dedicated to the MYRRHA reactor in which it is presented the application of the refined methodology from preceding experiments. Within this section, we will detail the various steps and strategies implemented and offer a thorough examination of the results obtained. The section culminates with a discussion that will help identify the key elements that warrant additional research in the future for the advancement and improvement of our results.

5.1 TIARA Experiment

5.1.1 Overview and Simulation Design

In reference [15], a neutron source equivalent, generated from the proton-7Li target interactions, was utilized both for the generation of variance reduction parameters via ADVANTG, and within the final MCNP calculations. However, the use of the proton source in tandem with the neutron source-weight windows proved to be less effective than anticipated. This prompted the application of variance reduction techniques, specifically, the weight window generator (WWG) present within the MCNP6.2 code. Despite this, the proton source was not utilized in conjunction with variance reduction parameters from the ADVANTG code. As such, this experiment was chosen for validation purposes.

As presented in reference [23], the shortcoming of these efforts could be traced back to the limited proton data available in the nuclear data libraries. This lack particularly impacted the peak generated in the high energy region, causing MCNP to rely heavily on physics models for ^{7}Li, consequently leading to unsatisfactory results. An in-depth analysis of the full experimental data set revealed that the use of JENDL-4.0/HE [24] offered the most favorable agreement with the ^{7}Li target experiment, especially enhancing the accuracy of the peak in the high energy region. This revelation was crucial in steering future investigations in this field.

This finding has significant implications for our study, as it suggests that weight windows generated with ADVANTG from an equivalent neutron source can be used with the original proton source, provided the correct proton-induced nuclear data is available, resulting in high-quality performance calculation.

To test the ADVANTG code calculations two shielding cases were studied:

- 68 MeV proton source with 40 cm Fe shielding and no extra collimator.

- 68 MeV proton source with 100 cm concrete shielding and no extra collimator.

A series of simulations were conducted for each shielding case using varying types of sources and weight windows. The calculations were performed using different source distributions with and without weight windows generated with the ADVANTG code. Three different source distributions, which are equivalent neutron source, non-equivalent neutron source and original proton source, were investigated here. It is worth to mentioned that the final aim is not use neutron sources in the MCNP6.2 calculations but rather in the ADVANTG code to produce the weight windows. Nevertheless, their accuracy was still tested using them as a source in the MCNP6.2 simulations.

Initially, the input was run using the equivalent neutron source provided in the documentation to ensure that the simulation functioned correctly and the results could be replicated, as described

in the technical report [15]. More details about how the equivalent neutron source was generated for TIARA is find in the following subsection (5.1.2). The non-equivalent neutron source was created simply by replacing the original proton source coming from the accelerator with the neutrons on the SDEF card and by removing the target material from the geometry. In case of proton source, the original proton source distribution in terms of spatial an energy coming from the accelerator was kept the same, as well as the lithium target to take account for the proton interactions with the target that produce the secondary neutrons that are transferred through the shielding.

The nuclear data libraries used for the neutron and proton induced reactions are JEFF-3.3 and JENDL-4./HE, respectively. Simulations were run for 2E+09 particles, with an additional run of 1E+11 particles conducted for the proton source due to the poor results obtained in the first simulation. All MCNP simulations were executed using 72 CPUs.

Upon obtaining the weight windows with ADVANTG, the final MCNP runs were executed using them as an external input file (wwinp). The objective of this experiment was to demonstrate that weight windows obtained with an equivalent and non-equivalent neutron source could be used with proton sources, thereby improving the statistical quality of the simulations.

5.1.2 Equivalent Neutron Source

The equivalent neutron source for TIARA is derived from the technical report [15]. A brief explanation of how this source definition is applied within our methodology can be found in section 4.1 of this document.

5.1.3 ADVANTG Simulation Results

A total of four ADVANTG simulations were executed, two utilizing non-equivalent and equivalent neutron sources respectively, for each of the shielding scenarios analyzed. These simulations consistently employed the same input data and parameters as depicted in reference [15]. An elaboration of these parameters has been provided in previous chapters.

The parameters used in the ADVANTG input for all simulations, excluding the varying mesh parameters for each shielding scenario, are:

Parameter	Value
method	fwcadis
fwcadis_spatial_treatment	pathlength
fwcadis_response_weighting	False
library	HILO2K
denovo_x_blocks	2
denovo_y_blocks	2
denovo_z_blocks	2

Table 5.1: Key parameters used in the ADVANTG input for TIARA experiment.

The individual mesh parameters used in the simulations, which differ per shielding scenario, are presented in Annex A.

The simulations were conducted on a computational system furnished with 70 CPUs, with their respective run times compiled in Table 5.2.

Table 5.2: ADVATNG simulations run time comparison for TIARA experiment.

Shielding	Source	Run time [mm:ss]
100 cm Concrete	Eq. Neutron	24:43
100 cm Concrete	Non-Eq. Neutron	22:53
40 cm Iron	Eq. Neutron	40:19
40 cm Iron	Non-Eq. Neutron	38:16

In addition to the variance reduction parameters generated by ADVANTG, several insightful output files can be accessed. Specifically, the deterministic calculations offer a perspective on the adjoint neutron flux distribution across the geometry. Figures 5.1 and 5.2 display heat maps of the integral adjoint flux for both shielding cases, visualized utilizing the VisIt software tool [25]. These heat maps represent neutrons per square centimeter from a top-down perspective (for the geometrical representation, refer to Figure 4.2b). Regions represented by red hues signify higher levels of neutron flux, whereas those displayed in blue indicate lower flux values. The peak flux observed for 40 cm iron shielding and 100 cm concrete shielding are 2.47E+09 and 2.96E+09 n/cm2, respectively.
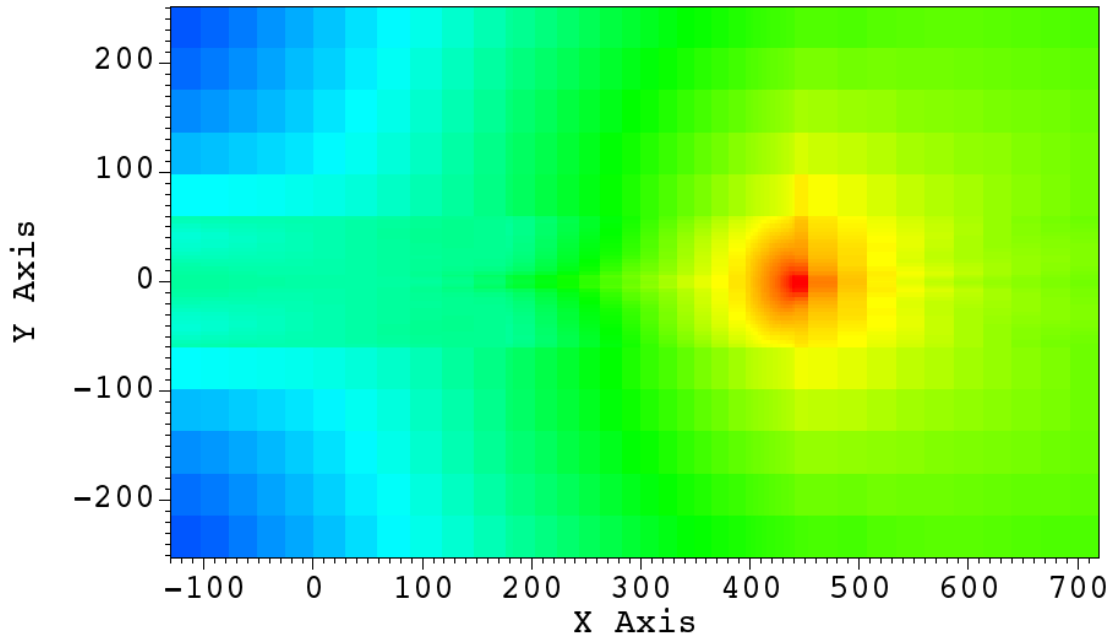
Figure 5.1: Heat map of the integral adjoint flux on XY plane for TIARA 40 cm iron shielding.
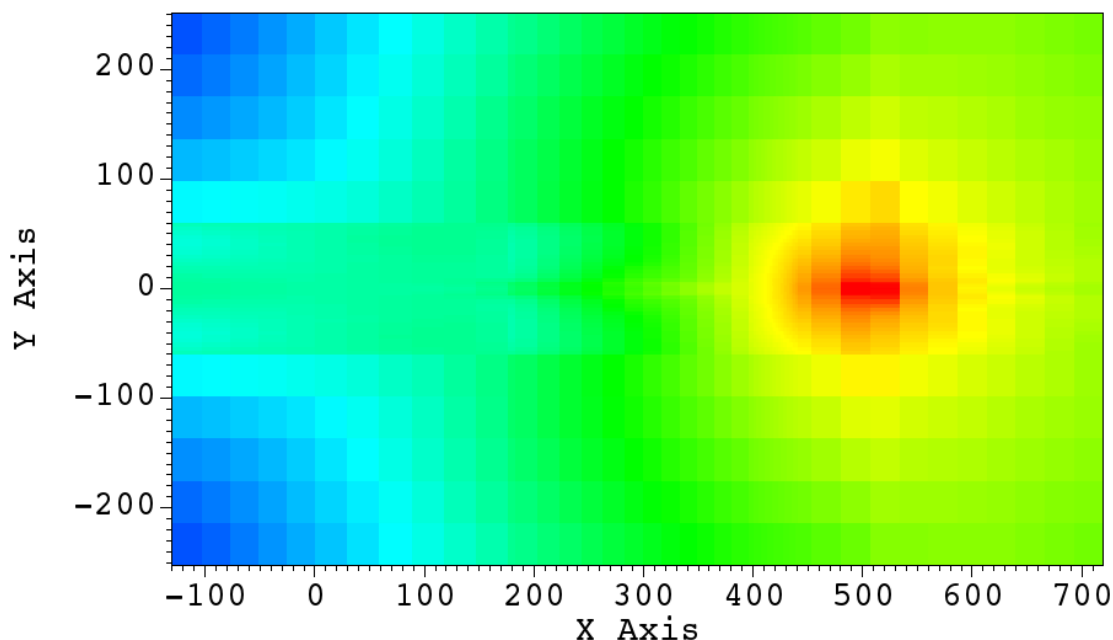
Figure 5.2: Heat map of the integral adjoint flux on XY plane for TIARA 100 cm concrete shielding.

5.1.4 MCNP Simulation Results

Table 5.3 provides a summary of the performance for the TIARA experiment simulations. The first column shows the shielding design, the second column shows the source type used in the MCNP calculations, the third column shows if the weight windows are used or not during the MCNP6.2 calculations. if they are not used, it is defined as 'none', which is equivalent to the analog calculations. if the weight windows are used in the MCNP6.2 calculations, then the type of source used in ADVANTG is described. Forth and fifth column give the calculation time and number of source histories, respectively, simulated in the MCNP6.2 calculations.

Table 5.3: MCNP simulation performance comparison for TIARA experiment with and without ADVANTG weight windows.

Shielding	Source	Weight Windows	Run time [hh:mm]	NPS
40 cm Iron	Eq. Neutron	None (analog)	00:20	2.00E+09
40 cm Iron	Non-Eq. Neutron	None (analog)	10:40	2.00E+09
40 cm Iron	Proton	None (analog)	00:10	2.00E+09
40 cm Iron	Proton	None (analog)	08:30	1.00E+11
40 cm Iron	Proton	Eq. Neutron	06:03	2.00E+09
40 cm Iron	Proton	Non-Eq.Neutron	Unfinished	-
100 cm Concrete	Eq. Neutron	None (analog)	00:23	2.00E+09
100 cm Concrete	Non-Eq. Neutron	None (analog)	01:29	2.00E+09
100 cm Concrete	Proton	None (analog)	00:10	2.00E+09
100 cm Concrete	Proton	None (analog)	07:30	1.00E+11
100 cm Concrete	Proton	Eq. Neutron	03:29	2.00E+09
100 cm Concrete	Proton	Non-Eq. Neutron	Unfinished	-

The analog calculation results obtained with equivalent, non-equivalent and proton sources are shown in Figures 5.5, 5.4 and 5.5 for the 40 cm iron shielding design performed with 2e9 nps, respectively. As it is seen that calculation statistics for the neutron sources are very good and in practice there is no need to apply any variance reduction technique. However, TIARA experiments were performed with thicker shielding materials, for which it is required to apply variance reduction methods. When it comes to the proton source, the results are very poor even when the NPS value is increased to the 1e11 as shown with the red plot of Figure 5.6. It is also seen that quasi-peak around the primary proton beam energy region (i.e, 68 MeV) is wrongly located with both neutron sources and as well as proton source. One can expect the same spectrum profile with the equivalent neutron source and the proton source, however as it is explained before that secondary neutron field is calculated with the proton interactions with the target material and so the results reflects the impact of the proton induced nuclear data library (i.e., JENDL-4.0/HE) used with the proton source. Though equivalent neutron source was obtained by using the measured neutron spectrum at the detector location. Therefore, the results obtained with both proton and equivalent neutron source are slightly different. It should be also noted that non-equivalent neutron source is not advisable to be used as a source in any MCNP calculation as it does not correspond to the neutron field produced from the proton-target interactions. Consequently, it will be only used to generate the ADVANTG weight windows and to determine their efficiency when used with MCNP6.2 code. Taking into account the time spent to produce the equivalent neutron source, it is a great worth to test whether weight windows produced with non-equivalent neutron source works.

Figure 5.6 shows the comparison of the experimental spectrum and the results of proton source without (i.e., analog) and with the weight windows produced with the equivalent neutron source. Even though the NPS value used for the analog calculations are two orders of magnitude higher than the case obtained with the weight windows, the calculation statistics are still poor.

It it worth mentioning that in the case of the simulation involving the proton source using the weight windows generated with the non-equivalent neutron source through ADVANTG, the simulation encountered issues and failed to complete, as indicated also in Table 5.3 as "unfinished". For a deeper understanding of what might have led to this situation, more information will be found in the subsection 5.1.6 within this section.
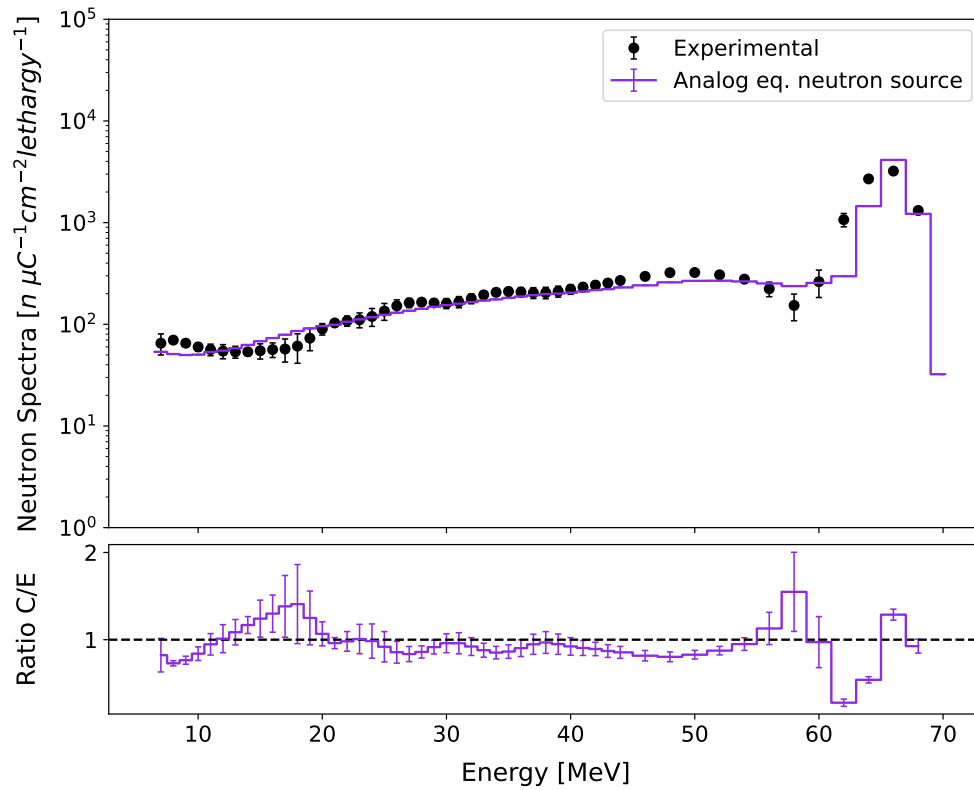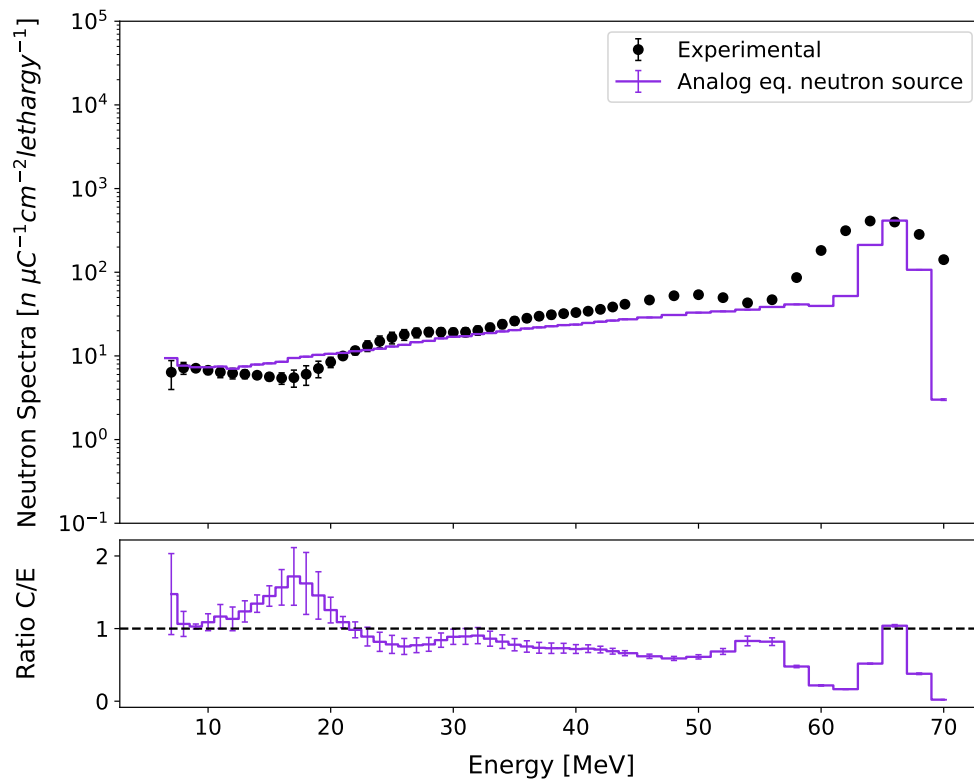
Figure 5.3: Comparison of experimental and analog MCNP simulation with equivalent neutron source for TIARA 40 cm iron shielding.
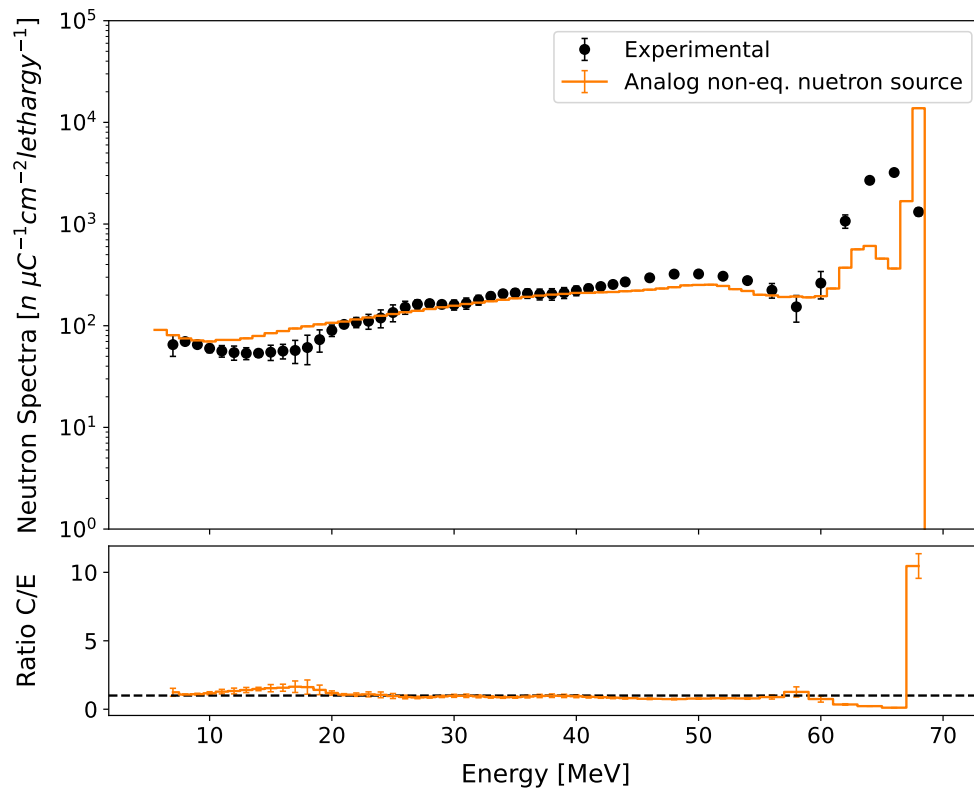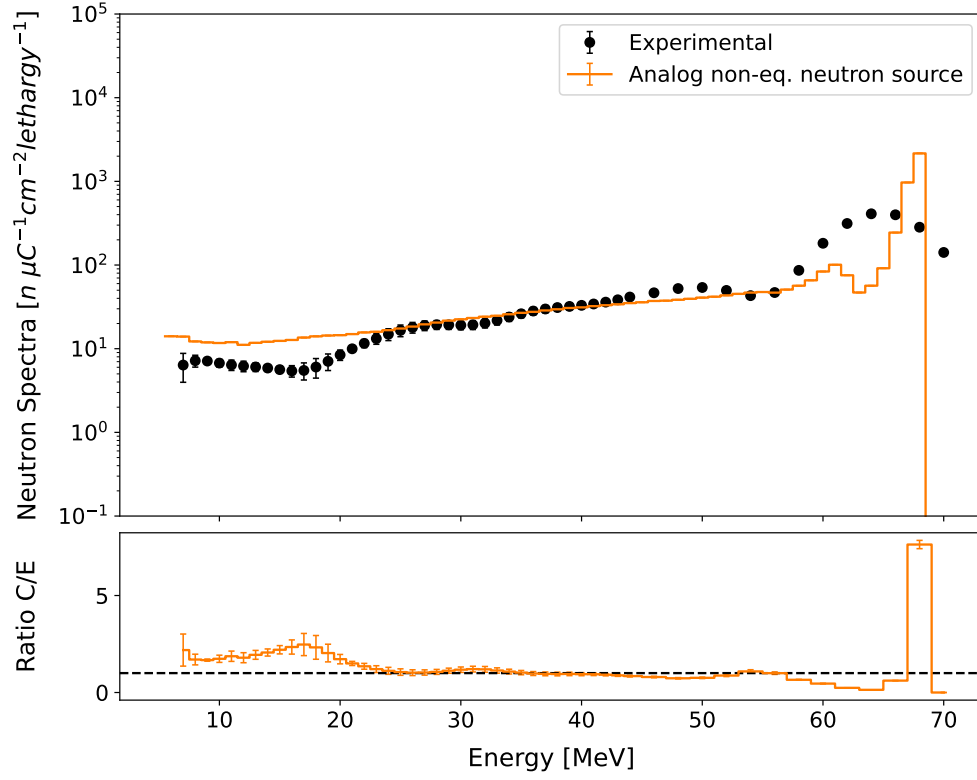

Figure 5.4: Comparison of experimental and analog MCNP simulation with non-equivalent neutron source for TIARA 40 cm iron shielding.
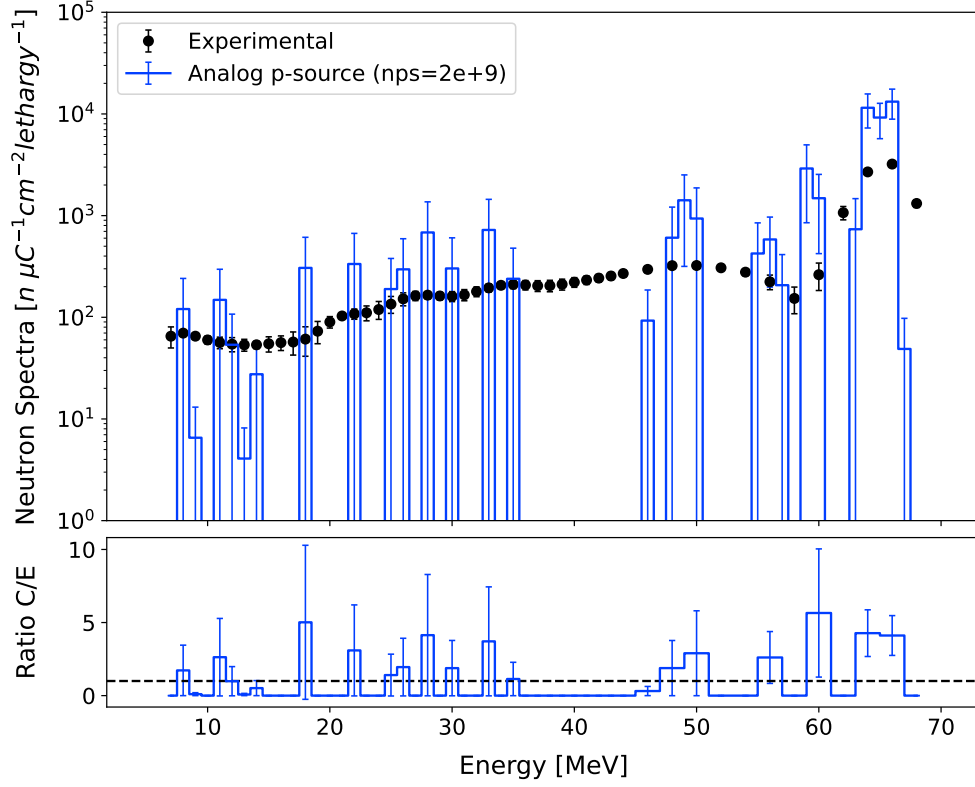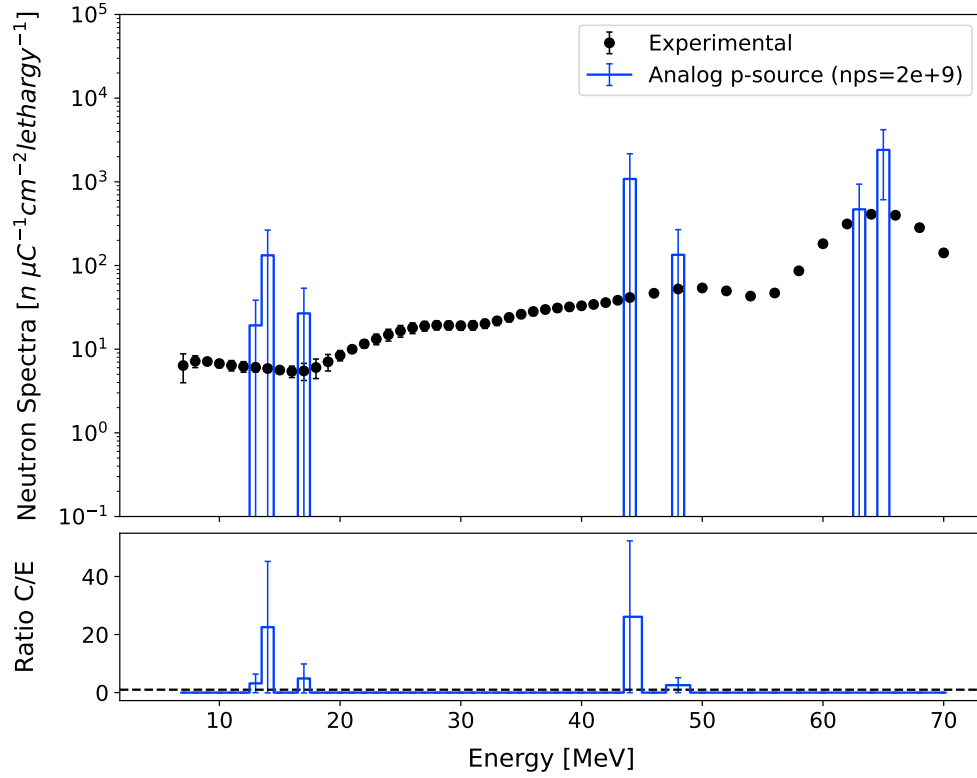
Figure 5.5: Comparison of experimental and analog MCNP simulation with proton source and NPS = 2E+09 for TIARA 40 cm iron shielding.
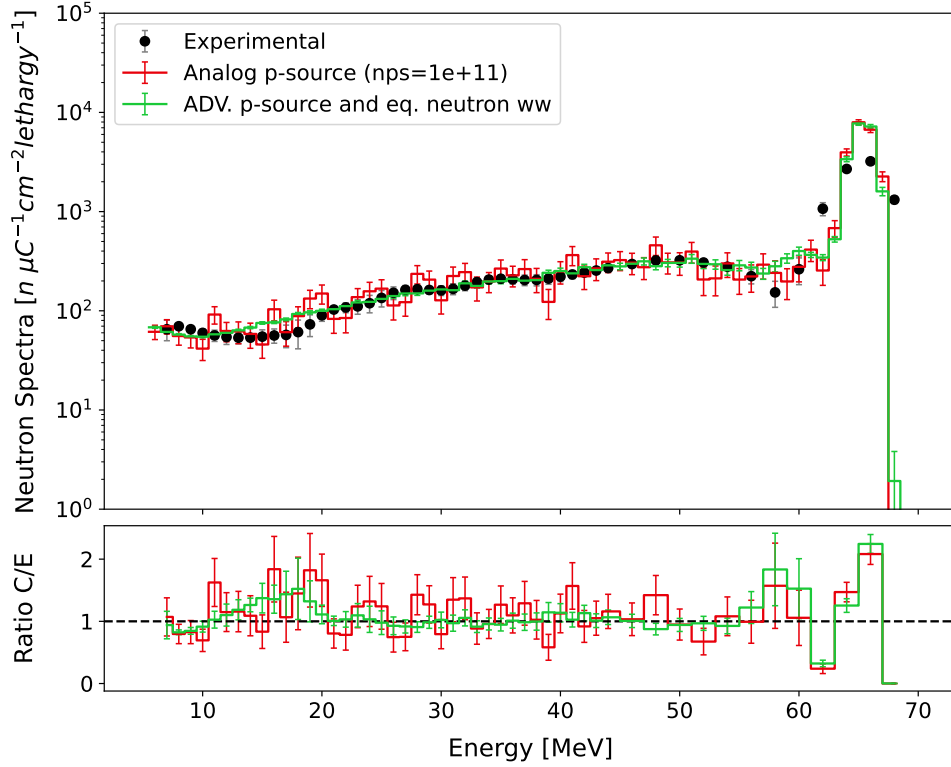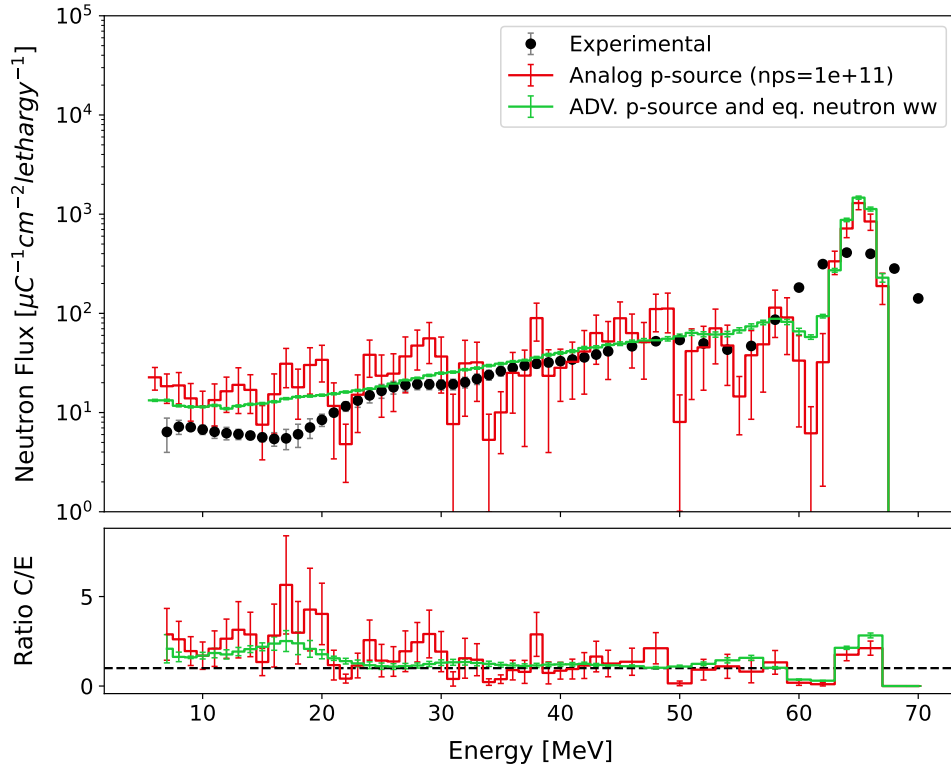

Figure 5.6: Comparison of experimental and calculational results before and after the use of ADVANTG with proton source for TIARA 40 cm iron shielding.

Figures 5.7, 5.8, and 5.9 present the results obtained using equivalent, non-equivalent neutron sources, and the original proton source for the 100 cm concrete shielding design, conducted with 2E+09 nps, respectively. These results broadly reflect the same trends and characteristics as those obtained with the 40 cm iron shielding. However, the performance of the proton source has deteriorated due to the increase on the shielding. This is noticeable even when the proton source is increased to 1E+11 nps, as displayed in Figure 5.10. It's clear from this figure that the simulation has yet to reach satisfactory convergence.

Similarly to the previous case, the simulation employing the proton source with non-equivalent neutron source produced weight windows once again failed to reach completion, as shown in Table 5.3.

Figure 5.7: Comparison of experimental and analog MCNP simulation with equivalent neutron source for TIARA 100 cm concrete shielding.

Figure 5.8: Comparison of experimental and analog MCNP simulation with non-equivalent neutron source for TIARA 100 cm concrete shielding.

Figure 5.9: Comparison of experimental and analog MCNP simulation with proton source and NPS = 2E+09 for 100 cm concrete shielding.

Figure 5.10: Comparison of experimental and calculational results before and after the use of ADVANTG with proton source for TIARA 100 cm concrete shielding.

The main conclusion that can be drawn from the results is that the use of ADVANTG weight windows significantly improves the simulation outcomes using a proton source while reducing the required simulation time for both shielding cases, as shown in Figures 5.6 and 5.10. However, it is worth noting that the high energy peak is overestimated for both cases, mainly due to the effect of the nuclear data as mentioned at the beginning of this section. This also highlights the fact that the weight windows obtained with the equivalent neutron source, worked accordingly with the proton source in the final MCNP6.2 calculation.

In addition, in the case of the 100 cm concrete shielding, the result is slightly overestimated for lower energies. In ref. [23], it was shown that results obtained with thicker shielding are slightly higher than the experimental values as well. The results are shown here with the proton source are the same with the those presented in ref. [23]. It is a reminder that the calculations in ref. [23] were done using the WWG implemented in MCNP6.2. This overestimation could be due to a dip in the experimental data caused by external factors such as environmental conditions or instrumental limitations, a decrease in elastic and inelastic scattering cross-sections for that range of energies, or a combination of both. To identify the exact reasons for this, further study should be conducted, but it will not be carried out in this work as it is beyond the scope of the thesis.

The analog equivalent neutron simulation works as expected and successfully replicates the simulations conducted in ref. [15]. The simulations slightly underestimate the response for high energies but have very good statistics (see Figures 5.3 and 5.7) with fast simulations.

Analog simulations using the non-equivalent neutron source can be quite time-consuming. For instance, the simulation for the 40 cm iron shielding took almost 11 hours to run, as shown in Table 5.3. Interestingly, the simulation time varied significantly depending on the shielding

material used. For the 100 cm concrete shielding, the simulation took considerably less time, clocking in at only 1.5 hours (see Table 5.3). Despite the good statistics for the number of particles simulated, the response in the high-energy peak showed considerable deviation from the experimental data. This discrepancy is evident in Figures 5.4 and 5.8, which compare the simulation results with the experimental data for the 40 cm iron and 100 cm concrete shieldings, respectively.

5.1.5   Performance Metrics

Based on our simulation results so far, it's important to look at specific metrics that will help us better understand the tally performance. This can be achieved by investigating the statistical checks of the MCNP2.6 code. These include relative error, slope, VOV, and FOM, which are printed in the MCNP6.2 output by default together with the tally results (e.g., flux, dose, heat, etc.) as a function of the NPS values. The results are shown here were obtained with the proton source using the variance reduction parameters obtained with ADVANTG code using the equivalent neutron source. These metrics provide a comprehensive overview of the accuracy and efficiency of our simulations. Figure 5.11 will visually compare these metrics for proton source simulations with and without applying the variance reduction techniques, for each shielding scenario.

As seen in Figures 5.11a and 5.11b, simulation incorporating weight windows yield lower relative errors and VOV, which is an indicator of tally convergence and should decrease with increasing NPS. The differences between matrices of analog and weight windows become more noticeable with increasing shielding, particularly evident in the case of the 100 cm concrete shielding. The VOV values with weight windows are already lower than 0.1, which is a quantity used to measure the relative statistical uncertainty in the estimated relative error, even at the beginning of nps value and consistent with the relative error behavior. Concerning the slope, the weight window simulation tends to exhibit a rapid decrease in the probability of extreme results, particularly in the case of 100 cm concrete shielding, where the slope remains consistently at 10. The analog simulations, on the other hand, maintains a high likelihood of extreme results with a slope value close to 0.

The FOM, which is a tally reliability indicator, would be expected to show a notable increase when transitioning from an analog simulation to one implementing weight windows. Yet, only a marginal FOM rise was observed, with an increase factor of eight or less. This outcome can be interpreted from two angles: the substantial computational time required by MCNP to read the external weight window file and implement the technique during the simulation, and the lack of full exploitation of the potential benefits of weight windows in these particular problems.

A high FOM value (see Equation 3.2), is beneficial as it proportionately reduces the computer time needed to achieve a desired precision level. In an ideal scenario, a well-behaved tally that has converged to the true (expected) value should maintain a nearly constant FOM, except possibly during the very early stages of a problem. In this case, the FOM values were found to be constant except at the initial NPS values, as expected. However, the increments in FOM values for both shielding cases proved to be rather small.

The use of a fine mesh to generate the variance reduction parameters can lead to an extensive weight windows file. Consequently, the time MCNP6.2 code takes to read this file may increase, which in turn could impact the efficiency of the calculations and consequently the FOM values. While the relative error values have improved with the introduction of weight windows, the marginal enhancement in FOM values suggests that further optimization may not be necessary.

The size of the weight windows file and the time spent to generate the weight window parameters depends heavily on the user's expertise. The users' ability to effectively manage these factors greatly influences the efficiency of the calculations. Further discussion on this topic can be found in subsection 5.1.6.
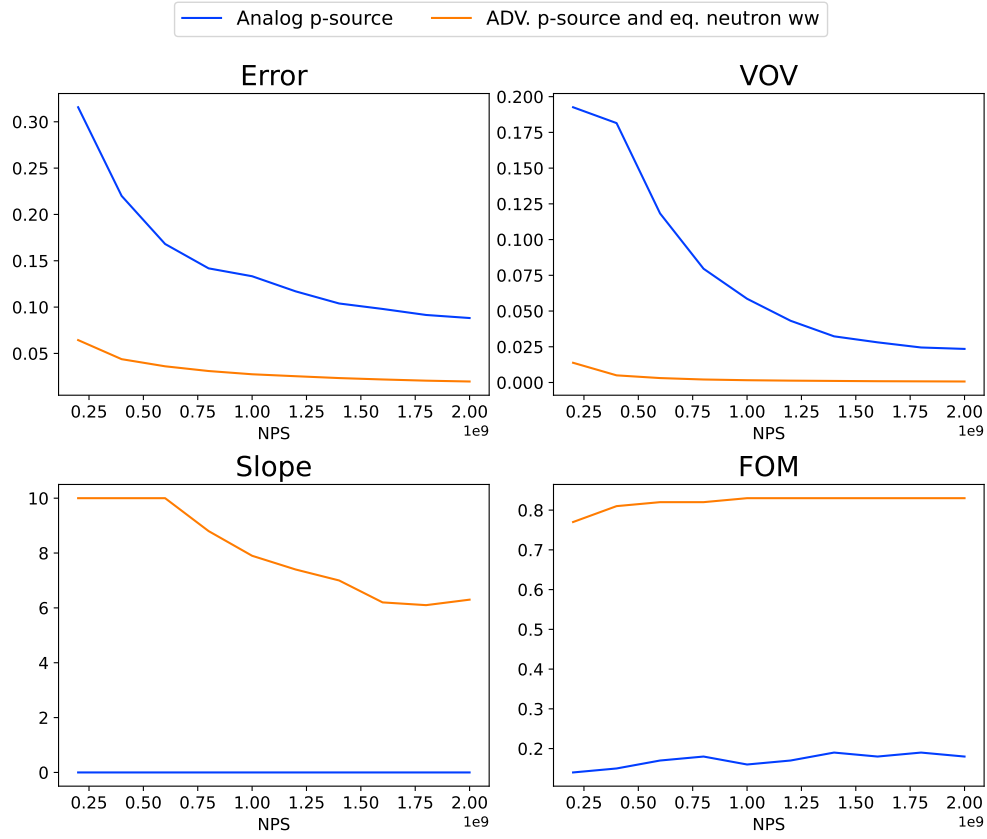
(a) TIARA 40 cm iron shielding.
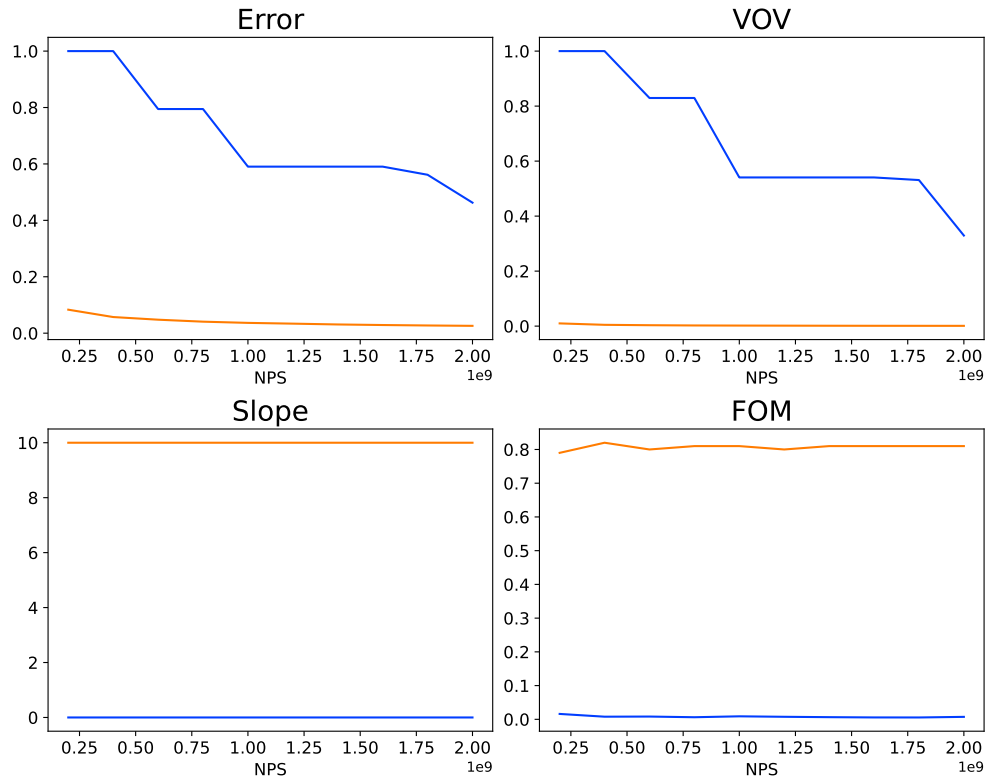
(b) TIARA 100 cm concrete shielding.

Figure 5.11: Performance metrics (Error, Slope, VOV, and FOM) in proton source MCNP simulations with and without weight windows across different NPS values for two different shielding cases: (a) 40 cm iron and (b) 100 cm concrete.

5.1.6 Discussion

Upon reviewing our findings, one might think that the equivalent neutron source used in analog calculations is a sufficient variance reduction technique. This effectiveness, may give us the idea that the usage of ADVANTG may not be essential for achieving satisfactory statistical outcomes in our simulations. However, it is important to keep in mind that the efficiency of results obtained through analog simulations is heavily dependent on particle energy and shielding thickness. While in these cases, these properties allowed analog simulations with an equivalent neutron source to have good efficiency in the simulations, it may not be the case for different values of incident energies, shielding thicknesses, materials, geometry, etc. On the other hand, weight windows enable continued improvement in simulation efficiency, independent of these parameters.

When it comes to the simulations that used the weight windows we got from the non-equivalent neutron source, it is important that we take a good look at what the results were. Table 5.3 shows that simulations with the proton source failed when the weight windows generated with the non-equivalent neutron source were used. To dig deeper into the causes, it's useful to look at the lower boundaries of weight windows created for the equivalent and non-equivalent sources for areas around the detectors and different energy levels in each shielding case. You can refer to Tables B.1 through B.4 in Annex B for a detailed look at these values. To get a better understanding, we can examine the disparities between these two data sets. To do so, Tables 5.4 and 5.5 present these differences. Specifically, these tables display the ratios of weight window values when obtained with both equivalent and non-equivalent neutron sources.

Table 5.4: Comparison of ADVANTG weight window lower bounds for TIARA experiment 40 cm iron shielding, using Equivalent Neutron Source vs. Non-Eq. Neutron Source, with relative differences in percentage.

Energy [MeV]	(439,0,0)	(441,0,0)	(454,0,0)
4.14E-07	-*	-*	2477
1.01E-04	2358	2372	2361
1.50E-02	2318	2305	2313
6.08E-01	2682	2659	2646
1.96E+01	5469	5116	4798
6.00E+01	8523	8028	7616
7.00E+01	8177	7828	7547

* Zero value for weight window lower bound.

Table 5.5: Comparison of ADVANTG weight window lower bounds for TIARA experiment 100 cm concrete shielding, using Equivalent Neutron Source vs. Non-Eq. Neutron Source, with relative differences in percentage.

Energy [MeV]	(468,0,0)	(501,0,0)	(514,0,0)
4.14E-07	1530	1528	1530
1.01E-04	1700	1525	4812
1.50E-02	3154	1567	6407
6.08E-01	6555	6018	9949
1.96E+01	9166	9298	17146
6.00E+01	14638	12346	16567
7.00E+01	15119	12567	16022

Upon closer examination of the data, two main observations can be made. The first observation is that the values of the lower boundaries for the weight windows are notably lower for the non-equivalent neutron source compared to those from the equivalent neutron source. Lower values of weight windows imply higher importance for the particles, as they are inversely proportional. Higher importances cause particles to split more, and as a result, the simulation becomes stuck and does not finish or becomes extremely inefficient. The second observation is that the difference in values significantly increases for energies close to the flux peak, which is approximately where the spectra differ the most and what potentially could be causing the problem with the simulation.

To emphasize the importance of employing the appropriate weight window mesh for ADVANTG, an MCNP simulation was conducted for the 100 cm concrete shielding, utilizing weight windows created with the same mesh as the one employed in the 40 cm iron shielding. Although the results were statistically comparable, the simulation took twice as long to finish when using the same number of particles. The meshes utilized in each case can be found in Annex A.

The simulations underscore the feasibility of applying weight windows to proton source problems derived from an equivalent neutron source. This not only suggests that the same methodology can be confidently implemented for the MYRRHA ADS configuration, but it also opens avenues for other applications. For instance, the methodology could be suitably adapted for beam dump shielding calculations at different beam energy sections of the MYRRHA LINAC. This versatile approach can potentially broaden the scope of our simulation capabilities.

5.2 KENS Shielding Experiment

5.2.1 Overview and Simulation Design

Drawing on the methodology employed in the TIARA experiment, three different types of sources were also used for this case: proton source, equivalent and non-equivalent neutron sources. A series of six simulations were performed, during which various parameters were evaluated. The experimental data available for these simulations are the reaction rates for the following reactions:

- Al27(n,α)Na24
- Bi209(n,4n)Bi206
- Bi209(n,5n)Bi205

- Bi209(n,6n)Bi204
- Bi209(n,7n)Bi203
- Bi209(n,8n)Bi202

These results were calculated by multiplying the cross-section of the reactions with the spectrum of the secondary neutrons produced either via the proton-target interactions when the source particle is the incident protons or via a the investigated neutron source interactions with the surrounding materials, shielding, etc. As the cross sections used are identical across all simulations, obtaining results that align closely with the experimental data would indicate a well-characterized neutron spectrum.

The neutron data library used for the MCNP particle transport simulations was JEFF-3.3, supplemented with JENDL-4.0/HE proton data library to account for missing nuclear data. Concerning the cross-sections associated with the reaction rates, ENDF-B/VI was used for bismuth reactions, while TENDL-2019 was utilized for the aluminium reaction, in line with the approach detailed in the reference paper [26].

After setting up the weight windows, we moved forward with the final MCNP runs, using these weight windows as our guide. For this experiment, we had a couple of main goals in mind. First, we wanted to check again if the weight windows we got from an equivalent neutron source could really work with a proton source. Second, we wanted to give the non-equivalent neutron source method another try, even though it didn't prove being a valid method in the TIARA experiment. By granting this method another chance, we anticipated gaining deeper insights into its efficacy, particularly in understanding why it either produces satisfactory results or fails to do so. An additional objective was to examine how the process of optimizing one or more detectors (or tallies) could influence the simulation and potentially modify the results.

Simultaneously, we have also undertaken some irradiation calculations focusing on the last detector. These calculations are essential in this study as they aim to evaluate the isotopic composition of a stainless steel sample placed in Slot-8. The primary goal is to understand how the reduction in the uncertainties of the spectrum impacts the induced activities of certain radionuclides produced in this sample due to the transmitted neutron flux interactions. These findings will not only augment our understanding of the impact of the spectrum uncertainties on the activation results, but could also yield valuable insights that could be directly applied to following work with the MYRRHA reactor.

5.2.2   Equivalent Neutron Source

As explained in more detail in the methodology chapter, we generated an equivalent neutron source using MCNP code. This source, defined as a point isotropic source, was collimated into a cone shape along the positive z-axis to simulate our experimental conditions (refer to Figure 4.5 in Section 4.2 for a schematic representation).

The neutron yield and flux, essential parameters in our study, were computed with the F1 tally function in MCNP. The yield and flux values are indicative of the number of neutrons produced per proton and the intensity of neutron radiation, respectively.

5.2.3   ADVANTG Simulation Results

Three ADVANTG simulations were carried out by optimizing the neutron spectra at different detector locations (i.e., slots). As the experimental reaction rates were performed at the detectors located through the concrete shielding, it was aimed to determine the impact of the detector location used to produce variance reduction parameters. This impact was determined by investigating the performance of the MCNP6.2 simulations when the previously generated variance reduction parameters used. Two of these utilized the equivalent neutron source; one optimized all detector slots, and the other focused solely on optimizing the last detector slot (Slot-8). Furthermore, an additional ADVANTG simulation was run with a non-equivalent neutron source, optimizing only slot 8. The meshes used for both types of optimization - for all slots and for slot 8 alone - can be found in Annex A. The run time for these simulations, performed using 70 CPUs, is presented in Table 5.6.

Table 5.6: ADVATNG simulations run time comparison for KENS shielding experiment.

Optimization	Source	Run time [mm:ss]
All Slots	Eq. Neutron	02:23
Slot 8	Eq. Neutron	02:25
Slot 8	Non-Eq. Neutron	02:25

The parameters used in the ADVANTG input for all simulations, excluding the varying mesh parameters for each type of optimization, are:

Parameter	Value
method	fwcadis
fwcadis_spatial_treatment	pathlength
fwcadis_response_weighting	False
library	HILO2K
denovo_x_blocks	2
denovo_y_blocks	2
denovo_z_blocks	2

Table 5.7: Key parameters used in the ADVANTG input for KENS shielding experiment.

Finally, to wrap up the simulation results, the heat maps showing the distribution of the integral adjoint neutron flux for the two distinct optimization types are presented in Figures 5.12 and

5.13. These results were found using the equivalent neutron source, but there's no clear difference when compared to heat maps made from non-equivalent neutron sources.
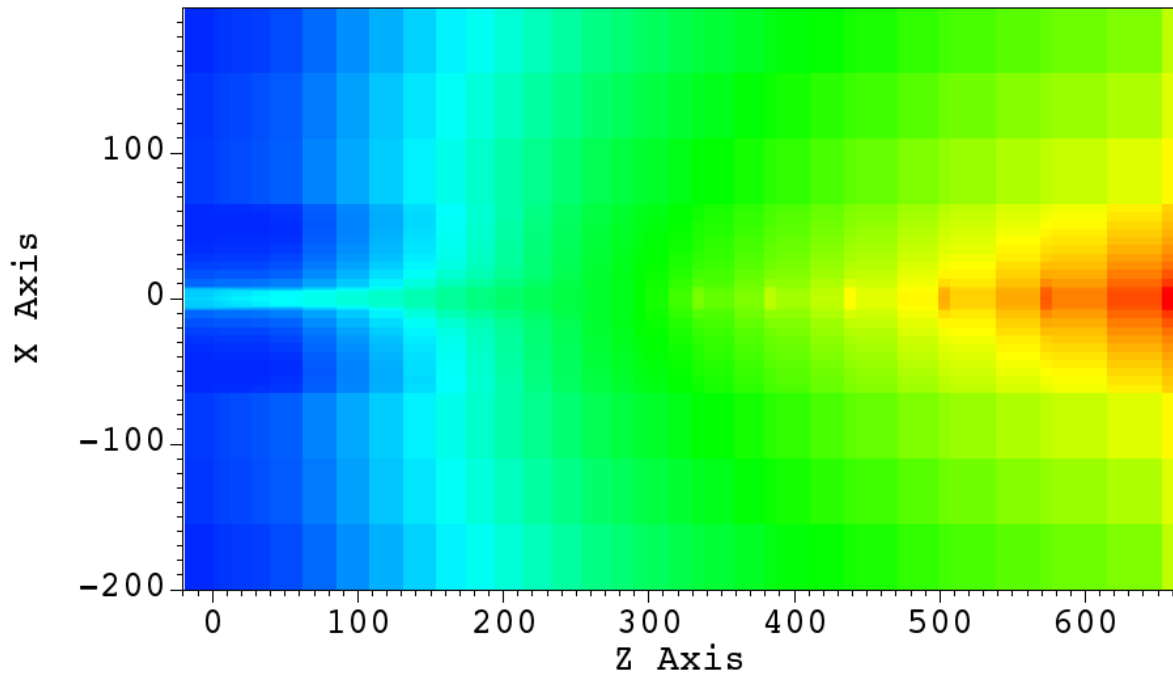
Figure 5.12: Heat map of the integral adjoint flux on XZ plane for KENS shielding experiment when optimizing all slots.
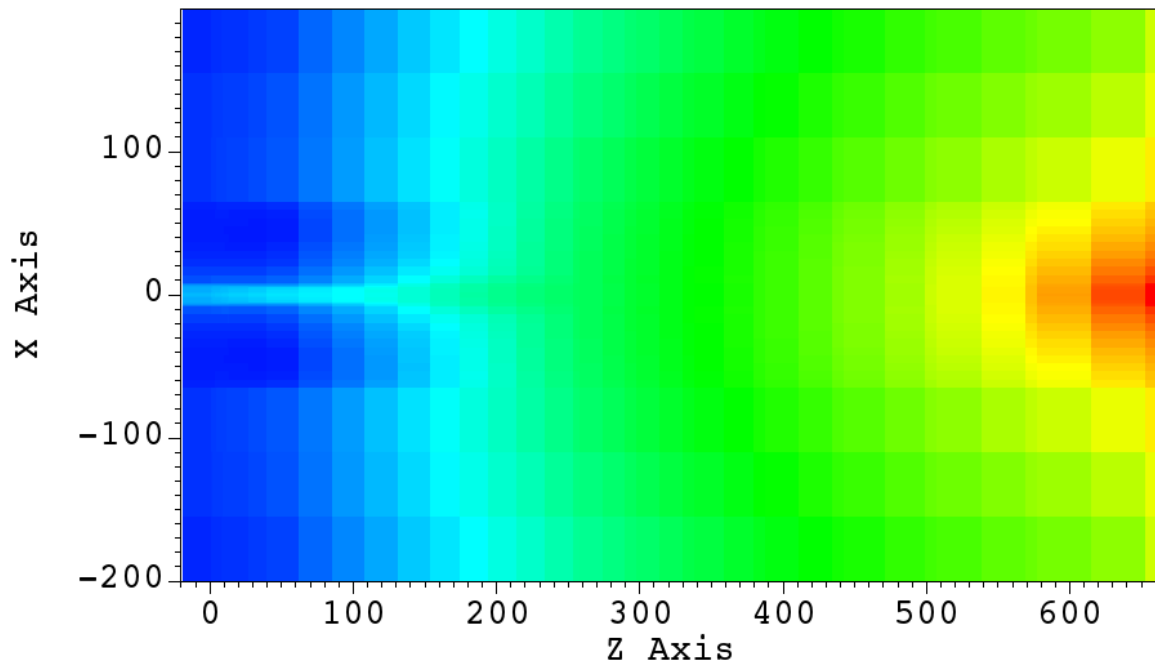
Figure 5.13: Heat map of the integral adjoint flux on XZ plane for KENS shielding experiment when optimizing slot 8.

5.2.4 MCNP Simulation Results

Table 5.8 shows the performance overview of the KENS shielding experiment simulations. The reaction rates calculated in the simulation and their comparison to experimental data can be found in Figures 5.14 through 5.17.

Table 5.8: MCNP simulation performance comparison for KENS shielding experiment with and without ADVANTG weight windows

Source	Weight Windows	Optimization	Run time [hh:mm]	NPS
Proton	None	None	77:33	2.00E+09
Non-Eq. Neutron	None	None	77:09	5.00E+08
Eq. Neutron	None	None	13:03	2.00E+09
Proton	Eq. Neutron	All-Slots	22:55	1.00E+06
Proton	Eq. Neutron	Slot-8	04:30	1.00E+06
Proton	Non-Eq. Neutron	Slot-8	00:30	1.00E+06
Proton	Non-Eq. Neutron	All-Slots	03:57	1.00E+06

Although Table 5.8 offers some valuable insights, it doesn't capture the complete picture of the simulation's performance. The main reason for this is that it doesn't include measures of the simulations' precision and accuracy. These important aspects are needed for a full and comprehensive understanding of how well our simulations are performing. Nevertheless, the table highlights clear differences in the simulation run time, in relation to the type of source and weight window optimization used. In this instance, the non-equivalent neutron source demonstrated the slowest response time when the analog calculations were performed, while the equivalent neutron source managed to simulate an equivalent number of particles to the proton source almost six times faster.

Moving to simulations utilizing weight windows, a clear disparity is evident between the optimization of a single detector and the optimization of all detectors in terms of simulation run time (see Table 5.6). Perhaps even more surprising is that the simulation employing the non-equivalent neutron source for weight window generation yielded the fastest results (i.e., 30 minutes for Slot-8 optimization and aproximately 4 hours for All-Slots optimization). This contrasts with the TIARA experiment, where simulations did not manage to finish. These results give us useful information, but to fully understand how well the simulations work, we also need to look at things like accuracy and precision. You can find more about these important details in Figures 5.14 to 5.16. This will help us get a complete picture of our calculations.

Figure 5.14 compares analog simulations for proton, equivalent, and non-equivalent neutron sources. Key observations include decreased accuracy and poor statistics from the proton source in heavily at the last two detectors or slots. The non-equivalent neutron source shows inaccuracy for small shielded distances (slot 1 and 2), warranting further spectrum analysis. While the equivalent neutron source tends to overestimate reaction rates in thin shielding (slots 1 and 2), it consistently produces results that align most closely with the experimental data and are consistent with the ones obtained from the proton source at the slots 5-6-7.
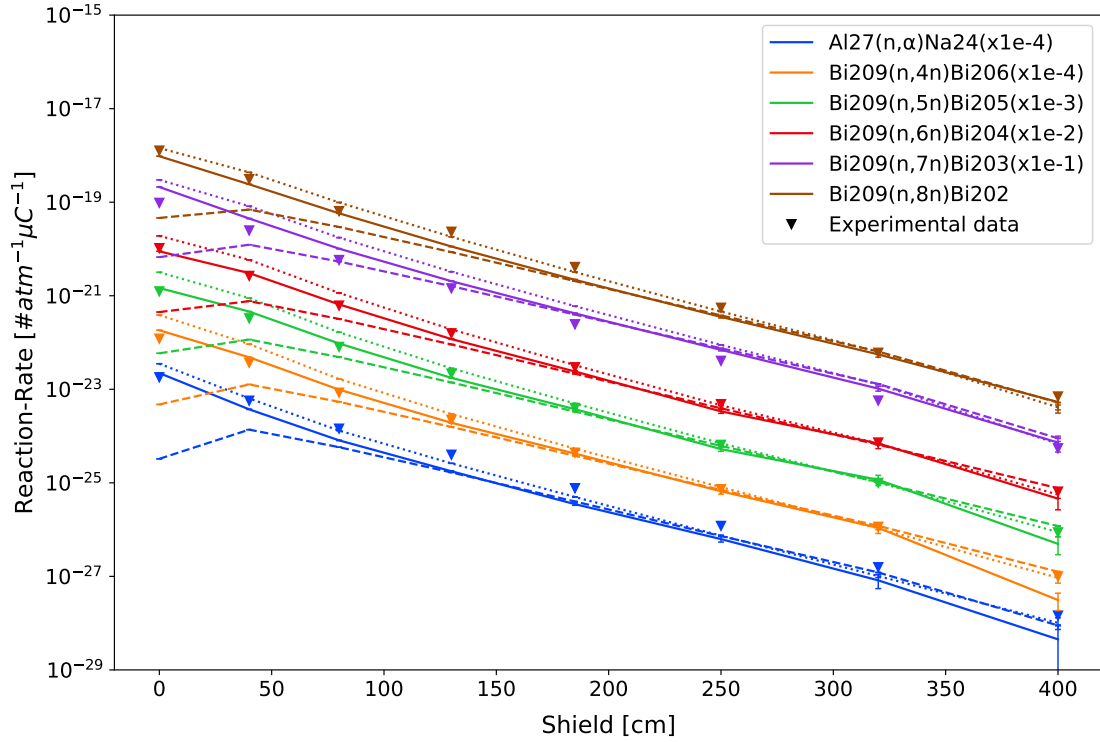
Figure 5.14: Comparison of experimental and calculational results of reaction rates with proton source (solid), equivalent neutron source (dotted) and non-equivalent neutron source (dashed) for KENS shielding experiment.

Figure 5.15 demonstrates that no substantial differences emerge when employing weight windows generated from equivalent and non-equivalent neutron sources. In both scenarios, there is an increase in the error as you move to areas with less shielding and a decrease in the accuracy of the reaction rate for the Al27(n,α)Na24. This appears to be a reasonable consequence given that the optimization is being performed for the final slot. A more comprehensive understanding of this phenomenon can be achieved by examining the neutron spectrum, which we will undertake following the analysis of the reaction rates.
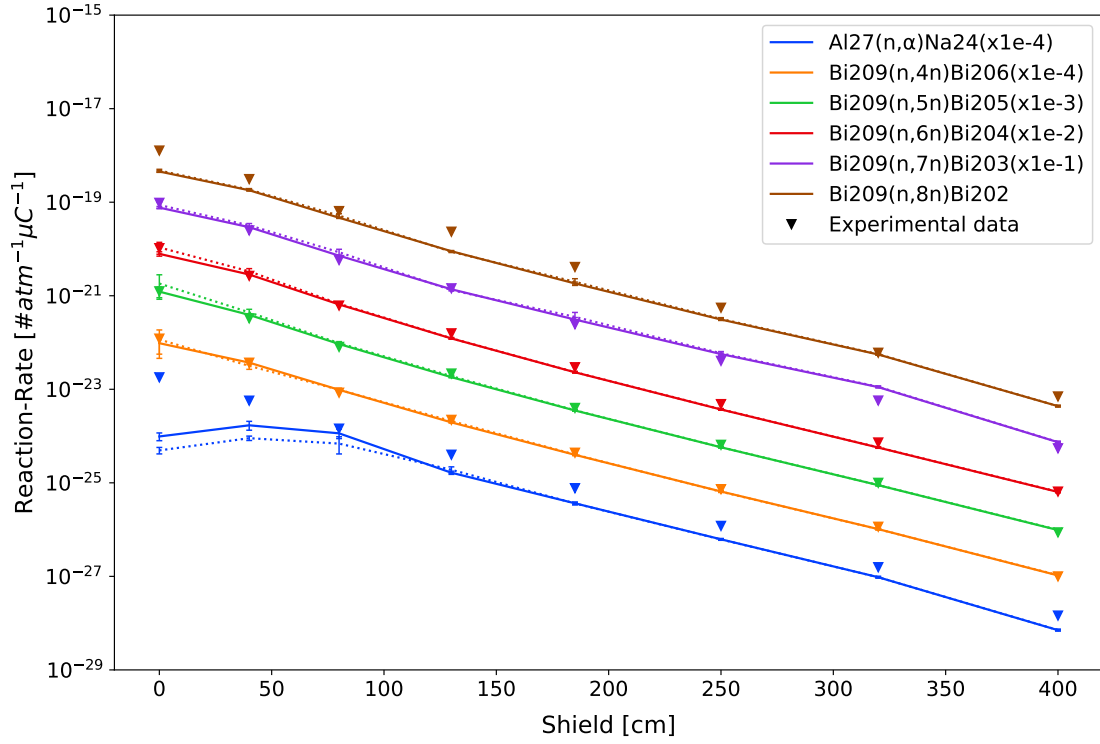
Figure 5.15: Comparison of experimental and calculational results for reaction rates using proton source and Slot-8 optimization with ADVANTG-generated WW from equivalent neutron source (solid) and non-equivalent neutron source (dotted) for KENS shielding experiment.

Figure 5.16 shows good statistical results for all shielding distances and reaction rates, with overall decent precision. As mentioned earlier, this comes at the cost of increased simulation run time (see Table 5.8). It is noteworthy that the differences seen here are even less pronounced than in the earlier scenario, which should be kept in mind during spectrum analysis. A final graph (see Figure 5.17) is included, displaying a comparison between analog and optimized results. These optimized results are selected based on the best fit from the different optimization simulations using proton source and weight windows generated from the equivalent neutron source. Further discussion regarding this is available in subsection 5.2.7.
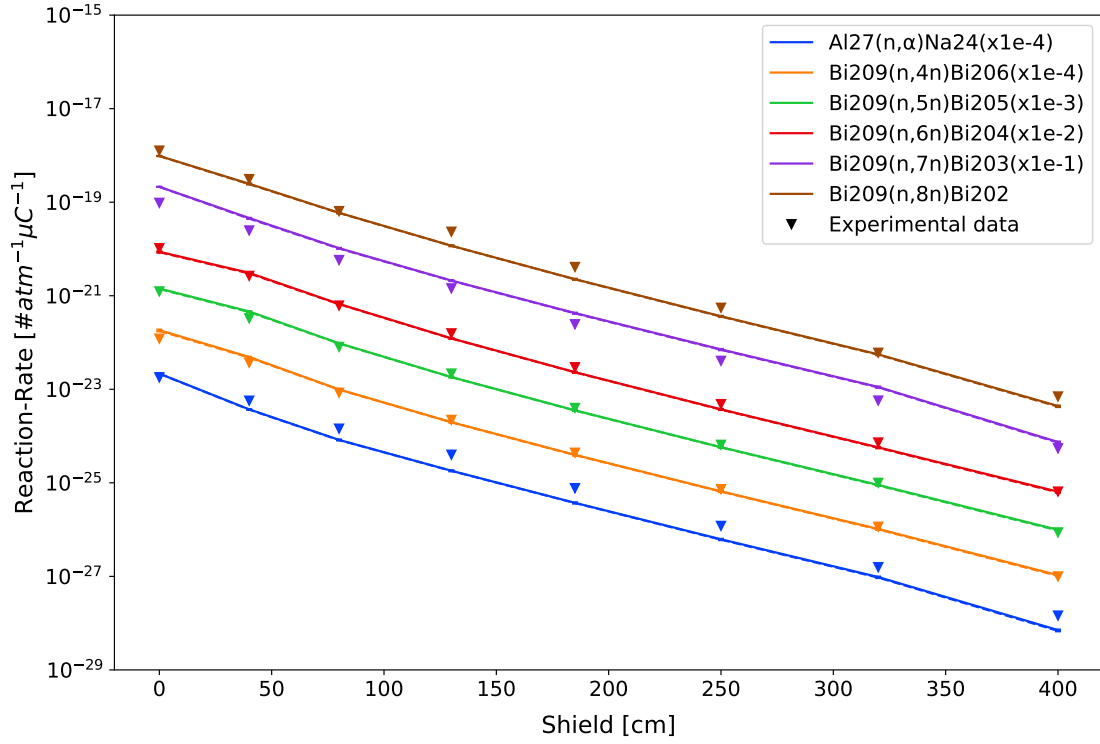
Figure 5.16: Comparison of experimental and calculational results for reaction rates using proton source and All-Slots optimization with ADVANTG-generated WW from equivalent neutron source (solid) and non-equivalent neutron source (dotted) for KENS shielding experiment.
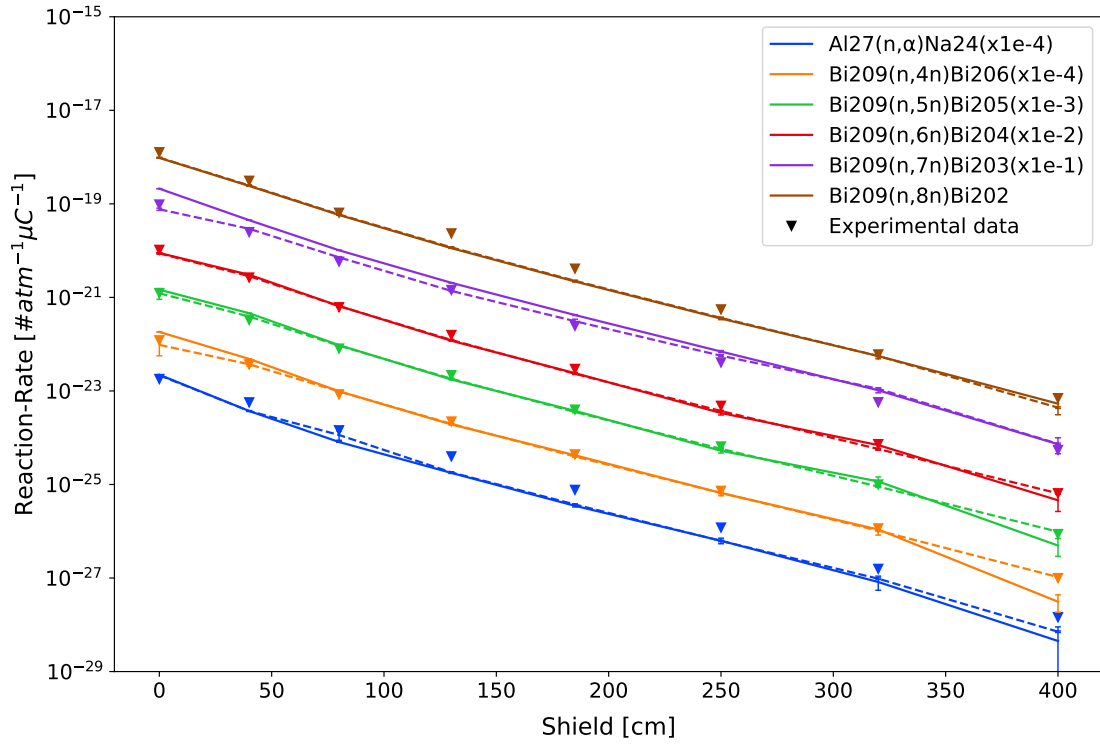
Figure 5.17: Comparison of experimental and calculational results before (solid) and after (dashed) the use of ADVANTG with proton source for KENS shielding experiment.

In order to understand better why the analog simulation with non-equivalent neutron source and simulations using weight windows generated with different spectra differ in their behaviour, it is interesting to have a look at the neutron spectrum. Specifically, we will focus on the neutron spectra at the initial (Slot-1) and final (Slot-8) slots, considering only energies above 1 MeV. This is because these reactions have a threshold in their cross sections for higher energies (¿ 1MeV) (refer to Section 4.2).

In Slot-1 (Figure 5.18), the proton and equivalent neutron sources show a very similar spectra. As a reminder, these spectra are generated in slot-1 and slot-8 from the neutrons that are produced via the proton-target interactions (i.e., spallation reaction at the target) in case of the proton source and from the neutron source that was created on the formerly proton-target interactions. In contrast, the non-equivalent neutron source has a different spectrum as expected, since it was biased by replacing the protons with the neutrons on the source definition. This source essentially consists of a beam of 500 MeV neutrons aimed directly at the detector area, so there is no target or specific definition employed. The spectrum in Figure 5.18 corresponds to the first slot and at that point, particles have not yet gone through any shielding, as the slot-1 is filled with the air and located at the inner left surface of the concrete shielding. Therefore no energy loss or attenuation has been possible. This accounts for the high neutron flux at 500 MeV, while the remainder of the spectrum can be explained by the backscattered particles that result from interaction with the shielding material and by particles generated in the surrounding materials, such as the iron collimator (see Figure 4.4).
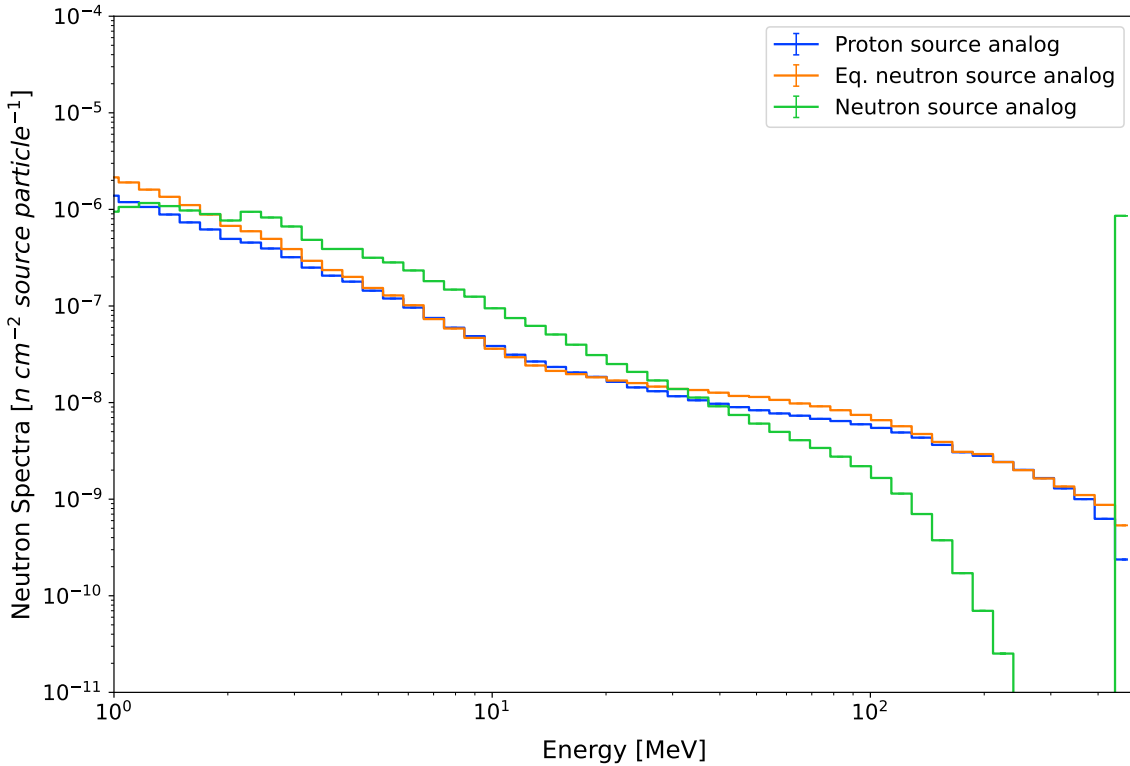
Figure 5.18: Neutron spectra obtained from analog MCNP simulations for Slot-1 of the KENS shielding experiment.

The spectrum in Slot-8 (Figure 5.19) presents not well converged results for all analog simulations, with the proton source delivering the least accurate results, as there are only values for a few energy intervals. The equivalent neutron source roughly follows the trend of the spectrum but with extremely high uncertainties, while the non-equivalent neutron source provides the

highest precision. For this last one, the spectrum is much clearer, as sufficient shielding has been present to scatter neutrons across all energy levels. Additionally, a peak of neutrons at 500 MeV is still observable.
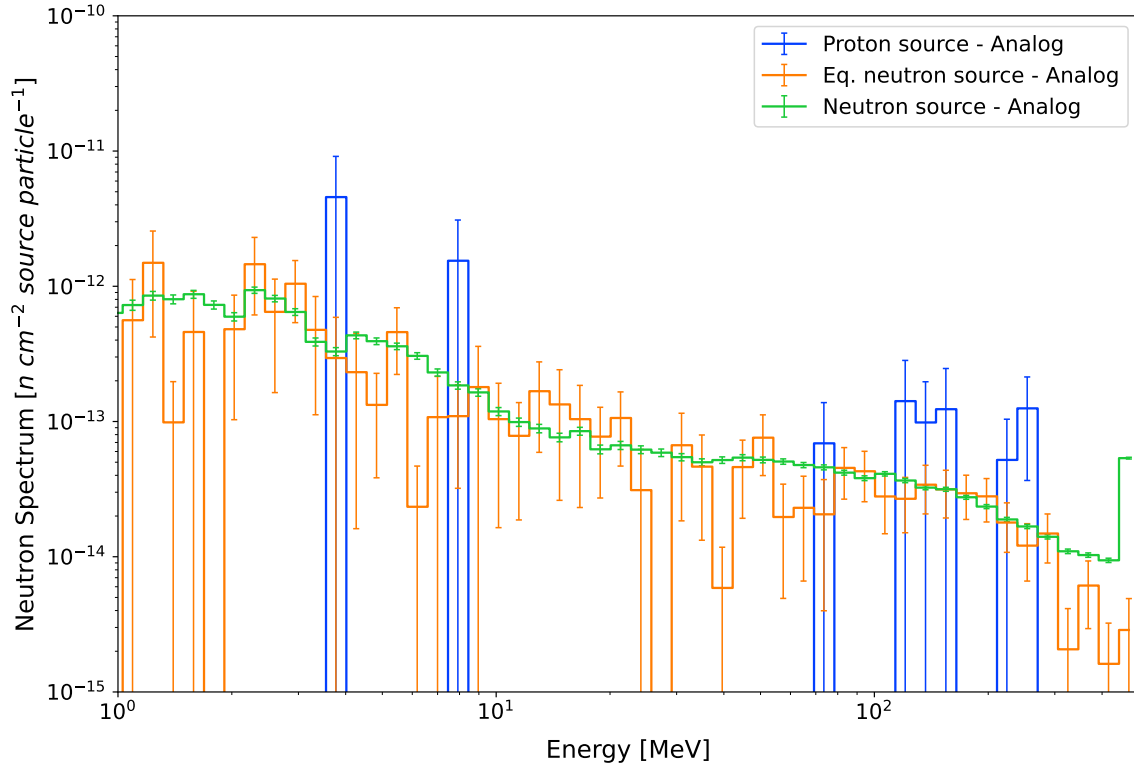
Figure 5.19: Neutron spectra obtained from analog MCNP simulations for Slot-8 of the KENS shielding experiment.

The spectra previously discussed are concerning the analog simulations, which were used to generate the weight windows. Figures 5.20 and 5.21 show a comparison of the spectra between the analog with proton source simulation and the simulations where weight windows were employed. For better understanding, the results for Slot-8 are presented first. This figure clearly illustrates how the spectra for all simulations employing the weight windows yield the same result with high accuracy and precision. This aligns with the expectations for ADVANTG weight window optimization of Slot-8.

Contrarily, our findings suggest that enhancing a region situated farther from the source (Slot-8) does not necessarily ensure better statistics in the preceding areas. This is emphasized by the neutron spectra results at Slot-1 (see Figure 5.21) for simulations utilizing weight windows optimized for the last slot, compared to the results where all slots are optimized. In the case of full-slot optimization, the spectrum aligns nearly perfectly with that generated by the analog proton source across all energy levels. Conversely, in simulations optimized solely for Slot-8, results align only for energies exceeding 100 MeV.
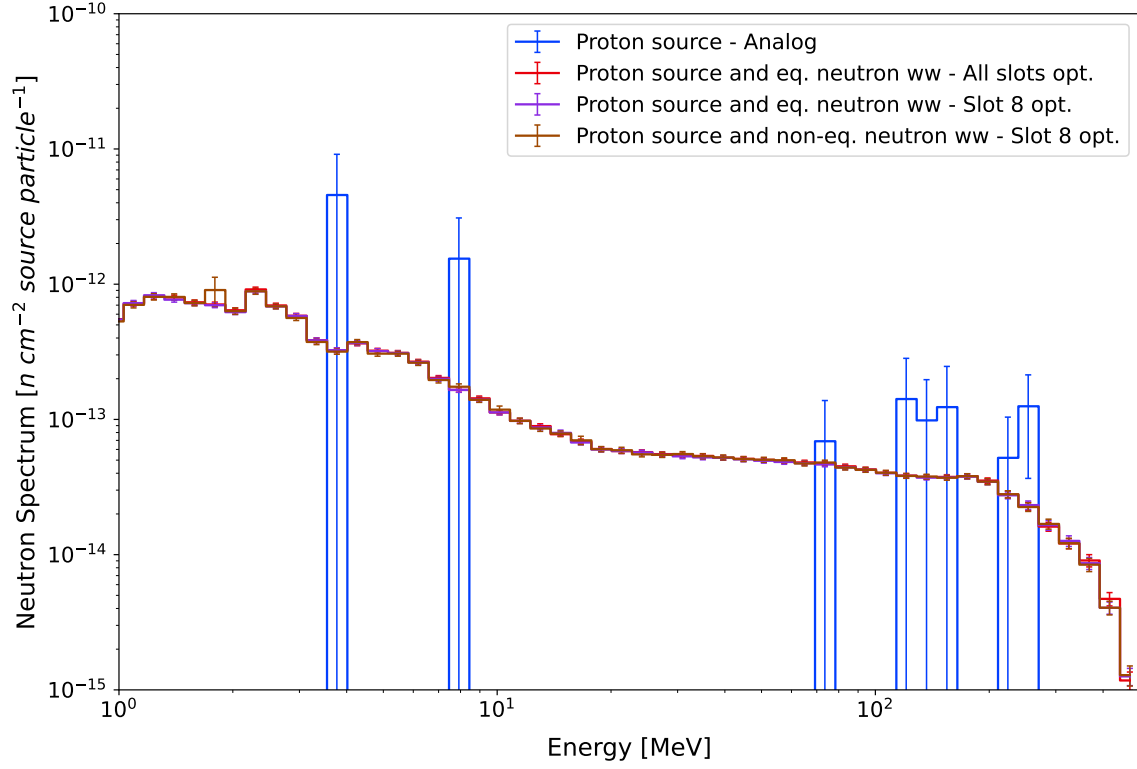
Figure 5.20: Neutron spectra obtained from MCNP simulations using proton source for Slot-8 of the KENS shielding experiment.
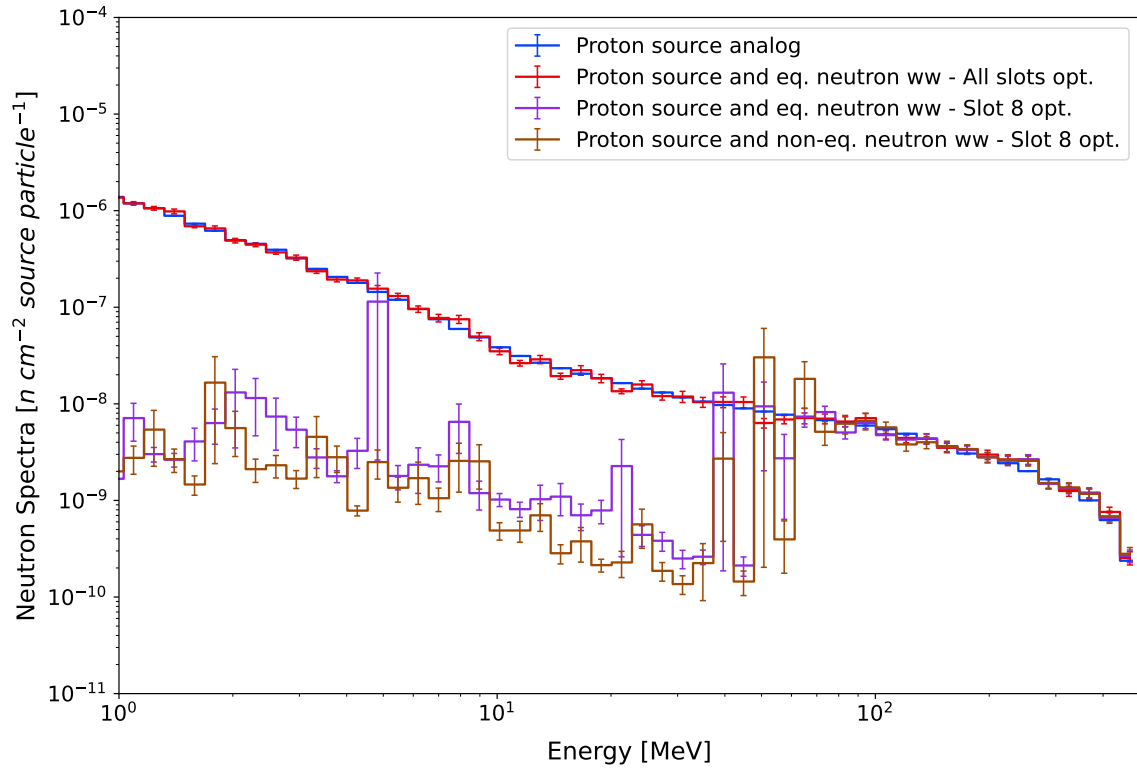
Figure 5.21: Neutron spectra obtained from MCNP simulations using proton source for Slot-1 of the KENS shielding experiment.

5.2.5 Performance Metrics

Following the method we used with TIARA, it could be beneficial to explore the performance metrics for these calculations. In this case, we are presenting the metrics for two MCNP tallies: one in Slot-1 and another in Slot-8. We conducted a comparison between the analog proton source simulation and several other simulations using weight windows. To put these results on the same graphs for easier comparison, two x-axes were used in Figures 5.22 and 5.23. The bottom axis represents the scale for the analog simulations, where 2E+09 particles were simulated. The top axis represents the scale for MCNP enhanced simulations, where 1E+06 particles were simulated. Y-axis' are the values corresponding to the relative error, VOV, slope and FOM.

The results presented in Figure 5.22 highlight the significant improvements in tally results due to the application of variance reduction techniques, which is observable across all measured parameters. The differences between simulations employing different weight windows are negligible for both error and VOV. However, when it comes to the slope parameter, Slot 8 with a non-equivalent neutron source demonstrates a quicker attainment of steady state compared to others. This specific simulation also delivers the best FOM. Importantly, these graphs illustrate the differences in FOM when varying the optimization approach, such as optimizing a single slot versus multiple slots, or when choosing between equivalent or non-equivalent neutron sources.
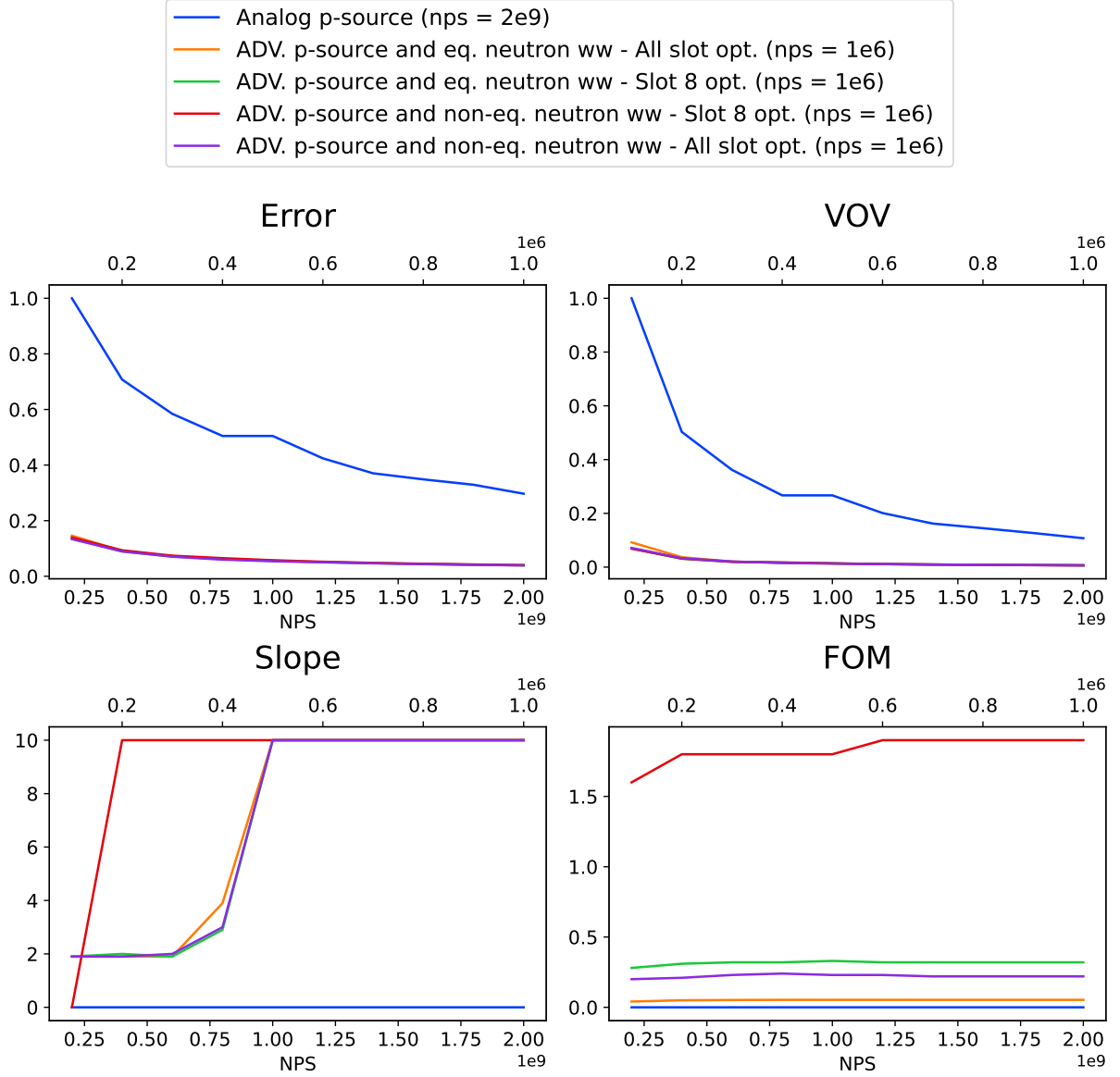
Figure 5.22: Comparison of Slot-8 performance metrics (error, slope, VOV, and FOM) in KENS shielding experiment: Proton source MCNP simulations with versus without weight windows across different NPS values.

When looking at the results from Figure 5.23 caution has to be taken since it is important to keep in mind that slot-1 is close to the source and filled with air, therefore variance reduction techniques should not be necessary and may slow down simulation and worsen the performance metrics. Nevertheless, when understood within the appropriate context, this information can be valuable in deepening our understanding of the phenomena associated with the application of weight windows.
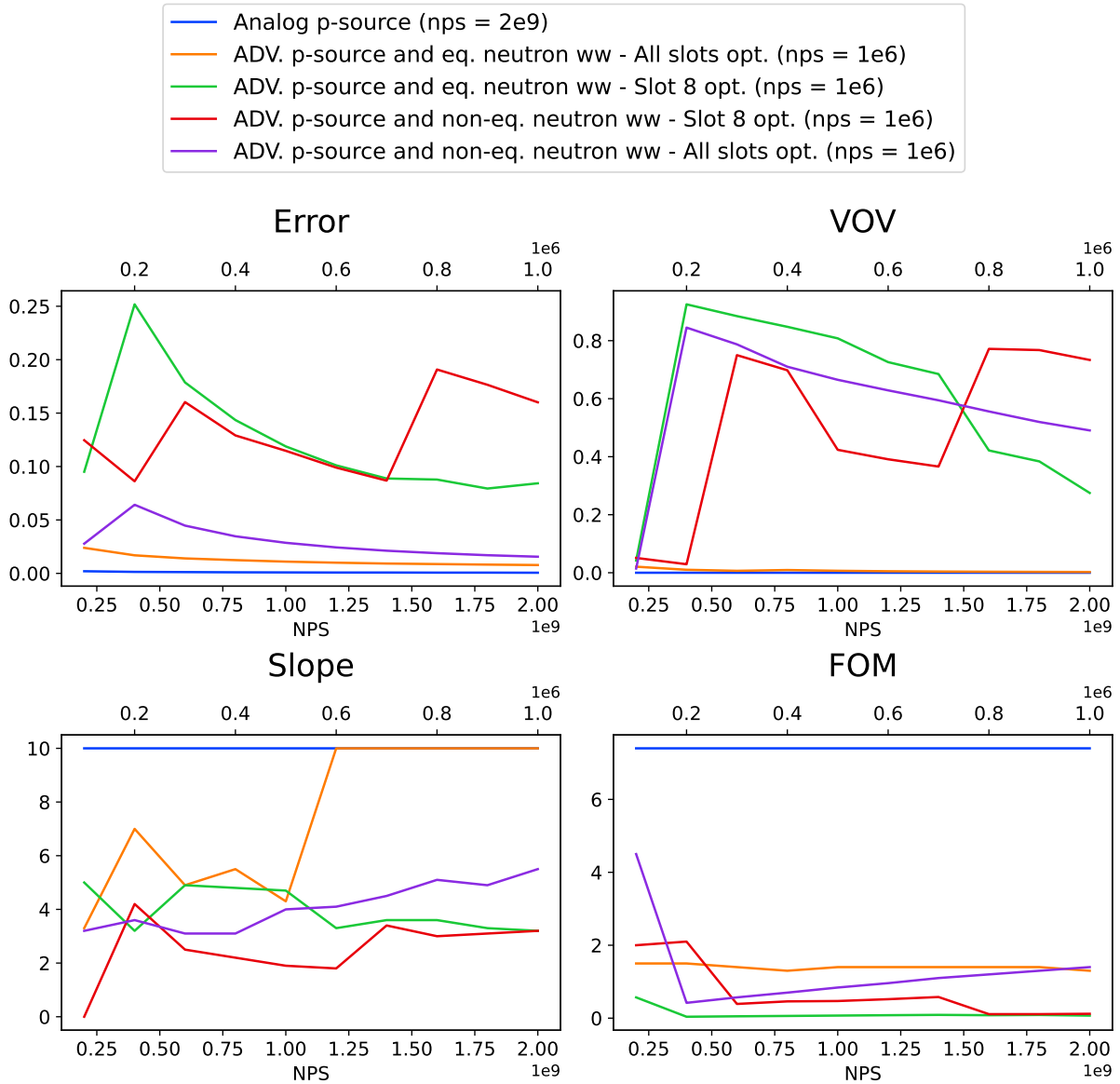
Figure 5.23: Comparison of Slot-1 performance metrics (error, slope, VOV, and FOM) in KENS shielding experiment: Proton source MCNP simulations with versus without weight windows across different NPS values.

In summary, among various simulations utilizing weight windows, the All-Slot optimization with non-equivalent neutron sources offers the best performance in measured parameters. Conversely, the same All-Slot optimization employing equivalent neutron sources displays a promising trend across all parameters but with a slower evolution concerning the number of particles simulated. Simulations involving the optimization of slot-8 exhibit considerable variability in behavior. Examining the FOM, it appears logical that the analog simulation attains the highest value. This is because the other simulations apply various variance reduction techniques, which, despite increasing computational time, do not bring about a significant impact on the tally results.

5.2.6   Irradiation Calculations

The motivation behind this exercise comes from the ref. [see below!], in which it was proven that it is possible to obtain an acceptable relative error (i.e., 5%) for the average neutron flux without obtaining the well-sampled flux spectrum. This is very important when there are strong resonances in the spectrum, which can cause different mean values of the reaction rates if the whole spectrum is not fully converged. Without examining the spectrum, to do the further calculations just based on the relative error of the average flux might give wrong results. This motivated us to investigate how the induced activities in the activated materials are impacted from the spectrum uncertainties and also the relative error of the average flux.

For the irradiation calculations, a stainless steel sample with the same composition as the antici-pated MYRRHA's reactor vessel was placed in Slot-8. The irradiation conditions considered for the illustrative purposes of activation results are 1 year of continues irradiation with 2mA beam current. Considering the results obtained with the analog proton were useless due to the poor statistics even with the high NPS values (See figure 5.21), we only give the results obtained with the weight windows. A series of MCNP simulations using weight windows were then conducted to obtain flux results with varying levels of uncertainty. The weight windows employed in these simulations were derived from the equivalent neutron source, with optimization applied to all slots. The resulting spectra for slot-8, showcasing the various levels of uncertainties, are depicted in Figure 5.24. As is evident, the error bars diminish as the uncertainty in the flux is reduced. This demonstrates that the reduction in flux error directly impacts the neutron spectrum, which is subsequently utilized for irradiation calculations in the ALEPH2 depletion code.
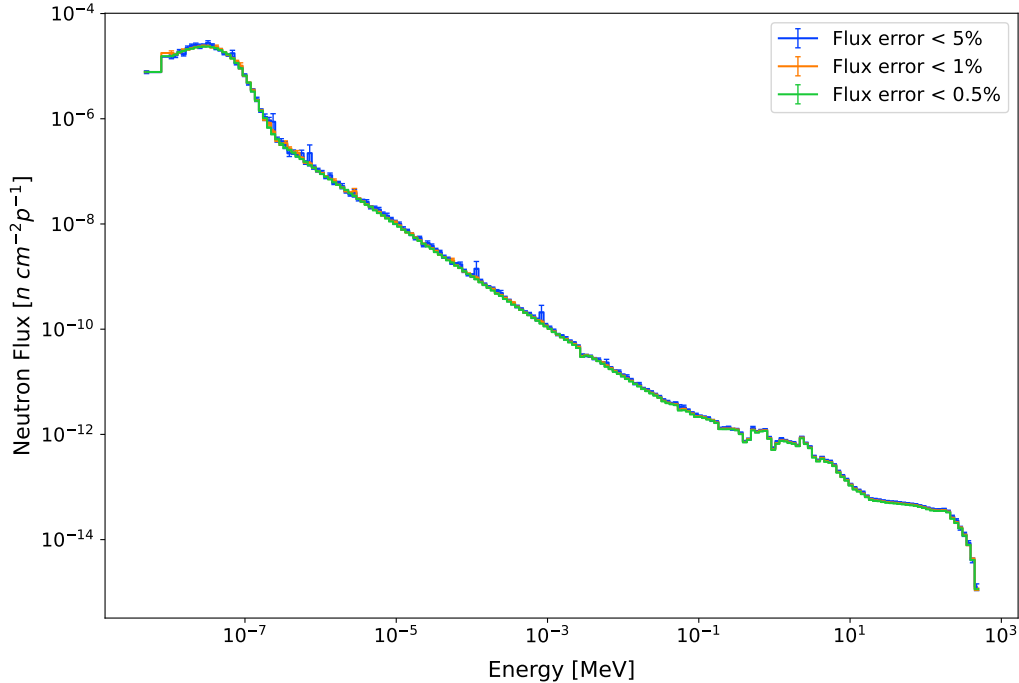
Figure 5.24: Neutron spectra at Slot-8 obtained from MCNP simulations using proton source and All-Slot optimization for different levels of uncertainties of the KENS shielding experiment.

From a radiation protection perspective, gamma emitters are of primary interest in order to handle with the radioactive waste and protect the workers from the high gamma dose rates. ALEPH allows us to identify all gamma emitters. The major ones among them, as shown in Figure 5.25, account for more than 99.5% of the gamma dose.
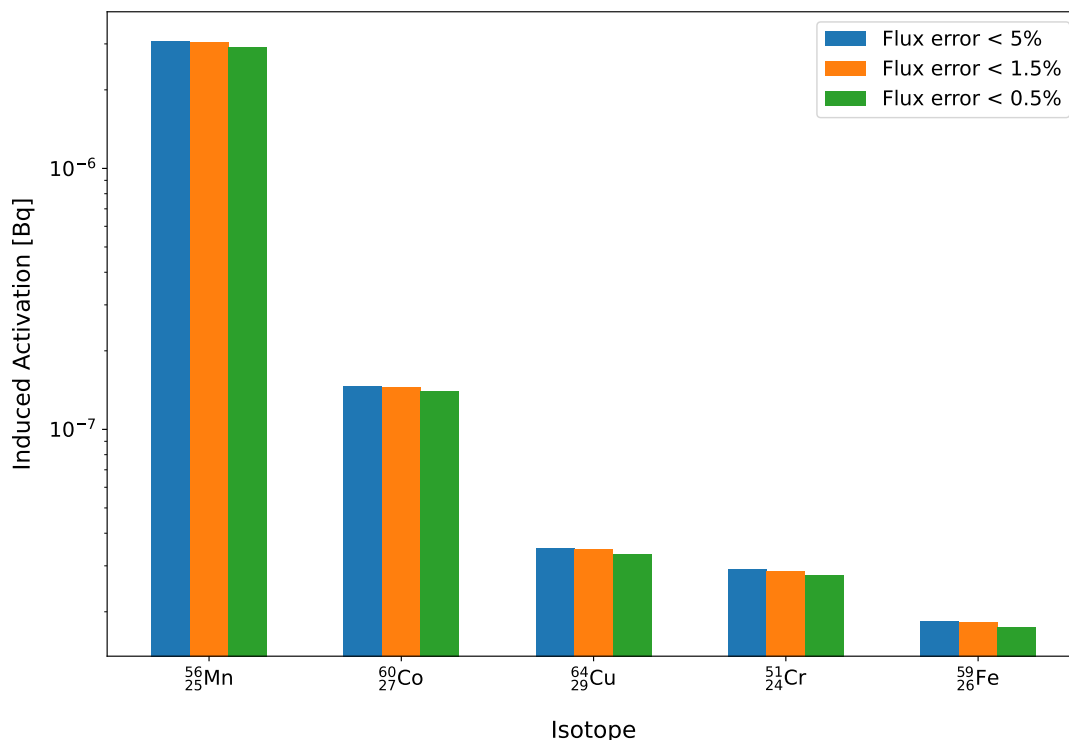
Figure 5.25: Induced activities of main gamma emitters in the activated steel sample after 1 year of irradiation.

Upon examining the total activity of the sample, it was found that these major isotopes account for approximately 85.5% of it. In this scenario, individual activity contributions of dominant radionuclides to the total activation of the steel sample remain constant. There is a reduction in activity of 3.86% and 5.29% when the flux error is lowered from around 5% to 1.5% and 0.5% respectively. As a conclusion, it is proven that improving the spectral convergence reflected also to the relative error of the average flux leads to substantial reductions in the isotopic production rates.

It is also crucial to ascertain whether any of these isotopes are derived from reactions that have a threshold in their cross section, as this could potentially influence the results based on the precision of the spectrum near the threshold areas. The uniform reduction across all isotopes analysed suggests that no threshold reactions are involved in this case. However, it is worthwhile to further investigate the reactions producing these isotopes. ALEPH provides this information, which can be viewed in Table 5.9. For this case all isotopes come from radiative neutron capture (MT=102) which as expected have no threshold in their cross section. However, it is not the case for MYRRHA sub-critical core, for which there are many threshold reaction channels available. Therefore, before doing the ALEPH calculations It is required to have well-converged detailed neutron spectra. For the KENS experiment, obtained spectrum doesn't have resonance region and also the weight windows utilized spectra are well converged.

Table 5.9: Production reactions for main gamma emitters.

Daughter	Parent	MT
^{56}Mn	^{55}Mn	102
^{60}Co	^{59}Co	102
^{64}Cu	^{63}Cu	102
^{51}Cr	^{50}Cr	102
^{59}Fe	^{58}Fe	102

5.2.7   Discussion

There are some key points that require further explanation, while others need to be emphasized or elaborated upon. Throughout this section we aim to address all of these to ensure a thorough understanding of the results obtained in the KENS shielding experiment.

Figure 5.17 displayed optimized results for simulations using weight windows from the equivalent neutron source. This implies that, among the two simulation results obtained (All-Slots and Slot-8 optimization), the best fit with the available experimental data was selected at each point. However, it's not accurate to assume that results in Slot-8 would solely derive from the simulation optimizing this specific slot, with the remaining results drawn from the all-slots simulation. In fact, even within Slot-8 data, certain reactions yielded results closer to the experimental data when using the All-Slots weight window optimization. Similarly, for some reactions in slots 3-7, simulations optimizing slot-8 provided a better fit than those where all slots were optimized.

In section 5.2.4, we discussed how optimizing results for more distant regions does not necessarily enhance them for preceding ones. What can be inferred, though, is that the computational effort required for optimizing various areas is significantly greater than focusing solely on one small region. Consequently, the design of the ADVANTG optimization mesh should be heavily influenced by the simulation's goals and the targeted performance level.

Unlike the scenario in the TIARA experiment where simulations using weight windows from a non-equivalent neutron source became unresponsive, in this instance they successfully completed and were even computationally faster than those utilizing an equivalent neutron source. The reasons behind this can be found by examining the lower bounds generated with ADVANTG in the external weight window file. It is insightful yet again to compare these values for each case to understand why this occurs. To analyze these values, we focus on areas surrounding Slot-1 and 8 across different energy ranges. We will use the weight window values obtained with the equivalent neutron source with all slots optimization as an arbitrary reference for the comparison. The relative differences between these values can be seen in Tables 5.10 through 5.12. The precise values for each one of them are available in the Annex B in Tables B.5 through B.8.

The first key aspect to point out is that values of lower bounds that come from non-equivalent neutron source are generally higher than those ones from equivalent neutron source (contrary to the case in TIARA). This means importances are lower which means that particles are not over splitted and actually more of them are be killed due to Russian roulette. As a result the MCNP run does not get stuck at certain NPS values. Tables 5.10 and 5.12 reveal variations in weight window values across different locations. The coordinates displayed in each column represent the geometric points where the weight window value is obtained. It's notable how significant the differences are in the weight windows around Slot-1 when only Slot-8 is optimized. As a result,

fewer particles will be tracked in these areas. This might decrease the computational time but also reduces the statistical data gathered from these regions. The impact of this reduction can be seen in the increased uncertainties shown in Figure 5.21 for these simulations.

Table 5.10: Comparison between Slot-8 and All-Slot optimizations using equivalent neutron source: Lower bounds of ADVANTG weight window values at different coordinates around slots 1 and 8 in the KENS experiment, presented with relative percentage differences.

Energy [MeV]	(0,0,254)	(0,0,258)	(0,0,654)	(0,0,662)
1.11E+00	4.18E+15	4.89E+15	1.73	0.43
3.01E+00	2.33E+10	4.11E+10	1.98	0.28
1.00E+01	1.51E+09	4.01E+09	1.90	0.00
2.50E+01	6.68E+07	1.69E+08	1.64	0.30
8.00E+01	1.97E+04	5.14E+04	2.80	0.24
1.80E+02	1.22E+03	2.19E+03	3.31	0.57
3.00E+02	5.50E+02	1.26E+03	3.31	0.63

Table 5.11: Comparison between All-Slots optimizations using non-equivalent and equivalent neutron sources: Lower bounds of ADVANTG weight window values at different coordinates around slots 1 and 8 in the KENS experiment, presented with relative percentage differences.

Energy [MeV]	(0,0,254)	(0,0,258)	(0,0,654)	(0,0,662)
1.11E+00	22.62	16.88	88.58	89.41
3.01E+00	12.00	45.08	88.83	89.28
1.00E+01	8.19	18.95	88.90	89.29
2.50E+01	8.98	8.97	88.91	89.29
8.00E+01	14.81	28.44	88.65	88.68
1.80E+02	50.38	16.38	87.72	86.19
3.00E+02	62.50	34.65	87.50	86.58

Table 5.12: Comparison between Slot-8 optimization using a non-equivalent neutron source and All-Slot optimization using an equivalent neutron source: Lower bounds of ADVANTG weight window values at different coordinates around slots 1 and 8 in the KENS experiment, presented with relative percentage differences.

Energy [MeV]	(0,0,254)	(0,0,258)	(0,0,654)	(0,0,662)
1.11E+00	3.68E+16	4.31E+16	824	849
3.01E+00	2.10E+11	3.71E+11	839	838
1.00E+01	1.38E+10	3.64E+10	841	839
2.50E+01	6.08E+08	1.54E+09	843	837
8.00E+01	1.81E+05	4.71E+05	830	788
1.80E+02	1.18E+04	2.70E+04	761	630
3.00E+02	5.64E+03	1.19E+04	743	648

Probably, the most important observation is that the lower bound values derived from a non-equivalent neutron source are generally higher than those obtained from an equivalent neutron

source (unlike in the TIARA case). This indicates that importances are lower, which implies that particles are not split as much, and more of them will be eliminated due to Russian roulette. Tables 5.10 and 5.12 highlight the substantial differences in weight windows around Slot-1 when only Slot-8 is optimized. As a result, fewer particles will be tracked in these areas, which will reduce the computational time but also worsen the statistics in the affected regions. This is reflected in the larger uncertainties demonstrated in Figure 5.21 for these simulations.

5.3 MYRRHA

5.3.1 Overview and Simulation Design

Upon successful testing and verification of the methodology we aimed to employ in the TIARA and KENS shielding experiments, the focus was shifted towards the application of these techniques to the MYRRHA reactor. The MYRRHA reactor can operate in two configurations: critical or subcritical. In the critical configuration, the core has an effective neutron multiplication factor (k_{eff}) of 1, indicating a stable, self-sustaining fission chain reaction. Conversely, in the subcritical configuration, the MYRRHA reactor operates as an ADS. In this setup, a 600 MeV proton beam is directed into the core's center, specifically towards the spallation target assembly. Here, the protons interact with Lead-Bismuth Eutectic (LBE), which serves as the spallation target. This interaction generates secondary neutrons, thereby initiating the fission chain reaction within the core. Consequently, when MYRRHA operates as an ADS, $k_{eff} < 1$, denoting that an external neutron source is required to sustain the fission process.

Our primary objective in this simulation was to reduce uncertainties linked to Monte Carlo methods within the vessel of MYRRHA. In achieving this, we utilized MCNP6.2 simulations, employing the JEFF-3.1.2 nuclear data library. Our particular interest was in the activation of materials, specifically the stainless-steel vessel materials. By doing so, we aimed to accurately assess the decay time required after 40 years of operation, which is crucial for enabling more precise activity dose calculations for workers when decommissioning begins.

Our workflow to tackle this problem resembled our approach in previous case studies. Initially, we carried out a series of analogous MCNP simulations to gain a deeper understanding of how uncertainties augment as the distance from the core increases. Our focus was not only on the uncertainties in neutron flux but also on those that propagate into the neutron spectrum. This aspect is significantly important to our study as the spectrum is integral to irradiation calculations. As demonstrated in Section 5.2.6, it can considerably influence the results. Subsequently, our work centered on the creation of an equivalent neutron source. This task presented a significant challenge, wherein various strategies were considered; for more detail, refer to Section 5.3.2. Once we obtained the equivalent neutron source, we executed several ADVANTG simulations, testing different parameters. The process finished with the conduction of final MCNP simulations to verify our results using the variance reduction parameters acquired from ADVANTG.

The first step involves examining the flux via a set of analog MCNP simulations, and understanding how the error propagates into the spectrum at varying distances from the reactor core. Figure 5.26 illustrates a continuous logarithmic decrease in the neutron flux across the LBE, along with some noticeable dips when passing through the stainless steel constituting the primary and safety vessels.

Furthermore, the uncertainties associated with the flux noticeably increase as the distance from the source expands. Table 5.13 provides the neutron flux uncertainty values for various points along the x-axis. The influence of the primary vessel on the neutron flux is clear; there are more interactions between the particles and the material, thereby preventing the particles from reaching farther regions and drastically reducing the statistics.

This simulation was performed using 5.0E+06 source particles (NPS), making use of 144 CPUs. The entire process required a duration of five days to reach completion.
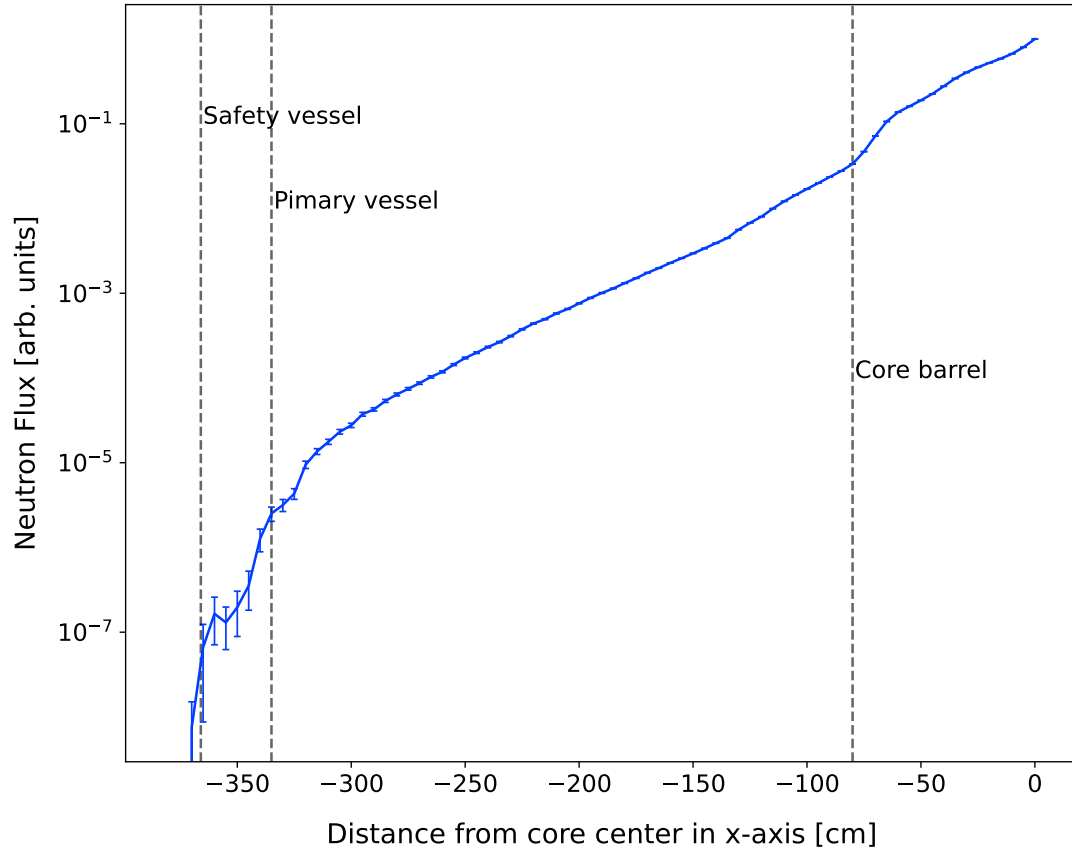
Figure 5.26: Analog MCNP simulation of neutron flux along the x-axis in MYRRHA reactor.

Table 5.13: Neutron flux uncertainties at varying distances along the x-axis from the center of MYRRHA reactor.

X [cm]	Uncertainty [%]
-50	0.07
-100	0.14
-300	1.41
-340	14.52

Figures 5.27, 5.28, and 5.29 below illustrate the neutron spectrum at various depths of shielding, demonstrating the impact of increased flux uncertainties on the spectrum. The augmentation in uncertainties is accompanied by a lack of proper convergence in the spectrum itself. As highlighted in Section 5.2.6, this can have significant implications for irradiation calculations, particularly when threshold reactions are involved. It is worth noting that Figure 5.29 presents the spectrum within an area between the primary vessel and the safety vessel. Calculations for the neutron spectrum at the distance of the safety vessel yielded poorer results, escalating the uncertainties in the spectrum to more than 37%.
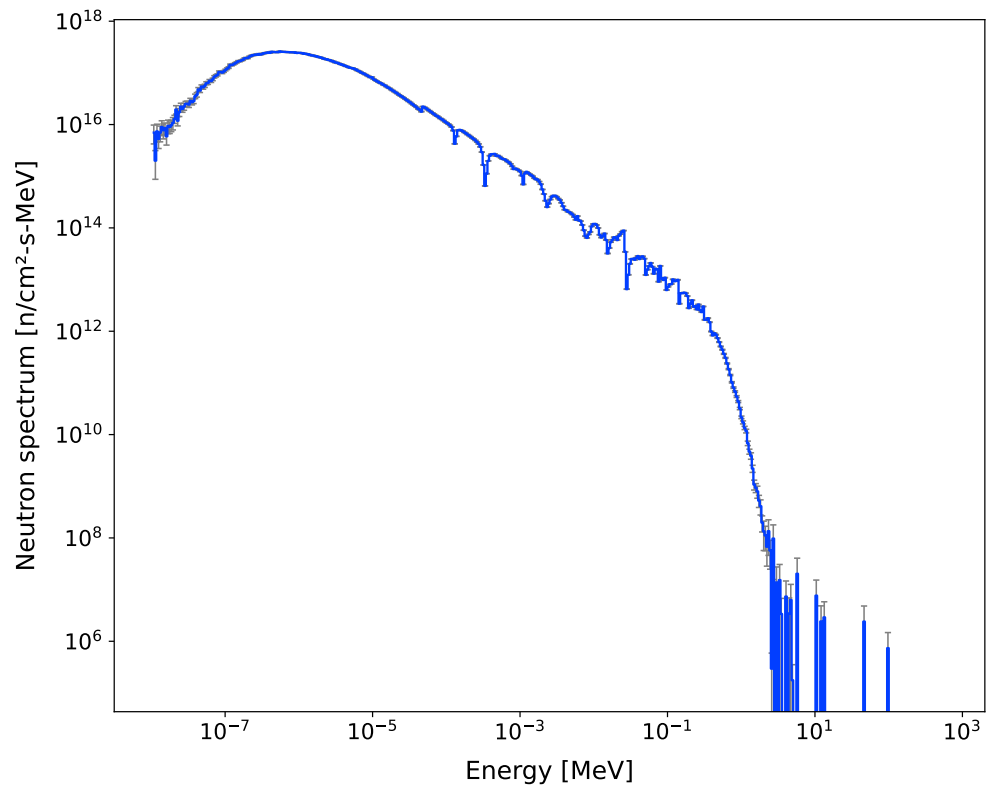
Figure 5.27: Neutron spectrum at a distance of 100 cm in the x-axis from the center of the MYRRHA reactor core.
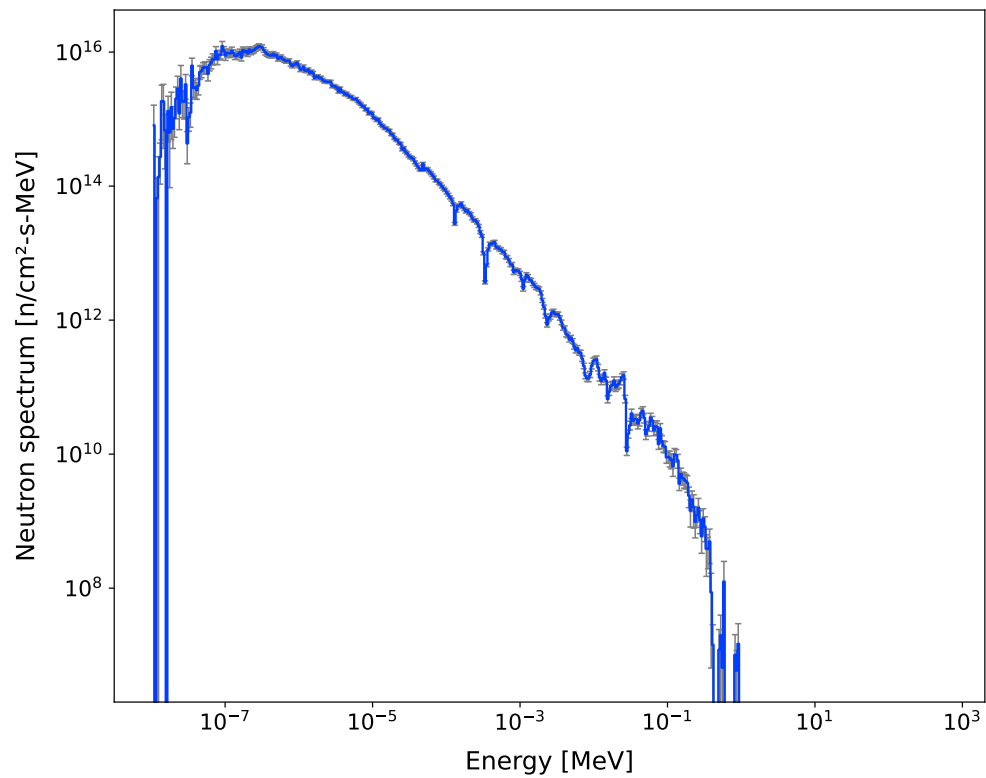
Figure 5.28: Neutron spectrum at a distance of 300 cm in the x-axis from the center of the MYRRHA reactor core.
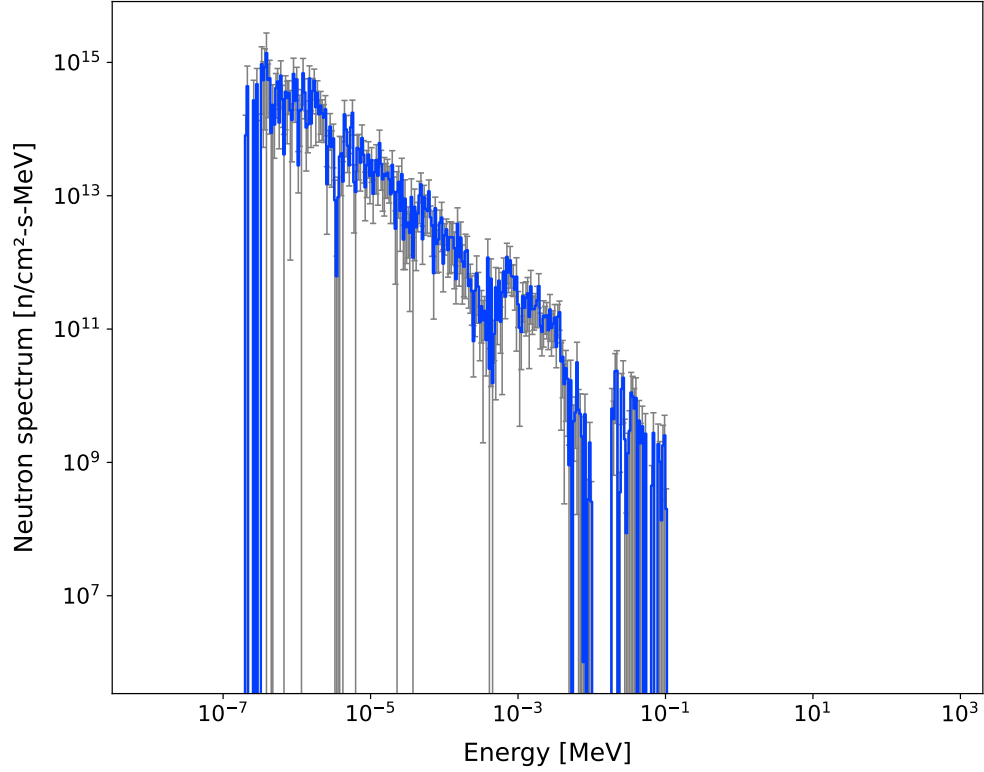
Figure 5.29: Neutron spectrum at a distance of 340 cm in the x-axis from the center of the MYRRHA reactor core.

5.3.2 Equivalent Neutron Source

The critical configuration has a more isotropic neutron distribution, while the subcritical one is less balanced due to the way the reactions are induced with the proton beam aimed at the spallation target assembly. This difference is important for our study and will have to be taken into consideration when we creating the fixed source for our neutron calculations. Because the subcritical configuration is the most complex, we focused our efforts on making a fixed source that could accurately mimic this setup while being compatible with ADVANTG software. It was our hope that this same source definition would apply satisfactorily to the more isotropic profile of the critical configuration as well.

Unlike previous scenarios where secondary neutrons were generated exclusively in the spallation target, MYRRHA involves the entire core undergoing fission. These fissions contribute to the chain reaction that maintains the reactor's operation when active. Furthermore, the spallation target is not a single material component, as in the case of TIARA (Lithium-7) or the KENS shielding experiment (Tungsten). Instead, it comprises an entire assembly filled with LBE coolant, which functions as the spallation target. This setup distributes the material over a larger volume.

A primary constraint we face when defining the fixed source for compatibility with ADVANTG is that it allows only one independent distribution. Any other defined distributions must be dependent on this primary one. Consequently, if we make a source definition using the energy parameter'erg' as an independent distribution, any additional parameters we wish to incorporate into the source definition (such as position 'pos' or direction 'dir') must be dependent on the energy distribution. This presents a challenge, as the position and energy, or direction of particles

and energy, are not necessarily related, making the definition of one distribution as dependent on the other infeasible.

To generate the fixed source, it is necessary to extract relevant data from the core. This data must encompass comprehensive information that allows the subsequent definition of an appropriate fixed source that exhibits a similar behavior to a critical source. Thus, the data of interest should include aspects such as neutron flux, spectra, and direction at various positions. This data would be obtained through analog MCNP simulations. However, prior to this, it is crucial to delineate the approach to be adopted, given that there are multiple potential strategies, as assessed initially, that could feasibly be implemented. These strategies include:

1. **Utilizing the Surface Source Write (SSW) card of MCNP, in conjunction with the MCPL tool to interpret the data.** The SSW would be defined at the core barrel. This specific MCNP card logs every particle that reaches a particular surface in a certain direction, recording the exact position, energy, direction, and weight of each particle. This information is saved in a .w file that can be accessed via the MCPL tool. By retrieving this information, a fixed source could be defined adjacent to the core barrel, thereby ensuring that the particles emitted outside the barrel maintain the same properties as those in the original simulation.

2. **Establishing the fixed source at the spallation target assembly.** All protons coming from the LINAC react within the spallation target, thereby creating the secondary neutrons that subsequently induce fission reactions. This approach entails obtaining the neutron particle information at the surface of the spallation target assembly. In this scenario, the fixed source is only delineated within the spallation target assembly. By accurately defining the properties of the secondary neutrons produced post-spallation, the rest of the core would keep the original behavior exhibited with the proton source. As one might anticipate, this approach would result in a highly anisotropic fixed source, due to the directional orientation of the protons derived from the accelerator.

3. **Developing the fixed source across the entire core volume.** This approach needs that the reactor's core is thoroughly tallied with an appropriate mesh in MCNP. Once the data is recorded, numerous isotropic point sources could be established throughout the core volume, ensuring the final results mirror the behavior of the critical core. In terms of creating the mesh, two possibilities were examined:

   (a) Cylindrical coarse mesh.
   (b) Cylindrical mesh at the fuel assembly level.

The most effective approach, proven by the results, was found to be the last one described above (3b). This will be further detailed below. Nonetheless, the other strategies retain their relevance and were explored to varying degrees. To provide a comprehensive understanding of what worked and what did not, detailed information regarding these approaches can be found in Annex C.

The method we used involved looking at each fuel assembly in the reactor core one by one. For this, we created individual mesh for each assembly using the FMESH4 MCNP tally. This tool lets us make either round (cylindrical) or square (rectangular) meshes. Since the fuel assemblies in MYRRHA's core are shaped like hexagons, we thought a cylindrical mesh would be more fitting (see Figure 5.30). Remember, the goal here is to gather the right data to create isotropic point sources across the whole core. This data is derived from the FMESH4 tally, whereby each voxel defined within the mesh tally enables the definition of an isotropic source.
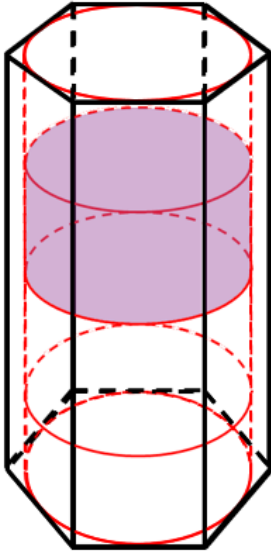
Figure 5.30: Scheme of the FA geometry (black) and the mesh used for tallying (red) with one of its voxels shaded in purple.

This methodology does, however, encounter a challenge. Specifically, the smaller the voxel size, the greater the number of isotropic point sources, thereby improving the core definition. Conversely, the reduction in voxel size tends to worsen the statistical output for each energy bin, potentially affecting the point source definition and introducing undesirable biasing. As such, it becomes essential to find a balance in the size of the voxels as defined via the FMESH4 tally. The illustration provided in Figure 5.30 - where the voxels are indicated in a distinctive shade of purple - serves as a visual representation of the fuel assembly geometry, showcasing the mesh layout with its axial divisions. Ideally, the voxels should encompass as many points as possible without compromising the convergence in the tally results for each voxel.

One of the essential steps involved the specification of the exact volume that would be tallied, which depended on the number of assemblies to be covered by the mesh and the vertical extent of coverage. Various possibilities, such as covering only fuel assemblies or incorporating cooling and reflector assemblies, and covering different heights such as the entire assembly versus the active height, were explored. After conducting multiple tests to ascertain the effects of different parameters, an optimal setup was determined based on statistical accuracy and computational time-efficiency. This optimal setup includes:

- A cylindrical mesh specific to each fuel assembly, excluding cooling or reflector assemblies.

- An axial height for each cylindrical mesh equal to the active height of 70cm.

- Each cylindrical mesh is divided axially into 14 divisions, resulting in voxels of 5cm height each.

Generating the equivalent neutron source is a two-step process. First, we acquire the tally results. Second, we need to convert the information from these tallies into a format compatible with the SDEF card in MCNP6.2, which also works with ADVANTG3.2. While MCNP6.2 offers various ways to structure these SDEF cards, not all of these methods are compatible with AD-VANTG3.2. Notably, when using ADVANTG, the source definitions have certain constraints; the most significant being the allowance of only one independent distribution. On top of that, there are specific limitations inherent to MCNP's source definitions that may pose challenges. For example, MCNP6.2 only permits distribution numbers (used to define the type of distributions) from 1 to 999 when setting up a source. As a result, it is not feasible to assign a unique distribution to each individual voxel in the mesh.

The SDEF card, designed by considering all these factors, is extensively explained in Annex D. The whole card is stored in an external txt file, which MCNP can then access using the 'Read file' card. The initial line of the source definition is as follows:

```
sdef erg=d1 pos=ferg=d500 wgt=1.0 par=n
```

This line indicates that energy is treated as the independent distribution following 'd1', while position follows a distribution that is dependent on the energy, defined as 'd500'. The particle weight is not adjusted in the source definition since it will be managed by the weight windows, and the particles emitted are neutrons. Given the way this source definition is structured, the maximum energy bins compatible with MCNP's restrictions amount to 498 bins.

It's worth noting that this source definition doesn't contain any directional bias; this means all point sources will emit particles isotropically. By doing this, we introduce a significant bias to the equivalent neutron source, which needs to be thoroughly tested to ensure its proper functioning and verify that it does not alter the neutron flux or spectrum, particularly in regions close to the vessel where the irradiation calculations will be conducted.

The entire process, including the tally definition of the core region, data extraction from the FMESH4 tally results, and the creation of the external source file with the SDEF card, has been automated using Python. The actual codes, due to their length, are not included in this document. However, readers interested in them can reach out to the author.

5.3.3 ADVANTG Simulations

Optimizing ADVANTG mesh, as proved in TIARA and KENS shielding experiments, is key for obtaining efficient results on the final MCNP run. Lessons learned in those cases can help us determine the correct mesh that should be used, nonetheless, MYRRHA has an extra difficulty that was not present in either of previous cases. This are the fission that occurs in the core, which creates an additional source of particles that will also be affected by the weight windows and that were not present before. ADVANTG forces to include inside the mesh all the source inside the geometry, which means a mesh has to be defined in the core region. How this mesh should be defined and how may it affect the final MCNP simulation is something that has not been able to be verified with previous scenarios and therefore had to be tested directly with MYRRHA's input. Also, another difference is the material in which particles propagate. This is particularly important for the size of the mesh across the shielding area. For TIARA it was used iron or concrete, for KENS it was concrete, here we have LBE. The change of materials affects the mean free path which might be relevant for mesh size definition of the weight windows.

Optimizing the ADVANTG mesh, as demonstrated in the TIARA and KENS shielding experiments, is key for obtaining efficient results in the final MCNP run. The insights gained from these instances can guide us in deciding the appropriate mesh to use. However, the MYRRHA scenario adds an extra layer of complexity, not encountered in the previous cases. This arises due to fissions occurring in the core, which generates an additional source of particles. These particles are also influenced by the weight windows and were not a factor in previous scenarios.

ADVANTG forces the inclusion of all sources within the geometry in the mesh, implying that a mesh must be defined in the core region. The way this mesh should be established and its potential impact on the final MCNP simulation could not be verified through prior scenarios, and therefore, had to be tested directly using MYRRHA's input. Additionally, the material through which the particles propagate varies, which significantly influences the mesh size across the shielding area. While iron or concrete was used for TIARA and concrete for KENS, MYRRHA involves LBE. The change in materials impacts the mean free path of neutrons, which may be a critical factor when defining the mesh size for the weight windows.

We tried to maintain the ADVANTG input parameters as consistent as possible with those employed in previous scenarios (TIARA and KENS), aiming to prevent the introduction of

any new bias. Table 5.14 displays the main parameters used in the ADVANTG input. For parameters such as 'denovo_x_blocks', 'denovo_y_blocks', and 'denovo_z_blocks', optimization was performed to make full use of the 72-CPU cluster capabilities. These values were dependent on the mesh definition and were adjusted for optimization. For more details on this, refer to [1]. Each conducted simulation took less than an hour.

Parameter	Value
method	fwcadis
fwcadis_spatial_treatment	pathlength
fwcadis_response_weighting	False
library	HILO2K

Table 5.14: Key parameters used in the ADVANTG input for KENS shielding experiment.

We tested several meshes by varying the following parameters:

- The volume encompassed by the mesh. Given MYRRHA's considerably larger geometry compared to TIARA and KENS, covering the entire mesh is possible, but it leads to longer computational times. An alternative could be covering the core and the region towards the vessel in one axis direction (the least shielded one). Here, the mesh's height is also relevant, it could span the active height, the fuel assembly (FA) height, the barrel height, or the entire height of the geometry.

- Mesh size in the core and non-critical areas. The core must be included in the mesh, but the mesh's fine-tuning inside the core can vary. A finer mesh would increase the computations when running the final MCNP simulation, particularly due to the high particle density in that region. Conversely, a very coarse mesh might not provide enough detail for calculations, and many particles might be killed before reaching the vessel (where we want to improve statistics). Also, if the mesh spans the entire geometry, the mesh size in the regions where particle tracking is not our focus must be defined and the same problematic arises.

- Mesh size in the area of interest. Prior experiments have shown that a finer mesh near the detectors yields satisfactory results when used with MCNP. This suggests that the mesh in areas surrounding the vessel should be sufficiently small (the same size as those used in TIARA and KENS – 2-5cm). As for the mesh across the shielding, different sizes require testing to ensure the proper splitting of neutrons.

Even with the knowledge gathered from the validation and verification process, it's clear that finding the optimal mesh in such complex geometry involves much trial and error. As evidenced in Sections 5.1 and 5.2, the chosen mesh significantly influences the final MCNP run, it can either enhance efficiency if well-defined, or severely impede it to the point where simulations won't finish due to excessive particle splitting. As of now, we have not found the ideal balance where statistics in the vessel are improved when using weight windows. The most persistent issue has been that simulations often get stuck at a certain number of NPS due to oversplitting. Therefore, no additional results can be provided in this section.

5.3.4 MCNP Simulations

The initial MCNP simulation retrieves reactor data for creating the fixed source, as detailed
in Section 5.3.2. Accuracy is critical at this stage, as any bias or uncertainty will propagate
to subsequent steps. FMESH4 tallies facilitate data retrieval, with one required for each fuel
assembly. A Python script was developed to automate this potentially error-prone and time-
consuming task, generating MCNP6.2 FMESH4 tallies for direct copying to the input. An
example of these tallies is shown below.

```
fc4 FA_4
FMESH4:n GEOM=cyl ORIGIN=-36.200,0.000,-35.000 AXS=0,0,1 VEC=1,0,0
         IMESH=5.225 IINTS=1
         JMESH=70 JINTS=14
         KMESH=1 KINTS=1
         EMESH=1e-08 496log 600
         OUT=COL
```

For this example a cylindrical mesh is defined following the description provided in Figure 5.30
and in 498 energy bins from 1.0E-08 to 600 MeV. For better understanding of the FMESH4
definition refer to [2].

The same simulation used to obtain the neutron spectrum generated this data, utilizing 5.0E+06
source particles (NPS) and 144 CPUs. The entire computation process spanned five days. We
assumed the equivalent neutron source to be working correctly if the radial, axial, and angular
neutron flux distributions obtained using the equivalent neutron source matched those obtained
using the proton source. To confirm the effective performance of the equivalent neutron source,
it was necessary to carry out some MCNP simulations to obtain and examine the neutron flux
distributions. Both simulations, with original proton source and equivalent neutron source were
run for 24 hours using 72 CPUs. In that time, NPS for proton source reached 1.5E+06 and NPS
for the equivalent neutron source 1.96E+07.

Figure 5.31 illustrates the radial distribution along the x-axis when $(y, z) = (0, 0)$. It is notewor-
thy that this corresponds almost perfectly with the original proton source across all distances.
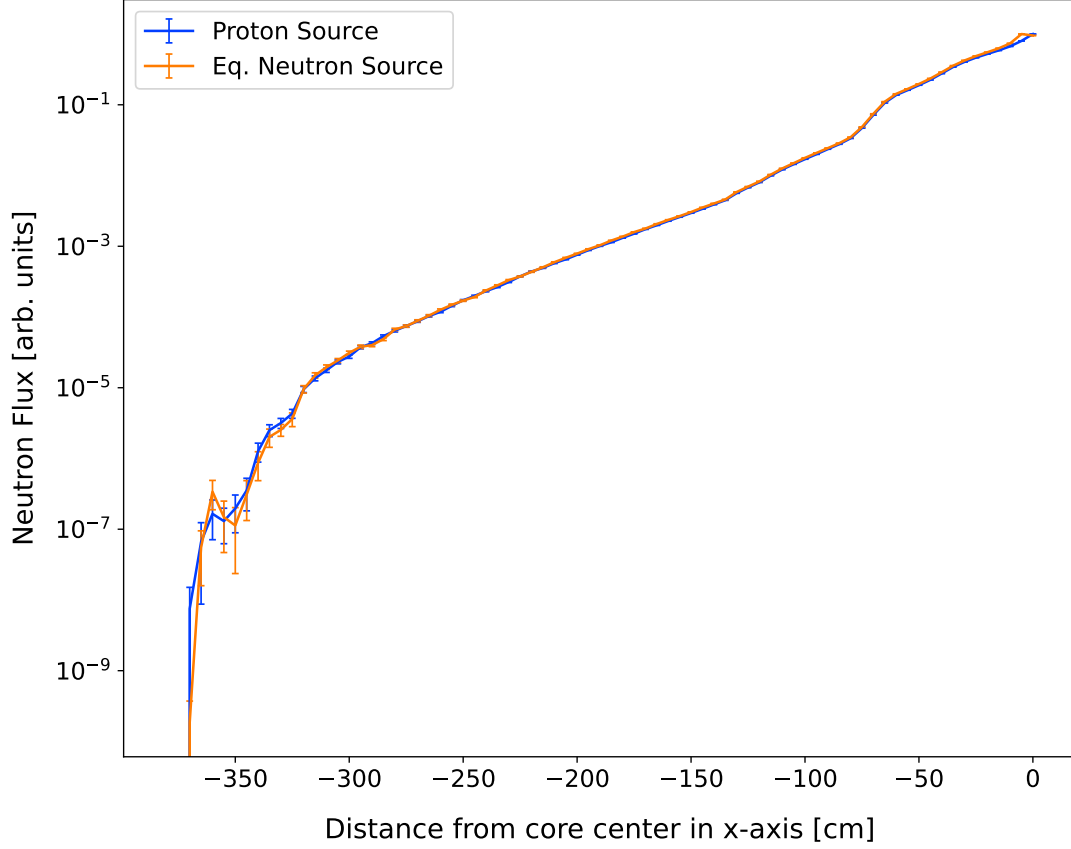
Figure 5.31: Radial neutron flux comparison along the x-axis for $(y, z) = (0, 0)$: Proton source vs. Equivalent neutron source.

Figure 5.32 through 5.35 present the axial neutron flux at various distances along the x-axis from the center of MYRRHA's core. As observed, the outcomes align nearly perfectly across all distances. At 300 cm, the results begin to show signs of incomplete convergence, however it is still clear that the profiles displayed by both simulations share a strong resemblance.
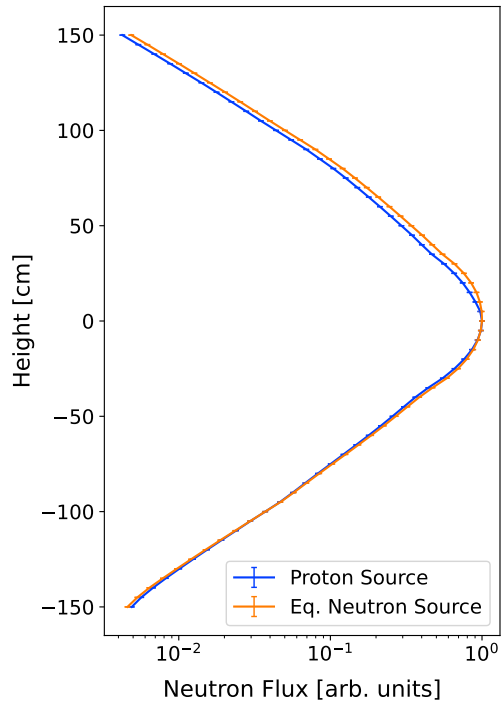
Figure 5.32: Axial neutron flux comparison at x=25 cm: Proton source vs. Equivalent neutron source.
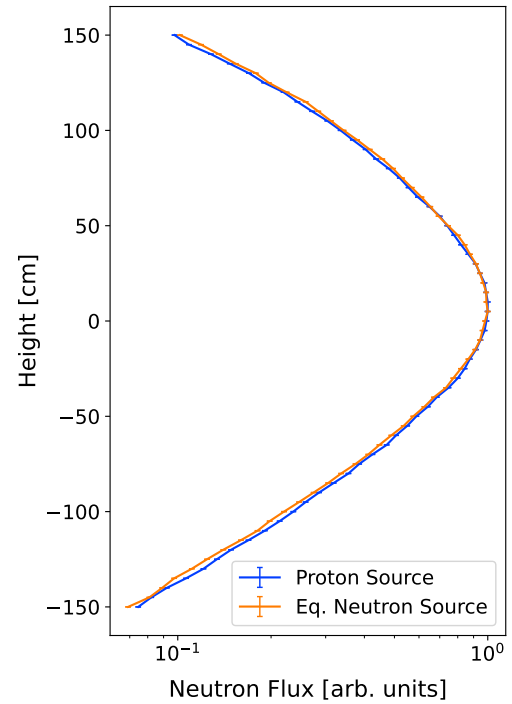
Figure 5.33: Axial neutron flux comparison at x=150 cm: Proton source vs. Equivalent neutron source.
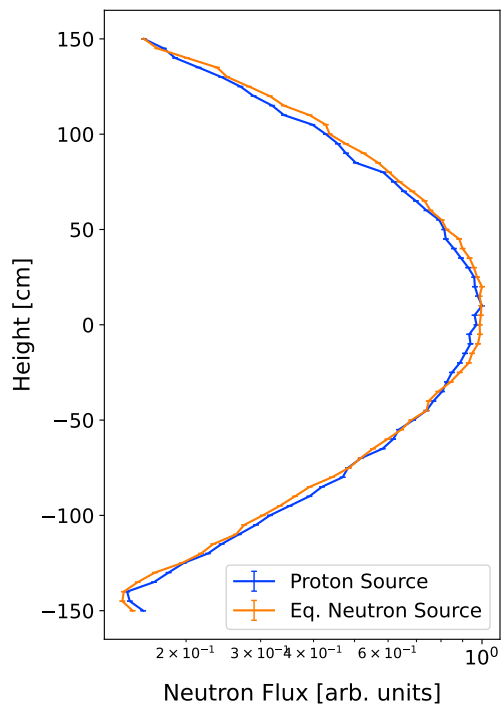
Figure 5.34: Axial neutron flux comparison at x=200 cm: Proton source vs. Equivalent neutron source.
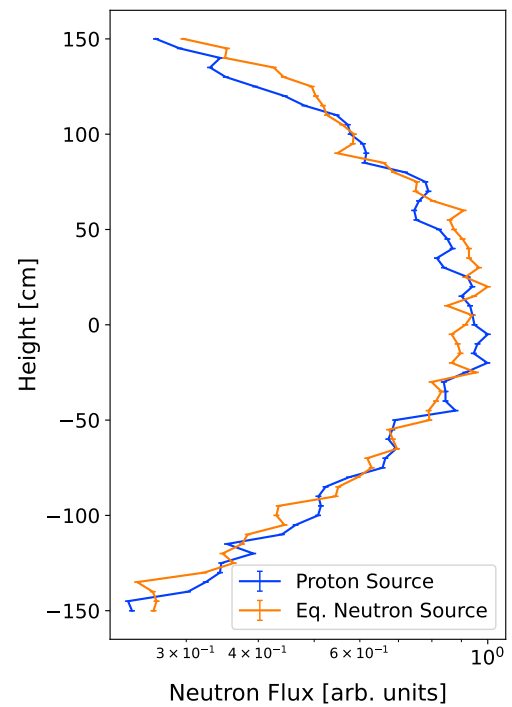
Figure 5.35: Axial neutron flux comparison at x=300 cm: Proton source vs. Equivalent neutron source.

Figures 5.36 and 5.37 illustrate the angular neutron flux distribution at $z = 0$ for distances of

150 cm and 300 cm, respectively, along the x-axis from the center of MYRRHA's core. For these cases, only one third of the entire core was tallied owing to the reactor's symmetry. These results highlight the effect that various components of the reactor have on the neutron flux. As neutrons traverse different elements such as the primary pump chimneys and the PHX chimneys, the flux values increase and decrease accordingly (refer to Figure 3.6 for the geometry).
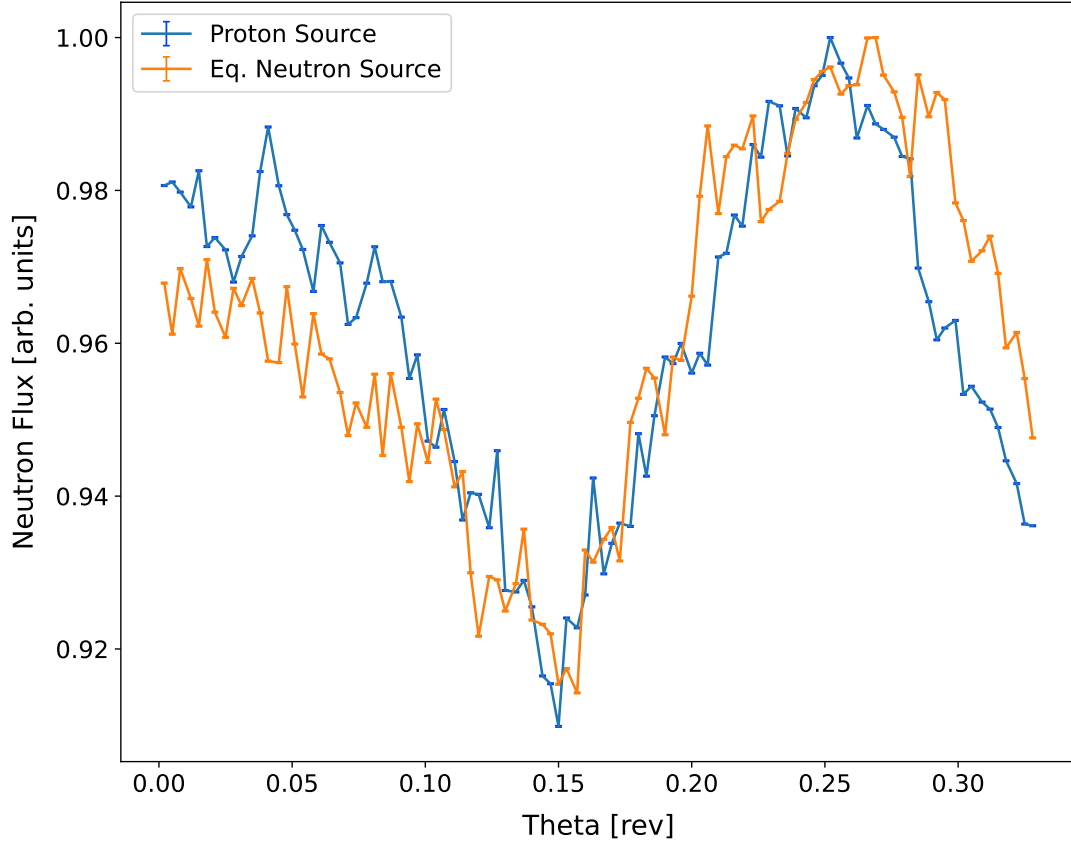
Figure 5.36: Angular neutron flux at $(x, z) = (150, 0)$ cm: Proton source vs. Equivalent neutron source.
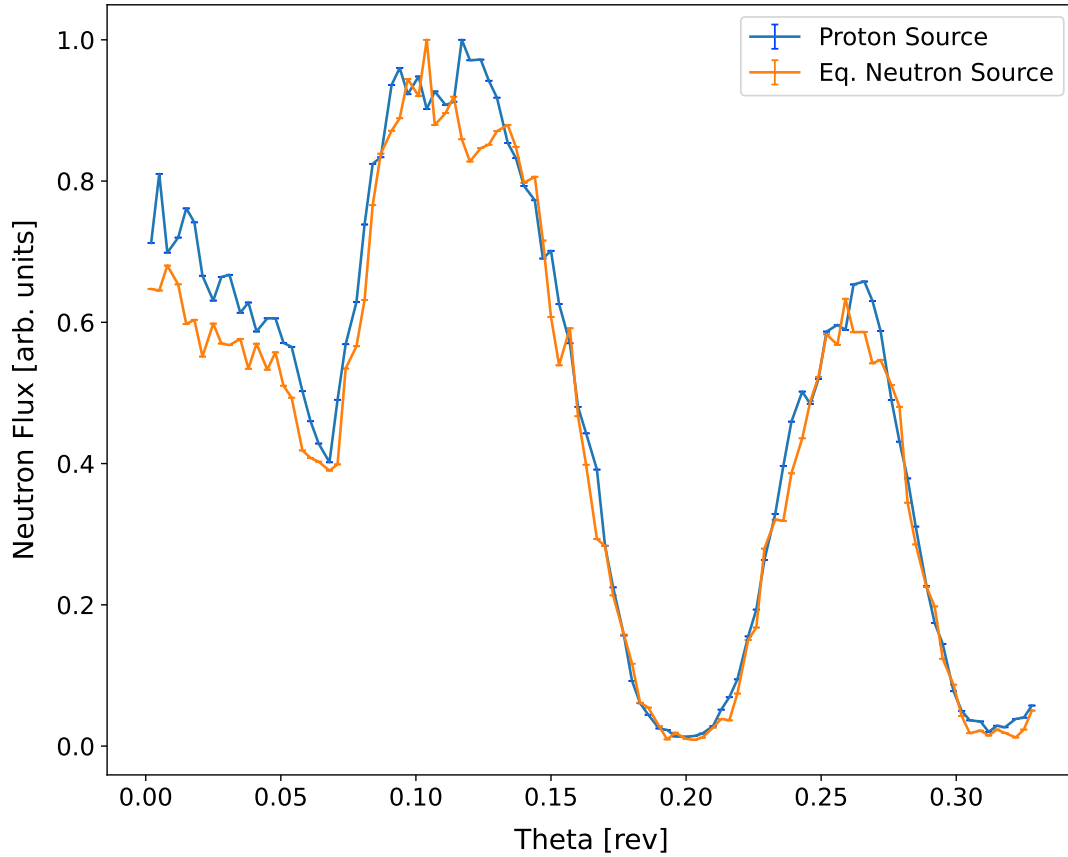
Figure 5.37: Angular neutron flux at $(x, z) = (300, 0)$ cm: Proton source vs. Equivalent neutron source.

After comparing radial, axial, and angular distributions for the proton and fixed sources, we can affirm the equivalent neutron source's behavior is sufficiently accurate for ADVANTG calculations in subcritical core configurations.

We also evaluated whether the source definition and methodology could be adapted for the critical core configuration. This necessitated a new set of simulations, beginning with an MCNP tally of the reactor's core to derive data for the fixed source. This simulation employed the critical core configuration of the MYRRHA reactor, running for 100 cycles with 2.0E+05 particles per cycle and 72 CPUs. We then created a fixed source similar to the one used before (see Annex D).

Figure 5.38 displays the radial distribution comparison along the x-axis at $(y, z) = (0, 0)$. The neutron flux remains consistent across the axis, with slight variations at the core's inner edge and end. The latter, potentially due to poor statistics in that region. Figures 5.39 through 5.42 illustrate the axial neutron distribution at various x-axis distances. Each demonstrates a high degree of similarity between the critical core and fixed source simulations. Comparable observations can be made from Figures 5.43 and 5.44, where the simulations align closely, mirroring previous findings. The influence of differing core materials is also reflected in the neutron flux.
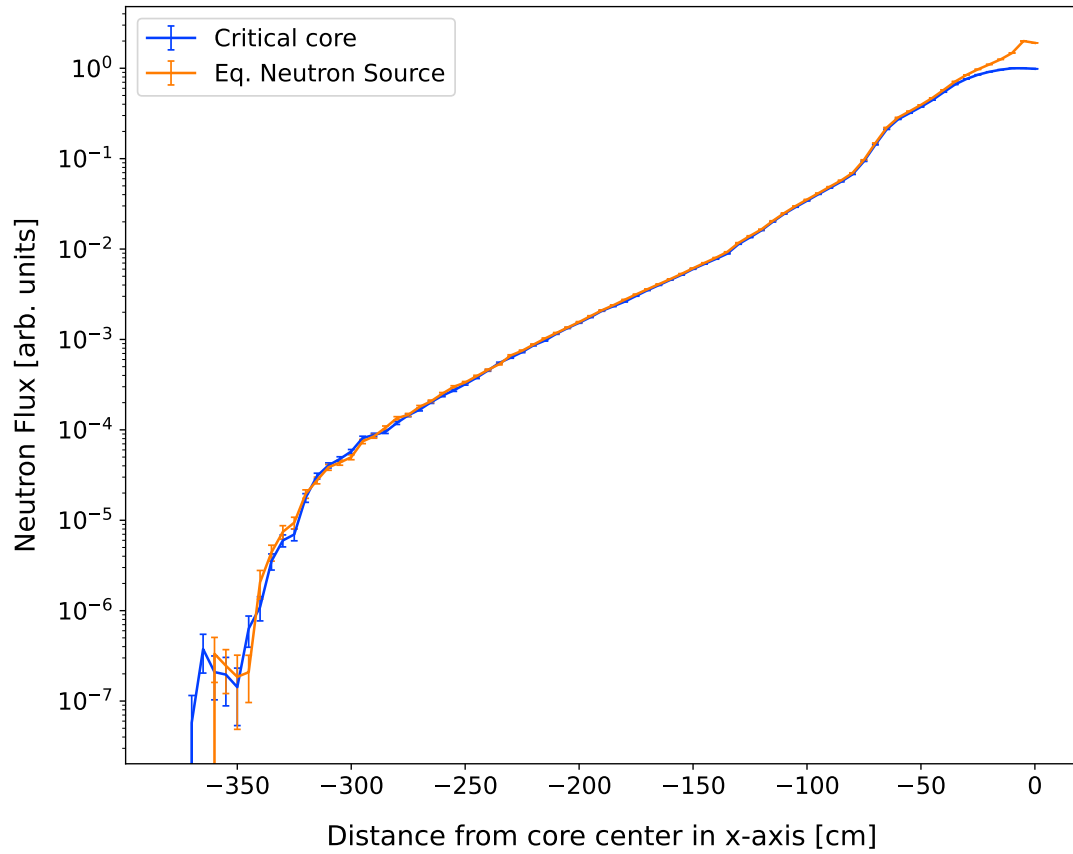
Figure 5.38: Radial neutron flux comparison along the x-axis for $(y, z) = (0, 0)$: Critical source vs. Equivalent neutron source.
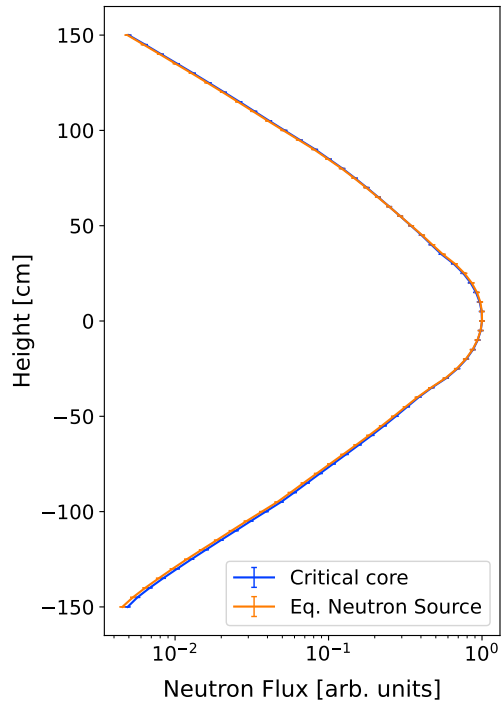
Figure 5.39: Axial neutron flux comparison at x=25 cm: Critical source vs. Equivalent neutron source.
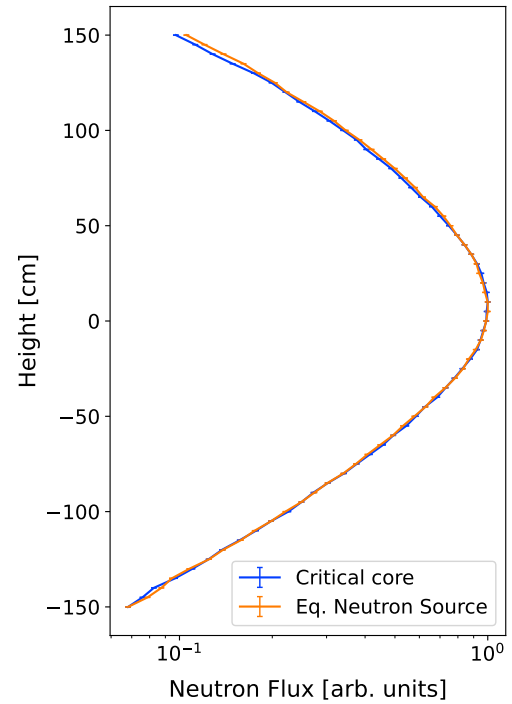
Figure 5.40: Axial neutron flux comparison at x=150 cm: Critical source vs. Equivalent neutron source.
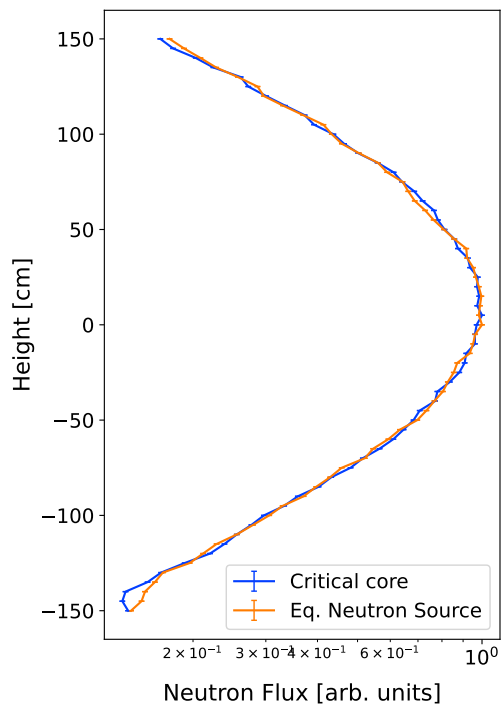
Figure 5.41: Axial neutron flux comparison at x=200 cm: Critical source vs. Equivalent neutron source.
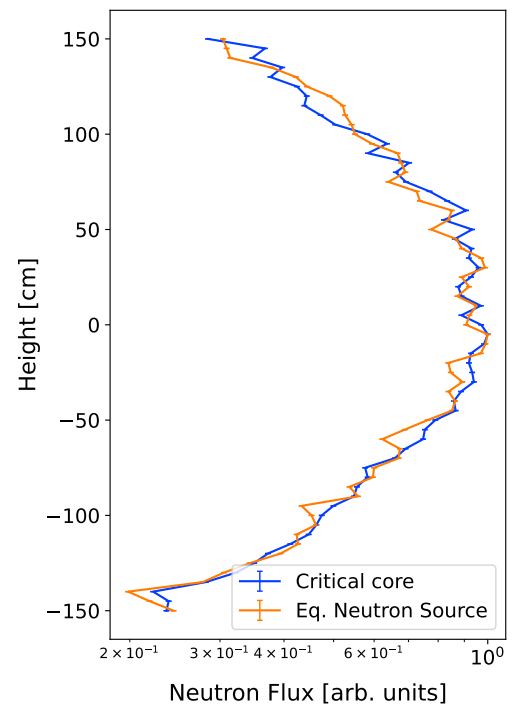
Figure 5.42: Axial neutron flux comparison at x=300 cm: Critical source vs. Equivalent neutron source.
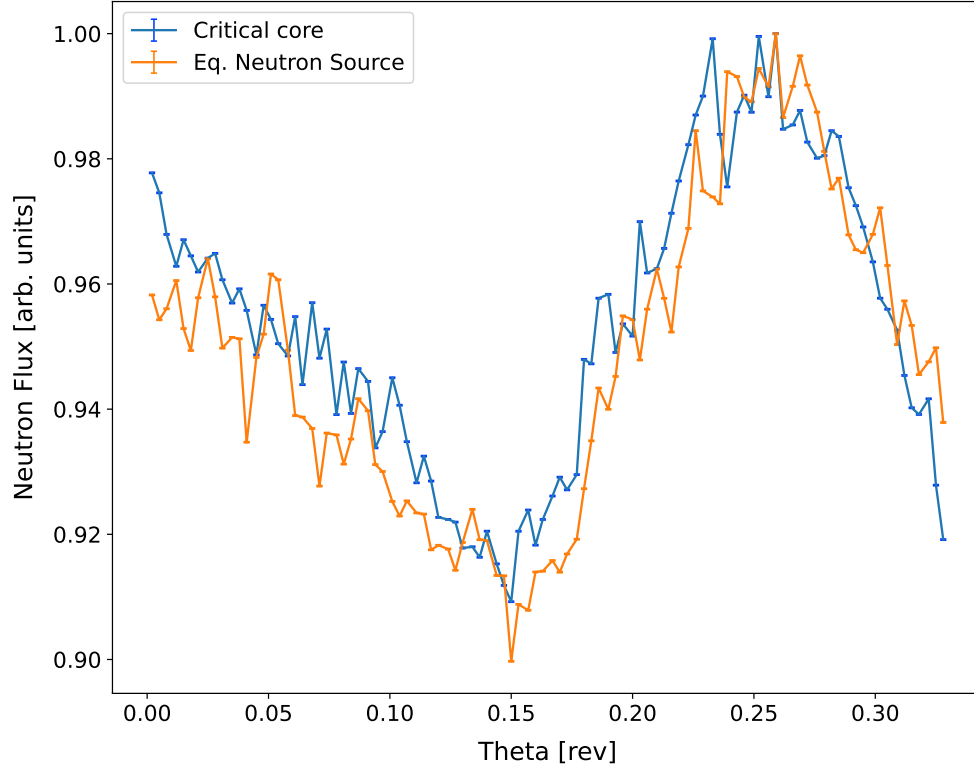
Figure 5.43: Angular neutron flux at $(x, z) = (150, 0)$ cm: Critical source vs. Equivalent neutron source.
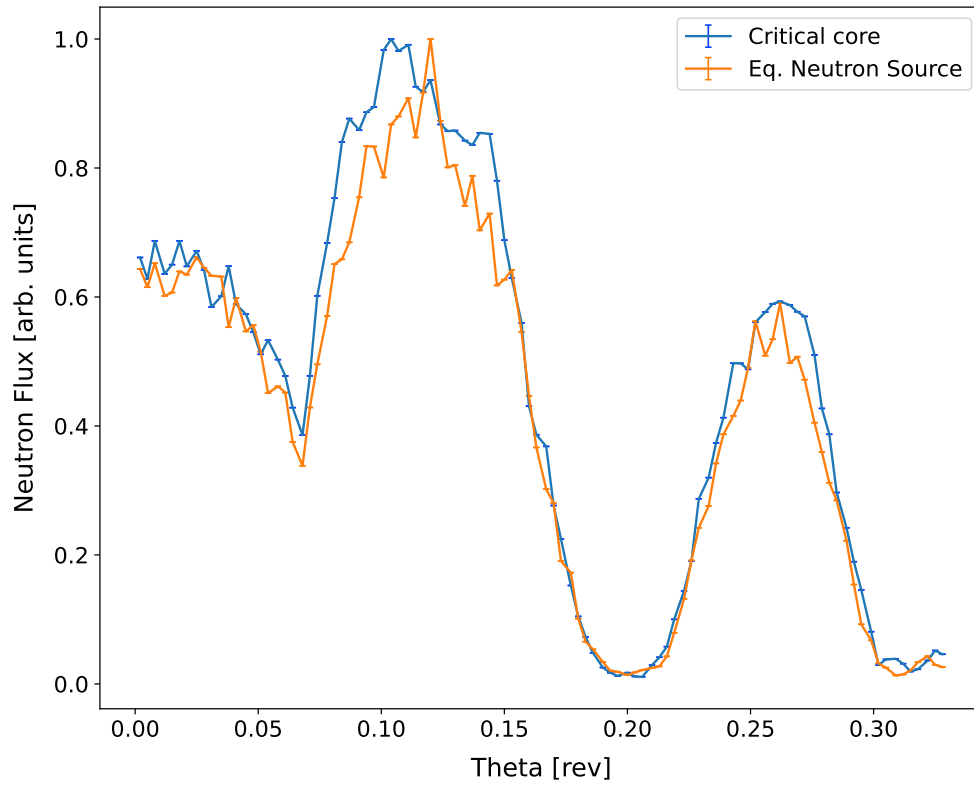
Figure 5.44: Angular neutron flux at $(x, z) = (300, 0)$ cm: Critical source vs. Equivalent neutron source.

As referenced in Section 5.3.3, we were unable to achieve successful outcomes from the final MCNP simulations run in conjunction with ADVANTG. Consequently, we could not analyze any irradiation calculations or performance metrics for MYRRHA. Nonetheless, significant progress was made, laying a robust groundwork for future investigations. Moreover, the results we did obtain offer valuable insights, which will be discussed in the following sections.

5.3.5 Discussion

It is crucial to point out that the fixed source developed in Section 5.3.2 is used only for the ADVANTG simulation. Its purpose is to compute the values for weight windows using deterministic calculations. In the final MCNP run, where the Monte Carlo simulation uses the previously ADVANTG-calculated weight windows, we go back to using the original source (proton beam or critical core). This step is taken to avoid any unwanted influence from the source.

However, as highlighted in Section 5.1 and cited in [15], the proper application of source biasing can indeed prove to be a valuable technique for variance reduction. By directing particles towards key areas, source biasing can bolster statistical results and reduce the time required for computations. In the context of MYRRHA specifically, the use of an equivalent neutron source in simulations has enabled us to achieve comparable statistical outcomes 10% faster, while still maintaining the simulation's accuracy in comparison to the original proton source or the criticality source.

Notwithstanding these improvements, we believe there's still potential for further refining the fixed source. In this instance, our comparison was limited to neutron flux distributions. For a more comprehensive analysis, we could also compare the neutron spectra at various locations, ensuring that the generated neutron spectrum aligns with the behavior of the original source's neutrons. This could lead to even better results that are closer to those from proton source and critical source simulations, while also reducing the time required for computations even more.

In addition to these points, it's worth noting that this approach presents an efficient and accessible way of applying variance reduction techniques to this particular problem (MYRRHA). This can be done without having to delve into the complexities of weight windows and ADVANTG, which require more specific knowledge and can be time-consuming to understand and implement. In other scenarios where statistics may need moderate improvement, this could serve as a suitable option.

6   CONCLUSIONS

In this chapter, we gather the conclusions drawn from all our research and experimental work. The knowledge we have gained from various sources and the simulations explained in Chapter 5 play a key role here. The conclusions are divided into four sections: Summary of Findings, Implications, Limitations, and Future Work. In each section, we focus on the unique conclusions we obtained from each of the three experiments: TIARA, KENS shielding experiment, and MYRRHA. Each experiment contributed valuable insights to our understanding.

Towards the end of this chapter, there is a section titled 'Final Conclusions'. Here, we draw overarching conclusions about the entire thesis, tying together all our learnings. This section offers a comprehensive summary of the work and marks the completion of this thesis.

6.1   Summary of Findings

The TIARA experiment was a key starting point in this thesis, demonstrating the viability of using an equivalent neutron source as a variance reduction technique for proton-driven problems. However, this finding's utility was observed to be dependent on specific factors such as particle energy and shielding thickness. Drawing from the research presented in [23], we also recognize the significant role that proton induced nuclear data can have on the accuracy of our findings. When it comes to the ADVANTG weight windows, it became apparent that fine-tuning the mesh is crucial, not just for the accuracy but also for improving computational speed. This was evident when the simulation run time increased upon using a mesh that was specifically optimized for concrete shielding, but then applied to iron shielding.

Transitioning into the KENS shielding experiment, we expanded upon the insights gleaned from TIARA. Interestingly, it was observed that optimizing for a specific slot does not automatically correlate with enhanced results for other slots. Moreover, a significant computational commitment for multi-area optimization doesn't always yield superior outcomes. Notably, this experiment also provided an intriguing counterpoint to the TIARA experiment. Contrary to TIARA's findings, the KENS experiment demonstrated that simulations utilizing weight windows from a non-equivalent neutron source can actually be computationally faster while getting satisfactory results, than those using an equivalent neutron source.

Regarding the irradiation calculations, the research has demonstrated that improvements in spectral convergence, which also meant the reduction in the relative error of the average flux, can result in substantial reductions in isotopic production rates. This was evidenced in the case of a stainless steel sample with the same composition as the anticipated MYRRHA's reactor vessel. In this instance, a decrease in flux error from around 5% to 1.5% and 0.5% led to a reduction in the activity of the sample by 3.86% and 5.29% respectively. Additionally, it was found that the total activity of the sample could be accounted for by a few dominant radionuclides, which contributed consistently to the overall activation of the steel sample.

Building upon the findings of both TIARA and KENS, the MYRRHA experiment examined the use of a fixed source in ADVANTG simulations for criticality problems, which proved to be a significant advantage in terms of efficiency. Though for our application, the fixed source is exclusive to ADVANTG simulations and not applied in the final MCNP run, this method managed to cut down computation time without compromising the simulation's accuracy. Drawing from the experience in TIARA and KENS, source biasing emerged as a powerful variance reduction technique. Notably, we achieved similar statistical results 10% faster compared to using

the original proton or criticality source. This advancement presents a marked improvement in computational speed and resource allocation.

6.2 Implications

The implications derived from our experiments are interconnected and provide valuable insights into variance reduction techniques and their applications. The TIARA experiment's observed effectiveness of an equivalent neutron source signals potential use in varied contexts, such as the MYRRHA ADS configuration or beam dump shielding calculations at different beam energy sections of the MYRRHA LINAC. Importantly, this finding also emphasizes the need for an appropriate weight window mesh for ADVANTG. The experiment revealed that using weight windows created with the same mesh as that used in the 40 cm iron shielding yields comparable statistical results, albeit requiring a longer simulation time.

Building upon these insights, the implications of the KENS shielding experiment are of substantial importance for the design and execution of similar projects. The experiment demonstrated that the ADVANTG optimization mesh design should be heavily influenced by the specific objectives of the simulation and the desired performance level. It also echoed the TIARA experiment's implications on the crucial role of careful weight window selection and optimization, as the performance variations of simulations using different weight windows became evident.

The findings on the irradiation calculations imply that control and precision over the spectral convergence can significantly influence the isotopic production rates. Therefore, in a practical application such as in the anticipated MYRRHA's reactor, focusing on achieving a well-converged neutron spectrum prior to running ALEPH calculations could lead to improved results and reduced uncertainties.

The MYRRHA experiment, while reinforcing the key takeaways from both TIARA and KENS, added some new dimensions to our understanding. First, it highlighted the power of source biasing to enhance statistical results and cut computational time, particularly evident in the context of MYRRHA. Second, it underscored the use of a fixed source in our simulations as an efficient and accessible method for applying variance reduction techniques. This approach, especially appealing due to its simplicity and the reduction of complexities associated with weight windows and ADVANTG, could be a promising option in scenarios requiring moderate statistical improvements. Taken together, these findings pave the way for more efficient and precise modeling and simulation in future research.

6.3 Limitations

Our study, while providing significant findings, was not without limitations, many of which are intertwined across the different experiments. The TIARA experiment, for instance, revealed a clear dependency of simulation outcomes on particle energy and shielding thickness. This dependency could pose a constraint on the applicability of these findings in scenarios where these parameters differ. Moreover, the use of weight windows derived from non-equivalent neutron sources showed potential weaknesses, as it failed in certain simulations, signalling limitations of this approach in some cases.

In contrast to the TIARA case, the non-equivalent neutron source for the KENS experiment yielded highly satisfactory results significantly faster than the equivalent-neutron source. However, it's crucial to note that these results may be influenced by the particular geometry, materi-

als, and setup of this specific experiment. Consequently, caution is advised when employing this approach in other contexts or experiments, as the same success might not be directly transferable. Additionally, the research on the KENS experiment did not account for situations where isotopes are derived from reactions that have a threshold in their cross section. This limitation is especially relevant in other scenarios, particularly for MYRRHA, where many threshold reactions can play a key role in determining the isotopic composition and radiation emissions.

Despite these challenges, the MYRRHA experiment offered valuable insights while shedding light on additional constraints of our study. Our comparison of the fixed source was limited to neutron flux distributions. For a more robust analysis, it would be pertinent to expand this comparison to include neutron spectra at various locations in future research. This expansion would ensure that the generated neutron spectrum aligns with the behaviour of the original source's neutrons. This limitation, together with those identified in the TIARA and KENS experiments, signifies areas for future improvement and research.

These limitations do not diminish the value of our findings but instead highlight areas for further exploration and refinement, proving that there is much to be learned and developed in this field.

6.4 Future Work

As we look towards the future of this research, the learnings from the TIARA, KENS, and MYRRHA experiments offer promising paths for exploration. The TIARA experiment emphasized the potential in expanding the application of weight windows to proton source problems, derived from an equivalent neutron source. Future studies could adapt this methodology for different settings, particularly those involving varied incident energies, shielding thicknesses, materials, and geometries. Concurrently, research could probe deeper into the reasons for simulation failures when using weight windows from non-equivalent neutron sources, a limitation noted in the TIARA experiment, and develop strategies to overcome this challenge.

Informed by the insights from the TIARA experiment and the specific challenges encountered in the KENS experiment, subsequent studies could concentrate on understanding the reasons behind the computational efficiency of simulations using weight windows from a non-equivalent neutron source. Additionally, future research should delve further into the reactions producing most relevant radionuclides in terms of emission and working dose, particularly focusing on potential threshold reactions and their influence on the results. The research should also consider the resonance region and how well-converged weight window utilized spectra can impact the outcomes. While the research for the KENS experiment did not feature a resonance region, and the weight windows utilized spectra were well converged, this may not be the case in other scenarios where further investigation might be needed.

The MYRRHA experiment presents valuable opportunities for future research, building on the foundations established in the work presented in this thesis. One of the primary areas for exploration is the optimization of the ADVANTG mesh. Achieving successful results in the final MCNP run highly depends on this aspect, suggesting its critical nature. Once significant progress is made in this area, future work could shift focus towards performing detailed irradiation calculations in the vessel. A comprehensive examination of the isotopic composition, the reactions involved, and the impact of neutron spectrum uncertainties could present invaluable insights. These investigations could advance our current understanding, pushing the envelope for more accurate and reliable results.

Moreover, an area of emphasis for future exploration should be refining the fixed source for

increased efficiency and accuracy. As discussed in the limitations of this study, expanding the comparative analysis to include neutron spectra at various locations could yield results more closely mirroring those from proton source and critical source simulations. This advancement could offer invaluable insights into achieving even more efficient computations and precise results, encapsulating the overarching goal of this research.

In sum, the future of this research field is wide open, promising opportunities for growth and refinement that can further our understanding and application of variance reduction techniques in proton source problems.

6.5   Final Conclusions

From this thesis, one key point should be underscored: optimizing the ADVANTG mesh is key for correctly obtaining weight window values, and thus effectively using this variance reduction method. Unfortunately, the path to success is not clearly marked - it demands significant expertise or an exhaustive approach of trial and error. This thesis seeks to illuminate this complex procedure, aspiring to pave the way for a comprehensive guide for future applications needing variance reduction techniques, particularly weight window techniques via ADVANTG.

Equally crucial is the need for an equivalent neutron source when applying ADVANTG in a proton-driven system. Crafting a dependable equivalent neutron source that mirrors the behavior of the proton-driven system can be a standalone variance reduction technique. This strategy could accelerate simulations, yielding more accurate statistical outcomes. If more refinement is needed, this step remains essential. For additional enhancements, we can turn to ADVANTG for weight window calculations, or even consider MCNP weight windows as an alternative.

In addition to the aforementioned concepts, the aspect of spectrum-driven uncertainty reduction holds significant weight in the context of irradiation calculations. This has been demonstrated even in the relatively simple scenario of KENS shielding experiments, where the production of all pertinent radionuclides resulted from radiative neutron capture. We can anticipate that these uncertainties will have a more pronounced effect when additional reactions, especially resonance or threshold reactions, come into play. However, it is crucial to note that the primary focus of this thesis has been on mitigating uncertainties arising from Monte Carlo simulations. This is primarily because, in the realm of deep shielding calculations, these uncertainties significantly influence the results. Yet, it is important to acknowledge the existence of other sources of uncertainties, particularly those related to nuclear data, that may require further attention for achieving more precise and conclusive results.

7 SOCIAL & PROFESSIONAL RESPONSABILITY

This chapter delves into the social and professional implications of the research conducted for this thesis. It aims to highlight the direct and indirect contributions of the research to broader social and professional contexts, addressing both the ethical considerations and the alignment with the Sustainable Development Goals (SDGs) outlined in the United Nations' 2030 Agenda for Sustainable Development. In this era of global challenges, research in all fields must adopt a responsible approach that considers its potential impact on society and the environment. This chapter will further divide into two sections: professional responsibility and social responsibility, along with sustainable development goals.

7.1 Professional Responsability

In conducting this thesis research, the professional responsibility associated with nuclear simulations and variance reduction techniques has been at the forefront. The ethical implications of nuclear research necessitate a highly responsible approach.

Firstly, the accurate representation of nuclear phenomena using MCNP6.2 and ADVANTG3.2 software tools is a critical professional obligation. Misrepresentation or misuse could potentially lead to incorrect conclusions, potentially threatening the safety and security of nuclear operations. Thus, the correct application and interpretation of these tools carry profound professional responsibility.

Secondly, the research's commitment to pursuing enhanced efficiency and accuracy in nuclear shielding simulations is an integral part of professional responsibility. Variance reduction techniques, source biasing, and weight windows are essential methodologies for improving the robustness of nuclear simulations. By furthering knowledge and understanding of these techniques, this thesis contributes to the professional growth and development of the field.

Finally, the professional responsibility extends to the dissemination of this research. The careful explanation of these advanced methodologies is intended to foster a broader understanding and to equip other researchers with the tools they need to advance in their work, thereby benefiting the entire professional community.

7.2 Social Responsibility and Sustainable Development Goals (SDGs)

The research aligns with several Sustainable Development Goals, demonstrating a commitment to addressing some of the most pressing challenges of our time:

- **SDG 7: Affordable and Clean Energy:** By enhancing the accuracy and efficiency of nuclear simulations, this research can contribute to safer, more efficient nuclear energy. Nuclear power is a low-carbon energy source, which can help reduce our reliance on fossil fuels and combat climate change.

- **SDG 9: Industry, Innovation and Infrastructure:** The advanced methodologies and techniques explored in this thesis contribute to innovation in the nuclear industry. Through this work, the capacity for scientific research and technological capabilities in this field is being enhanced.

- **SDG 13: Climate Action:** As mentioned under SDG 7, nuclear power is a low-carbon energy source. By improving the efficiency and safety of nuclear power through enhanced simulation techniques, this research contributes indirectly to the efforts to combat climate change.

- **SDG 17: Partnerships for the Goals:** The thesis emphasizes the importance of collaborative efforts, highlighting the need for ongoing cooperation between researchers, professionals, and institutions to optimize nuclear simulations. It encourages knowledge sharing and collaborative learning, vital for achieving any of the SDGs.

In conclusion, the research conducted in this thesis aligns with the principles of professional responsibility and contributes to several social and sustainability objectives. Through this work, we hope to foster a better understanding of variance reduction techniques in nuclear simulations and their potential for social and environmental impact.

8 PROJECT MANAGEMENT

Effective project management is a crucial aspect of any research undertaking. It helps to streamline tasks, allocate resources efficiently, ensure timely completion, and manage expenses within budget constraints. For our investigation into reducing spectrum-driven uncertainties with variance reduction techniques, we implemented a detailed project management plan to ensure the successful execution and completion of the study. This chapter will discuss the project management approach used in this research, with specific focus on two key aspects: planning and budget.

8.1 Planning

The planning phase was instrumental in charting the course of the project and establishing a roadmap for the tasks to be undertaken. The project was divided into broad and specific tasks, with appropriate timelines allocated for each. Table 8.1 and Figure 8.1 both represent the timeline and distribution of tasks for this master's thesis project. The project started on 1st September 2022 and ended on 31st May 2023. The tasks were divided into four main sections: Literature Review, Simulation & Experimentation, Data Analysis & Result Interpretation, and Thesis Writing & Review. Each of these sections had subtasks with their respective durations and timelines.

Table 8.1: Project Timeline and Task Distribution

Task	Duration (days)	Begin date	End date
Literature Review	30	1st Sept	30th Sept
- Study on Variance Reduction Techniques	15	1st Sept	15th Sept
- Examination of Previous Experiments	15	16th Sept	30th Sept
Simulation & Experimentation	70	1st Oct	10th Dec
- MCNP6.2 and ADVANTG3.2 Setup	10	1st Oct	10th Oct
- Simulation of TIARA	30	11th Oct	10th Nov
- Simulation of KENS	30	11th Nov	10th Dec
- Simulation of MYRRHA	25	11th Dec	5th Jan
Data Analysis & Result Interpretation	55	6th Jan	1st Mar
Thesis Writing & Review	90	2nd Mar	30th May
- Drafting	60	2nd Mar	30th Apr
- Review and Revision	30	1st May	30th May
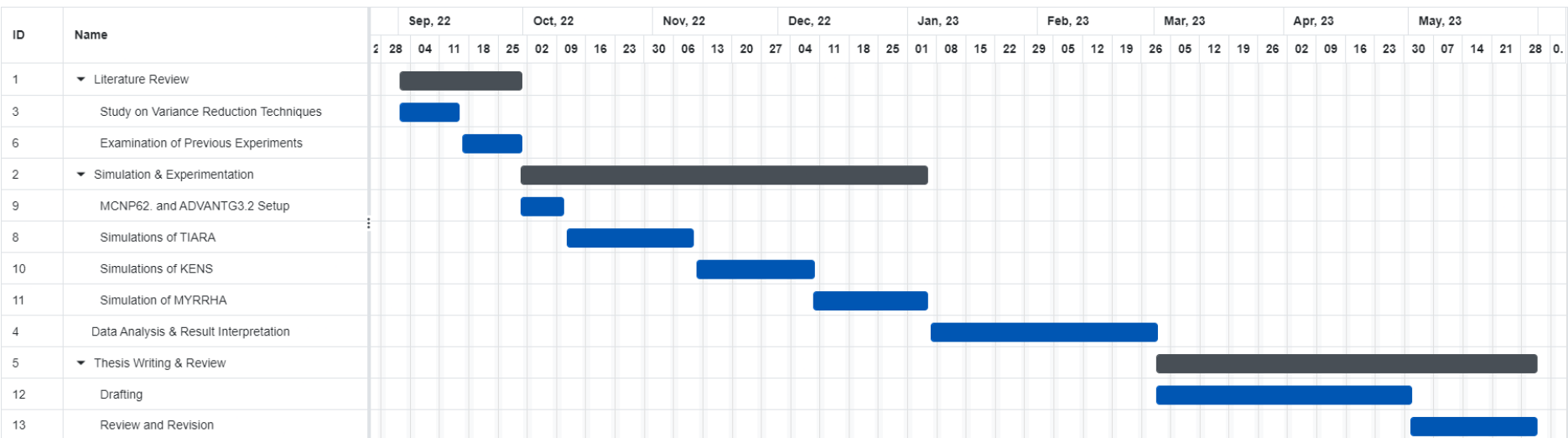
Figure 8.1: Gantt chart.

The most challenging tasks during the project were the Simulation & Experimentation and the Thesis Writing & Review. The Simulation & Experimentation section was challenging due to the complexity of setting up MCNP6.2 and ADVANTG3.2 and conducting simulations on TIARA, KENS, and MYRRHA. These tasks required a deep understanding of the systems and careful execution of the simulations. To overcome these challenges, I invested significant time in understanding the systems, consulted with experts, and conducted multiple trial runs before the actual simulations.

The Thesis Writing & Review section was also challenging due to the need for clear and concise presentation of the findings, drafting, and revising the thesis. The process of writing a thesis is iterative and requires a lot of patience and attention to detail. To tackle these challenges, I started writing early, sought feedback from my advisors regularly, and revised my drafts multiple times to ensure clarity and coherence.

8.2 Budget

The budget is a significant aspect of project management that determines the financial feasibility of the research. A comprehensive budgeting approach was employed to cater to workforce expenses and resource expenses, including the software licensing costs. Tables 8.2 and 8.3 summarize the expenses incurred during the duration of the project. The former illustrates workforce costs, including time and effort invested by the student, mentor, and co-mentor. The student spent a total of 1350 hours on the project, with a monthly financial support of 398.29€, resulting in an hourly cost of 2.77€. The mentors, both primary and co-mentor, contributed a total of 200 hours at a rate of 35€ per hour. The cumulative workforce expense stands at 10,739.50€.

Table 8.3 details the various resources required for the project. The cost of accommodation was significant, amounting to 3276.00€ for the nine-month period. Other resources, like the Dell Intel Core i5, MCNP6.2 license, ADVANTG3.2 license, and peripherals, were used for the same duration and had to be amortized accordingly. The cumulative resource expense amounts to 4388.50€.

Table 8.2: Workforce Expenses

Concept	Hours	Cost per hour (€)	Subtotal (€)
Student	1350	2.77	3739.50
Mentor	150	35.00	5250.00
Co-mentor	50	35.00	1750.00
Total			**10739.50**

Table 8.3: Resource Expenses

Concept	Cost (€)	Amort. (months)	Use (months)	Subtotal (€)
Accommodation	364.00	-	9	3276.00
Dell Intel Core i5	700.00	72	9	87.50
MCNP6.2 License	500.00	9	9	500.00
ADVANTG3.2 License	500.00	9	9	500.00
Peripherals	200.00	72	9	25.00
Overleaf LaTeX	0.00	-	-	0.00
Total				**4388.50**

The total project cost, including workforce and resource expenses, is given in Table 8.4. The amounts are subjected to a 21% tax, leading to a final project budget.

Table 8.4: Total Project Expenses

Concept	Cost (€)
Workforce	10739.50
Resources	4388.50
Subtotal	15128.00
Tax (21%)	3176.88
Total	**18304.88**

In conclusion, taking into account the workforce and resources expenses, and including a 21% tax, the final project budget amounts to 18,304.88€.

9 BIBLIOGRAPHY

References

[1] S. W. Mosher, S. R. Johnson, A. M. Bevill, A. M. Ibrahim, C. R. Daily, T. M. Evans, J. C. Wagner, J. O. Johnson, and R. E. Grove, *ADVANTG-An Automated Variance Reduction Parameter Generator*, 2015.

[2] C. J. Werner, J. Armstrong, F. B. Brown, L. Casswell, L. J. Cox, D. Dixon, R. A. Forster, J. T. Goorley, H. G. Hughes, J. Favorite, R. Martz, S. G. Mashnik, M. E. Rising, C. Solomon, A. Sood, J. E. Sweezy, A. Zukaitis, C. Anderson, J. S. Elson, J. W. Durkee, R. C. Johns, G. W. McKinney, G. E. McMath, J. S. Hendricks, D. B. Pelowitz, R. E. Prael, T. E. Booth, M. R. James, M. L. Fensin, T. A. Wilcox, and B. C. Kiedrowski, *MCNP USERS MANUAL*, 2017.

[3] L. A. N. Laboratory, "Mcnp® website." Available online: `https://mcnp.lanl.gov/`. Last accessed: 2023-02-2.

[4] A. Stankovskiy, G. Van Den Eynde, P. Baeten, C. Trakas, P. M. Demy, and L. Villatte, "Aleph2 - a general purpose monte carlo depletion code," *American Nuclear Society*, 7 2012.

[5] G. Van Rossum and F. L. Drake, "Python 3 reference manual." `http://www.python.org`, 2009.

[6] L. Fiorito, G. Zerovnik, A. Stankovskiy, G. Van den Eynde, and P.-E. Labeau, "Nuclear data uncertainty propagation to integral responses using sandy," *Annals of nuclear energy*, vol. 101, pp. 359–366, Mar. 2017. Score=10.

[7] T. E. Booth and T. Booth, "A sample problem for variance reduction in mcnp," tech. rep., Los Alamos National Laboratory, 1985.

[8] J. S. Hendricks and T. E. Booth, *MCNP Variance Reduction Overview*, 1985.

[9] M. Matijević, "Pca benchmark analysis using the advantg3.0.1/mcnp6.1.1b codes," tech. rep., International Centre for Theoretical Physics, 2017.

[10] J. C. Wagner, E. D. Blakeman, and D. E. Peplow, "Forward-weighted cadis method for global variance reduction monte carlo variance reduction with deterministic importance functions view project reactor pressure vessel neutron fluence analyses view project forward-weighted cadis method for global variance reduction," tech. rep., Oak Ridge National Laboratory, 2007.

[11] H. A. Abderrahim, P. Baeten, D. D. Bruyn, and R. Fernandez, "Myrrha - a multi-purpose fast spectrum research reactor," *Energy Conversion and Management*, vol. 63, pp. 4–10, 11 2012.

[12] H. A. Abderrahim, "Realization of a new large research infrastructure in belgium: Myrrha contribution for closing the nuclear fuel cycle making nuclear energy sustainable," *EPJ Web of Conferences*, vol. 246, p. 00012, 2020.

[13] S. Andriamonje, A. Angelopoulos, A. Apostolakis, F. Attale, L. Brillard, S. Buono, J. Calero, F. Carminati, F. Casagrande, P. Cennini, S. O. Charalambous, R. D. Moral, C. O. Eleftheriadis, E. Gailego, J. Galvez, L. Garcia-Tabares, C. Geles, I. Goulas, A. Giorni, E. Gonzalez, M. Hussonnois, J. Jaren, R. Klapisch, P. Kokkas, F. Lemeilleur, G. Lindecker,

A. O. Liolios, J. Loiseaux, C. Lopez, A. Lorente, M. Macri, J. Martinez-Val, H. Nifenecker, J. Gropesa, P. Pavlopoulos, J. Pinston, J. p Revol, C. Roche, C. Rubbia, J. R. eyb, L. Sakelhou, F. Saldana, F. Schussier, D. Trubert, J. Viano, S. Vieira, S. Vlachos, X. Li, and G. Zarris, "Experimental determination of the energy generated in nuclear cascades by a high energy beam," *Physics Letters*, vol. 3, pp. 697–709, 1995.

[14] D. Vandeplassche, L. M. Romão, and SCK·CEN, *Accelerator Driven Systems*. IEEE, 2012.

[15] B. Kos and I. A. Kodeli, "Indc international nuclear data committee mcnp modelling of the tiara sinbad shielding benchmark," tech. rep., IAEA, 2019. Last accessed: 2023-04-04.

[16] C. Konno, K. Ochiai, S. Sato, and M. Ohta, "Analyses of iron and concrete shielding experiments at jaea/tiara with jendl/he-2007, endf/b-vii.1 and fendl-3.0," *Fusion Engineering and Design*, vol. 98-99, pp. 2178–2181, 10 2015.

[17] I. Kodeli, A. Milocco, P. Ortego, and E. Sartori, "20 years of sinbad (shielding integral benchmark archive and database)," *Progress in Nuclear Science and Technology*, vol. 4, pp. 308–311, 2014.

[18] IAEA, "Conderc." Available online: `https://www-nds.iaea.org/conderc/tiara`, 2022. Last accessed: 2023-04-04.

[19] N. Nakao, H. Yashima, M. Kawai, K. Oishi, H. Nakashima, S. ichi Sasaki, K. Masumoto, M. Numajiri, T. Sanami, H. Matsumura, Q. Wang, A. Toyoda, K. Iijima, K. Takahashi, S. Ban, H. Hirayama, S. Muto, T. Nunomiya, S. Yonai, D. R. H. Rasolonjatovo, K. Terunuma, T. Nakamura, E. Kim, P. K. Sarkar, and A. Maruhashi, "Kens shielding experiment (1)-measurement of neutron attenuation through 4m concrete shield using a high energy neutron irradiation room," tech. rep., KEK, 2004.

[20] N. Nakao, "Kens shielding experiment at kek." Available online: `https://www.oecd-nea.org/science/wprs/shielding/sinbad/kens500/kenssh-a.htm`. Last accessed: 2023-04-12.

[21] N. Nakao, H. Yashima, M. Kawai, K. Oishi, H. Nakashima, K. Masumoto, H. Matsumura, S. Sasaki, M. Numajiri, T. Sanami, Q. Wang, A. Toyoda, K. Takahashi, K. Iijima, K. Eda, S. Ban, H. Hirayama, S. Muto, T. Nunomiya, S. Yonai, D. R. Rasolonjatovo, K. Terunuma, K. Yamauchi, P. K. Sarkar, E. Kim, T. Nakamura, and A. Maruhashi, "Arrangement of high-energy neutron irradiation field and shielding experiment using 4 m concrete at kens," *Radiation Protection Dosimetry*, vol. 116, pp. 553–557, 12 2005.

[22] L. Fiorito, "Neutron activation of the myrrha steel reactor components," tech. rep., SCK CEN, 2022.

[23] e. a. Y. Çelik, Yosuke Iwamoto, "Benchmarking of proton and neutron induced nuclear data with mcnp6.2 using sinbad experiments," *Nuclear Science and Engineering*, 2023.

[24] JAEA, "Nuclear data center." Available online: `https://wwwndc.jaea.go.jp/jendl/j40/j40.html`. Last accessed: 2023-06-06.

[25] O. Source, "Visit: scalable, open source, visualization and data analysis from laptop to lcf." Available online: `https://visit-dav.github.io/visit-website/index.html`. Last accessed: 2023-05-25.

[26] N. Nakao, H. Yashima, M. Kawai, K. Oishi, H. Nakashima, K. Masumoto, H. Matsumura, S. Sasaki, M. Numajiri, T. Sanami, Q. Wang, A. Toyoda, K. Takahashi, K. Iijima, K. Eda,

S. Ban, H. Hirayama, S. Muto, T. Nunomiya, S. Yonai, K. Terunuma, D. R. H. Rasolonja-tovo, K. Yamauchi, P. K. Sarkar, E. Kim, T. Nakamura, and A. Maruhashi, "Arrangement of high energy neutron irradiation field arrangement of high energy neutron irradiation field and shielding experiment using 4m concrete at kens and shielding experiment using 4m concrete at kens," tech. rep., Kyoto University Research Reactor Institute (KURRI), 2005.

[27] T. e. a. Kittelmann, "Monte carlo particle lists: Mcpl," *Computer Physics Communications*, vol. 218, pp. 17–42, 2017.

References

LIST OF TABLES

LIST OF FIGURES

GLOSSARY

ADS Accelerator-Driven System

ADVANTG Automated Variance Reduction Generator

BR2 Belgian Reactor 2

CADIS Consistent Adjoint Driven Importance Sampling

CERN European Council of Nuclear Research

CPU Central Processing Unit

FA Fuel Assembly

FASTEF Flexible Accelerator-driven System for Technology development and Experimental Facility

FP6 EUROTRANS Sixth Framework Programme of the European Union's EUROpean Research Programme for the TRANSmutation of high-level nuclear waste

IAEA International Atomic Energy Agency

IPS In-Pile test Section

JENDL Japanese Evaluated Nuclear Data Library

KENS KEK Spallation Neutron Source Facility

LBE Lead-Bismuth Eutectic

LINAC Linear Accelerator

MCNP Monte Carlo N-Particle code

MOX Mixture Of Oxides

MYRRHA Multi-purpose hYbrid Research Reactor for High-tech Applications

SDEF General Source Definition

SINBAD Shielding Integral Benchmark Archive and Database

SSW Surface Source Write

TIARA Takasaki Ion Accelerator for Advanced Radiation Application

XT-ADS eXperimental facility demonstrating the technical feasibility of Transmutation in an Accelerator-Driven System

Escuela Técnica Superior de Ingenieros Industriales (UPM)

ANNEXES

A   ADVANTG Code Fragments for Different Simulations

A.1   TIARA – Mesh used for 40cm Iron Shielding

```
1  mesh_x         -130.0 0.0 176.0 183.0 283.0 333.0 396.0 401.0 441.0 453.7
                   720.0
2  mesh_x_ints    5 6 1 5 3 4 1 20 1 10
3  mesh_y         -252.0 -60.0 -6.34 -5.44 5.46 6.36 60.02 252.02
4  mesh_y_ints    5 15 2 12 2 15 5
5  mesh_z         -315.0 -60.0 -20.0 -6.35 -5.45 5.45 6.35 60.0 285.0
6  mesh_z_ints    7 10 5 2 12 2 15 5
```

A.2   TIARA – Mesh used for 100cm Concrete Shielding

```
1  mesh_x         -130.0 0.0 176.0 183.0 283.0 333.0 396.0 401.0 501.0 513.7
                   720.0
2  mesh_x_ints    5 6 1 5 3 4 1 3 1 10
3  mesh_y         -252.0 -60.0 -6.34 -5.44 5.46 6.36 60.02 252.02
4  mesh_y_ints    5 15 2 12 2 15 5
5  mesh_z         -315.0 -60.0 -20.0 -6.35 -5.45 5.45 6.35 60.0 285.0
6  mesh_z_ints    7 10 5 2 12 2 15 5
```

A.3   KENS – Mesh used for optimization of all slot detectors

```
1  mesh_x         -200.0 -65.0 -8.0 -5.0 -4.44 4.43 5.0 8.0 65.0 200.0
2  mesh_x_ints    3 10 3 1 8 1 3 10 3
3  mesh_y         -200.0 -65.0 -8.0 -5.0 -4.44 4.43 5.0 8.0 65.0 200.0
4  mesh_y_ints    3 10 3 1 8 1 3 10 3
5  mesh_z         -20.0 0.0 13.09 38.6 153.6 253.6 258.1 289.6 297.6 329.6
                   337.6 379.6 387.6 434.6 442.6 499.6 507.6 569.6 577.6
                   653.6 661.6
6  mesh_z_ints    1 13 2 5 5 1 2 1 2 1 2 1 2 1 2 1 2 1 2 1
```

A.4   KENS – Mesh used for optimization of slot-8 detector

```
1  mesh_x         -200 -65 -8 -5 -4.445 4.43 5 8 65 200
2  mesh_x_ints    3 10 3 1 8 1 3 10 3
3  mesh_y         -200 -65 -8 -5 -4.445 4.43 5 8 65 200
4  mesh_y_ints    3 10 3 1 8 1 3 10 3
5  mesh_z         -20 0 13.09 38.6 153.6 253.6 258.1 289.6 297.6 329.6
                   337.6 379.6 387.6 434.6 442.6 499.6  507.6  569.6 577.6
                   653.6 661.6
6  mesh_z_ints    1 13 2 5 5 1 2 1 2 1 2 1 2 1 2 1 2 1 2 1
```

B ADVANTG Weight Window Lower Bounds for Different Simulations

Table B.1: ADVANTG weight window lower bounds in TIARA experiment 40 cm iron shielding, using Equivalent Neutron Source.

Energy [MeV]	(439,0,0)	(441,0,0)	(454,0,0)
4.14E-07	0.00E+00	0.00E+00	9.92E+02
1.01E-04	1.76E-02	2.62E-02	3.74E-02
1.50E-02	1.03E-04	1.40E-04	1.93E-04
6.08E-01	7.65E-06	8.94E-06	1.06E-05
1.96E+01	5.14E-06	6.05E-06	7.20E-06
6.00E+01	2.70E-06	3.17E-06	3.75E-06
7.00E+01	2.45E-06	2.87E-06	3.38E-06

Table B.2: ADVANTG weight window lower bounds in TIARA experiment 40 cm iron shielding, using Non-Eq. Neutron Source.

Energy [MeV]	(439,0,0)	(441,0,0)	(454,0,0)
4.14E-07	0.00E+00	0.00E+00	3.85E+01
1.01E-04	7.16E-04	1.06E-03	1.52E-03
1.50E-02	4.26E-06	5.82E-06	8.00E-06
6.08E-01	2.75E-07	3.24E-07	3.86E-07
1.96E+01	9.23E-08	1.16E-07	1.47E-07
6.00E+01	3.13E-08	3.90E-08	4.86E-08
7.00E+01	2.96E-08	3.62E-08	4.42E-08

Table B.3: ADVANTG weight window lower bounds in TIARA experiment 100 cm Concrete shielding, using Equivalent Neutron Source.

Energy [MeV]	(468,0,0)	(501,0,0)	(514,0,0)
4.14E-07	3.26E+05	8.74E+01	5.28E-04
1.01E-04	2.52E+05	6.42E+01	1.12E-04
1.50E-02	8.07E+04	4.95E+01	4.90E-05
6.08E-01	1.97E+02	1.45E-01	2.06E-05
1.96E+01	5.05E+01	6.25E-03	1.39E-05
6.00E+01	1.07E+00	6.92E-04	1.52E-05
7.00E+01	5.22E-01	4.94E-04	1.53E-05

Table B.4: ADVANTG weight window lower bounds in TIARA experiment 100 cm Concrete shielding, using Non-Eq. Neutron Source.

Energy [MeV]	(468,0,0)	(501,0,0)	(514,0,0)
4.14E-07	2.00E+04	5.37E+00	3.24E-05
1.01E-04	1.40E+04	3.95E+00	2.28E-06
1.50E-02	2.48E+03	2.97E+00	7.53E-07
6.08E-01	2.96E+00	2.37E-03	2.05E-07
1.96E+01	5.45E-01	6.65E-05	8.06E-08
6.00E+01	7.26E-03	5.56E-06	9.12E-08
7.00E+01	3.43E-03	3.90E-06	9.49E-08

Table B.5: ADVANTG weight window lower bounds for All-Slots optimization in KENS shielding experiment, using Equivalent Neutron Source.

Energy [MeV]	(0,0,254)	(0,0,258)	(0,0,654)	(0,0,662)
1.11E+00	1.30E-05	3.60E-06	9.83E-11	2.34E-11
3.01E+00	1.12E-05	2.80E-06	1.01E-10	3.57E-11
1.00E+01	6.87E-06	1.13E-06	1.05E-10	1.65E-11
2.50E+01	7.80E-06	1.58E-06	1.22E-10	3.34E-11
8.00E+01	5.35E-06	1.40E-06	1.43E-10	4.20E-11
1.80E+02	2.62E-06	8.78E-07	1.51E-10	5.22E-11
3.00E+02	1.41E-06	5.28E-07	1.21E-10	3.18E-11

Table B.6: ADVANTG weight window lower bounds for All-Slots optimization in KENS shielding experiment, using Non-Equivalent Neutron Source.

Energy [MeV]	(0,0,254)	(0,0,258)	(0,0,654)	(0,0,662)
1.11E+00	1.68E-05	3.08E-06	8.61E-10	2.21E-10
3.01E+00	1.00E-05	1.93E-06	9.04E-10	3.33E-10
1.00E+01	6.35E-06	9.50E-06	9.46E-10	1.54E-10
2.50E+01	8.57E-06	1.45E-06	1.10E-09	3.12E-10
8.00E+01	6.28E-06	1.09E-06	1.26E-09	3.71E-10
1.80E+02	5.28E-06	1.05E-06	1.23E-09	3.78E-10
3.00E+02	3.76E-06	8.08E-07	9.68E-10	2.37E-10

Table B.7: ADVANTG weight window lower bounds for Slot-8 optimization in KENS shielding experiment, using Equivalent Neutron Source.

Energy [MeV]	(0,0,254)	(0,0,258)	(0,0,654)	(0,0,662)
1.11E+00	5.44E+08	1.76E+08	1.00E-10	2.35E-11
3.01E+00	2.61E+03	1.15E+03	1.03E-10	3.58E-11
1.00E+01	1.04E+02	4.53E+01	1.07E-10	1.65E-11
2.50E+01	5.21E+00	2.67E+00	1.24E-10	3.35E-11
8.00E+01	1.06E-03	7.21E-04	1.47E-10	4.21E-11
1.80E+02	3.46E-05	2.64E-05	1.56E-10	5.25E-11
3.00E+02	9.16E-06	7.16E-06	1.25E-10	3.20E-11

Table B.8: ADVANTG weight window lower bounds for Slot-8 optimization in KENS shielding experiment, using Non-Equivalent Neutron Source.

Energy [MeV]	(0,0,254)	(0,0,258)	(0,0,654)	(0,0,662)
1.11E+00	4.79E+09	1.55E+09	9.08E-10	2.22E-10
3.01E+00	2.35E+04	1.04E+04	9.48E-10	3.35E-10
1.00E+01	9.47E+02	4.11E+02	9.88E-10	1.55E-10
2.50E+01	4.74E+01	2.43E+01	1.15E-09	3.13E-10
8.00E+01	9.70E-03	6.60E-03	1.33E-09	3.73E-10
1.80E+02	3.12E-04	2.38E-04	1.30E-09	3.81E-10
3.00E+02	8.10E-05	6.34E-05	1.02E-09	2.38E-10

C Explanation of different approaches to create a fixed source in MYRRHA

C.1 SSW + MCPL

Our initial approach to establishing a fixed source for ADVANTG involved leveraging the Surface Source Write (SSW) card feature of MCNP (Monte Carlo N-Particle). The SSW card enables the recording of neutron particles at the surface of the core barrel. This card serves as a component of a source definition that can be used in MCNP. In an initial simulation, particles are recorded on a user-specified surface or surfaces. Upon completion of the simulation, a .w file is generated, recording comprehensive data about each particle, including type, position, energy, direction, time of recording, and weight. A subsequent MCNP simulation employing the Surface Source Read (SSR) card allows this file to be utilized as a source for another simulation. This method allows for an increased number of particles in the second run compared to the first, achieved by MCNP modifying particle weights — a variance reduction technique. Unfortunately, this source definition is incompatible with ADVANTG, needing the search for alternatives.

The recorded data is saved in a .w file, replete with the required information for source creation. However, the file format, produced by MCNP, can not be read by standard text editors. To extract and interpret the data from this file, the MCPL tool is utilized. MCPL, an open-source tool [27], facilitates the extraction of information from the output file, making it accessible. This data can then be viewed through Python in a dataframe format, where each row corresponds to a recorded particle. It is important to note that as the recorded particle count increases, the size of the file and the computational power required to process it also escalate. Prolonged simulations may potentially result in memory errors when attempting to read the large output file produced by the SSW card. Figure C.1 illustrates the first few rows of the dataframe when interpreted using MCPL in Python.

	pdgcode	x	y	z	ekin	ux	uy	uz	time	weight
0	2112	-60.788765	49.668659	39.439140	0.009339	-0.965156	0.023600	-0.260609	0.002501	0.366042
1	2112	-60.355679	50.194042	38.813530	0.006996	-0.377641	0.386461	-0.841448	0.002517	0.363907
2	2112	52.858589	58.036366	-17.586275	0.000003	0.659113	0.511174	0.551607	0.033756	0.314640
3	2112	-70.598534	-34.323418	28.357437	0.823776	-0.818896	-0.418903	0.392340	0.004781	0.332165
4	2112	-69.630638	-36.246712	47.993221	0.129120	-0.633714	-0.535209	0.558532	0.005244	0.314142
...	...	...	...	...	...	...	...	...	...	...

Figure C.1: Example of dataframe containing the data recorded with SSW card of MCNP and read with MCPL tool.

Until this stage, we encountered no significant impediments. The primary challenge, however, was transforming the acquired data into an SDEF (Source Definition) source format compatible with ADVANTG. The gathered data constitutes discrete observations, which needs some form of aggregation to define distributions for the SDEF card. Yet again, we were confronted with ADVANTG's restrictions related to source definition, which allows for only one independent distribution.While we believed that this could potentially be achieved by partitioning particles into smaller regions and defining appropriate energy distributions, this would have needed extensive scripting. Moreover, it would have been a time-intensive task. Hence, before delving any further into this approach, we chose to explore other potential methodologies that might offer a more efficient solution.

C.2   Spallation Target Assembly

In our exploration, we considered a methodology involving the creation of a neutron source solely within the spallation target assembly. Here, protons from the accelerator enter the spallation target assembly and interact with the Lead-Bismuth Eutectic (LBE), resulting in the production of secondary neutrons. These neutrons then disperse into the core, inducing fission. We envisioned tracking these neutrons on the surface of the spallation target assembly and establishing numerous point sources adjacent to the surface to emulate the secondary neutrons generated.

However, this methodology presents several constraints. The most salient limitation is its exclusivity to subcritical configurations when MYRRHA operates as an Accelerator-Driven System (ADS). Furthermore, neutrons in the proximate region exhibit a significantly anisotropic distribution due to the influence of the proton beam, indicating preferential emission directions. This aspect must be contemplated when defining the source, thus imposing another complication due to ADVANTG's limitation of only permitting one independent distribution, with the remaining distributions being dependent.

While we brainstormed potential solutions to these challenges, the constraints, coupled with the time cost of implementing these ideas with uncertain outcomes, led us to abandon this strategy. Instead, we chose to concentrate on alternative approaches, potentially offering more robust and efficient solutions.

C.3   Entire Volume – Coarse Mesh

In this approach, we used a simpler mesh, less detailed than the one mentioned in Section 5.3.2 where we used the mesh at the FA level. Unlike the previous method where each fuel assembly needed its own FMESH4 tally, here, a single FMESH4 tally covers the entire geometry. Moreover, we're tallying the complete volume inside the core barrel. As shown in Figure C.2, we divided the mesh in three ways: axially (red), angularly (purple), and radially (blue). This leads to two types of voxels in the mesh, as seen in the figure: one shaped like a wedge (shown in blue), and another like a slice of a hollow cylinder (shown in green).[2] In the center of each voxel is were the isotropic point source will be located. In order to generate the data required to create the external SDEF card file, the simulation was run using 1.8E+06 particles. This simulation, which employed 72 CPUs, took 11 days and 5 hours to complete.

---

[2]The divisions you see in Figure C.2 are only representative. In the actual mesh, we calculated the divisions so that the green voxel had an area of about 25 cm^2.
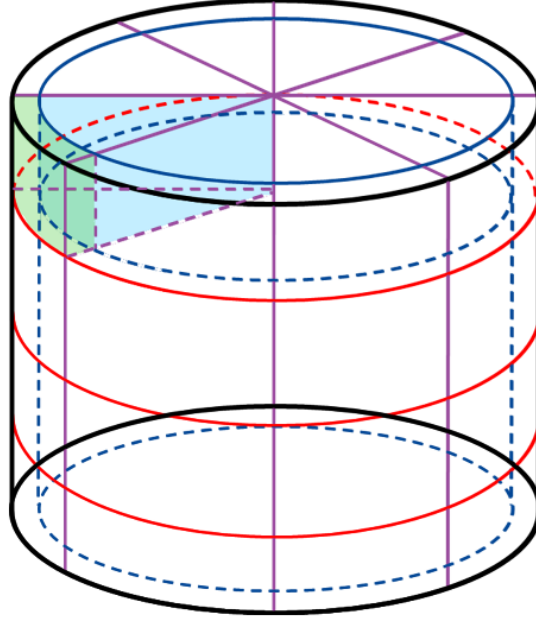
Figure C.2: Scheme of the core geometry (black) and the mesh used for tallying with two different types of voxels shaded in blue and green.

The scope of this approach, using this mesh type, was constrained by the maximum voxel quantity achievable with a single FMESH4 tally. Undoubtedly, additional FMESH4 tallies could be created - for instance, one for every originally defined axial segment - to amplify the voxel count per FMESH4. This method was computationally slightly more efficient for the simulation, as it used a single FMESH4 tally but covered a larger volume. However, when comparing the results with the original source, they were somewhat less accurate than those obtained with the FA level mesh. The comparative neutron flux distributions are provided below. Both simulations, using the original proton source and the equivalent neutron source, were conducted over a 24-hour period using 72 CPUs. During this time, the NPS for the proton source reached 1.5E+06, and the NPS for the equivalent neutron source reached 3.67E+07.

Figure C.3 presents the radial distribution along the x-axis when the coordinates (y,z) are at the origin. The distribution along the axis aligns remarkably well for all intermediate distances, yet deviates near the core center and, notably, in the distant regions where the vessel is positioned. This divergence could have significant implications for irradiation calculations in that area.
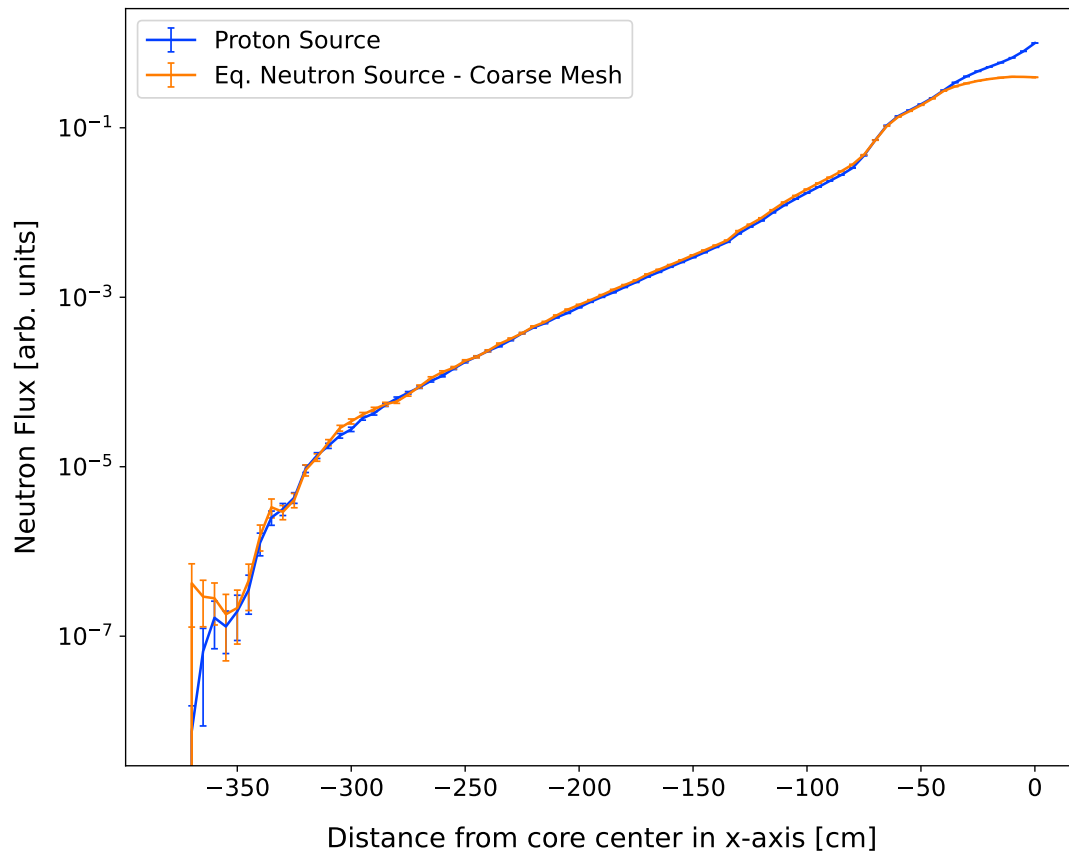
Figure C.3: Radial neutron flux comparison along the x-axis for $(y, z) = (0, 0)$: Proton source vs. Equivalent neutron source using coarse mesh.

Figures C.4 through C.7 illustrate the axial neutron flux at varying distances from the center of MYRRHA's core along the x-axis. It is noticeable that the result within the core (at x=25 cm) is slightly overestimated. At intermediate distances, the outcomes align almost flawlessly. However, at a distance of 300 cm, the results start to indicate incomplete convergence.

Figure C.4: Axial neutron flux comparison at x=25 cm: Proton source vs. Equivalent neutron source using coarse mesh.
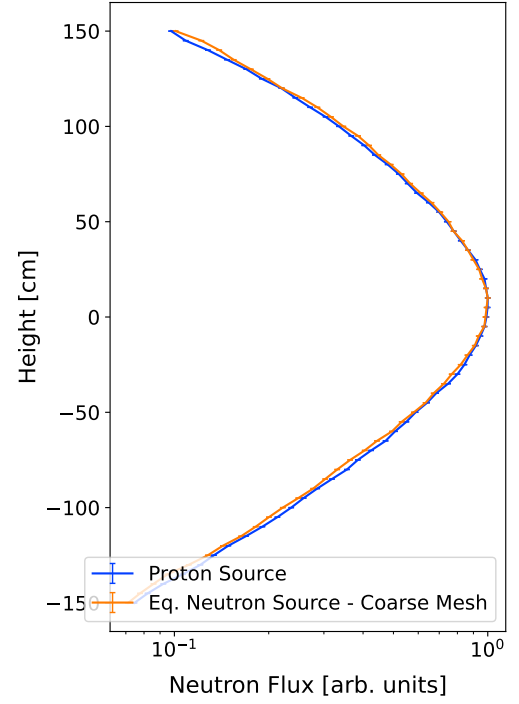
Figure C.5: Axial neutron flux comparison at x=150 cm: Proton source vs. Equivalent neutron source using coarse mesh.

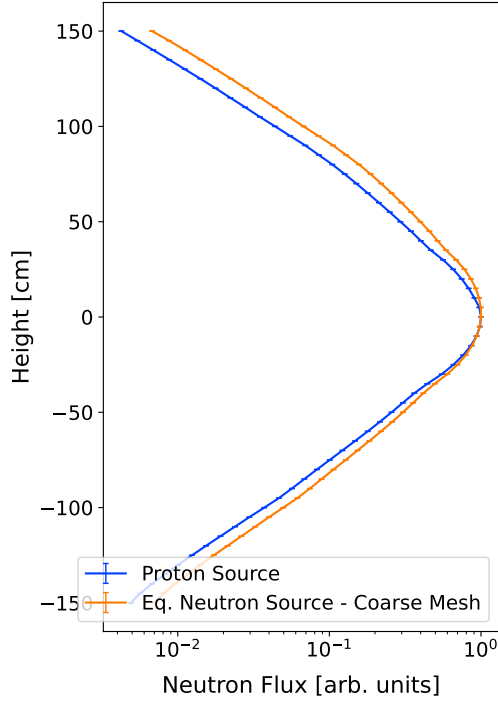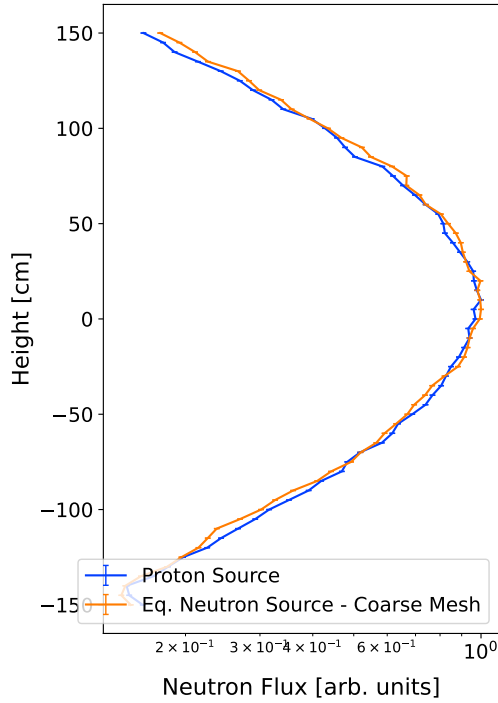**Figure C.6:** Axial neutron flux comparison at x=200 cm: Proton source vs. Equivalent neutron source using coarse mesh.
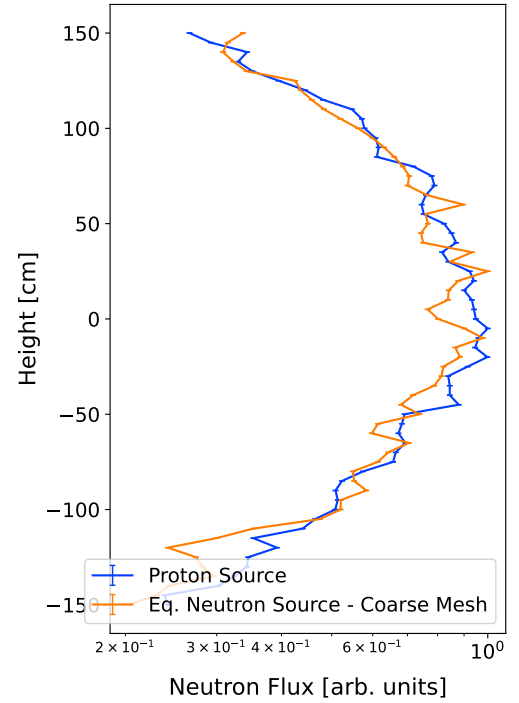
Figure C.7: Axial neutron flux comparison at x=300 cm: Proton source vs. Equivalent neutron source using coarse mesh.

Figures C.8 and C.9 depict the angular neutron flux distribution at z=0 for distances of 150 cm and 300 cm along the x-axis from the center of MYRRHA's core, respectively. Interestingly, the results in this instance are slightly supérior to those using the FA level mesh. This can potentially be attributed to the fact that the fixed source created in this scenario covers a larger volume and extends to greater radii compared to the one used in the previous study.

Figure C.8: Angular neutron flux at $(x, z) = (150, 0)$ cm: Proton source vs. Equivalent neutron source using coarse mesh.

Figure C.9: Angular neutron flux at $(x, z) = (300, 0)$ cm: Proton source vs. Equivalent neutron source using coarse mesh.
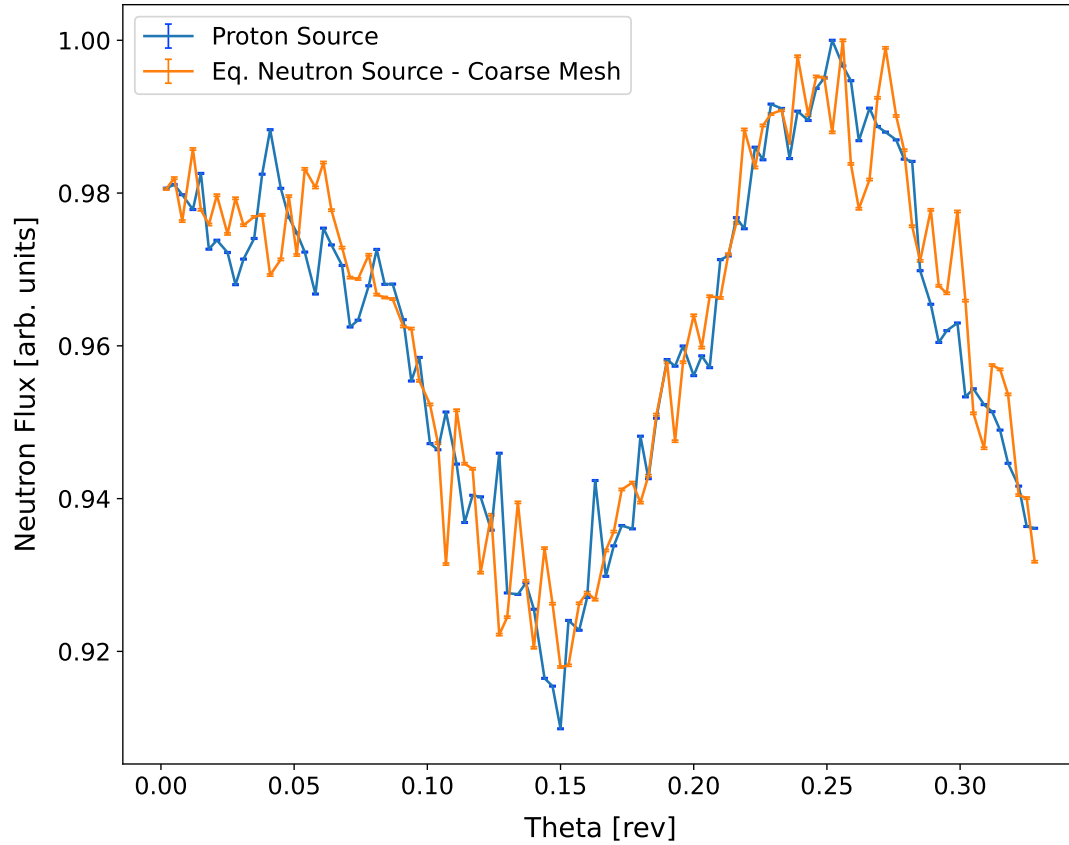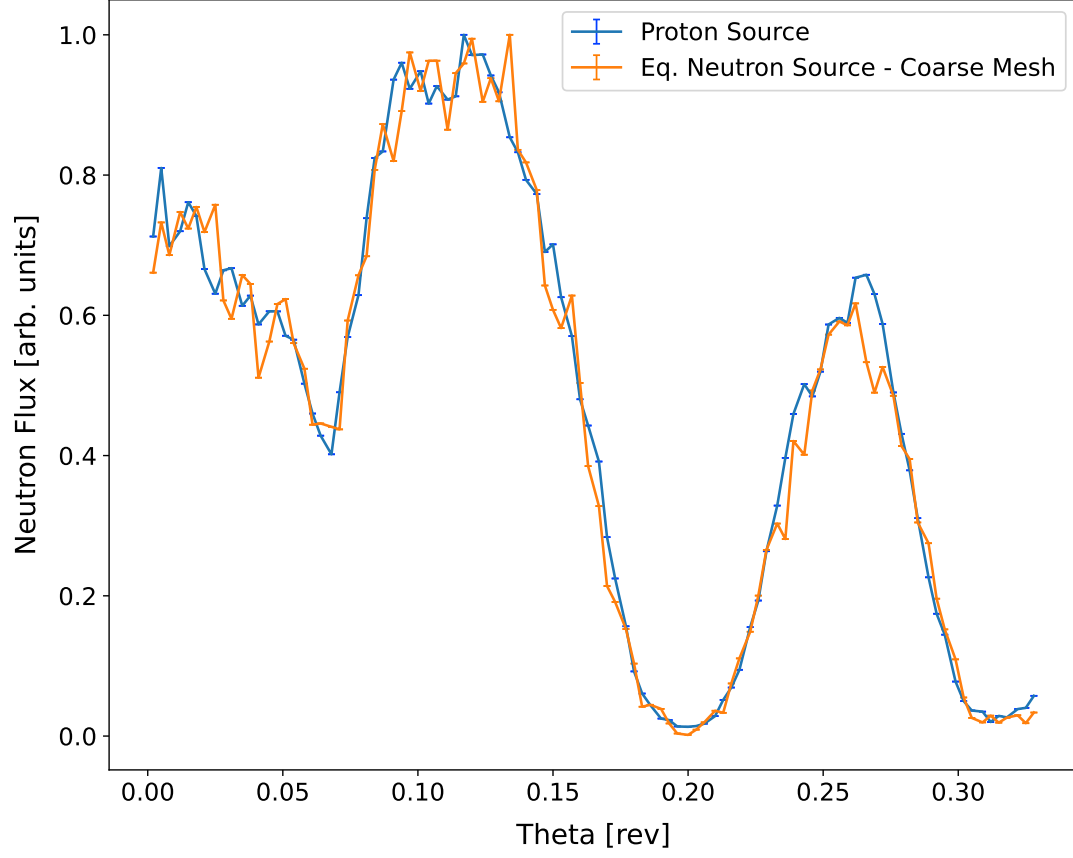
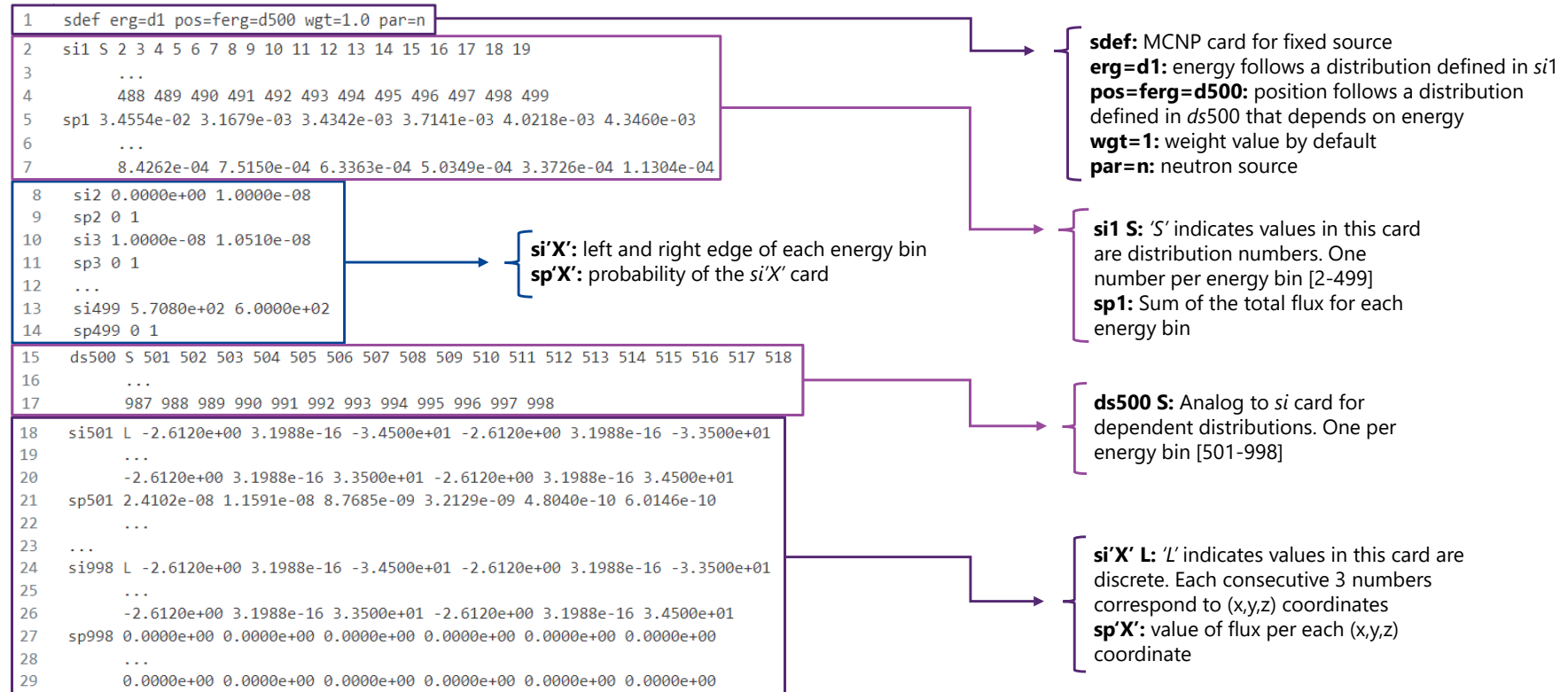# D   Explanation of SDEF card format for MCNP6.2 compatible with ADVANTG3.2


```
1    sdef erg=d1 pos=ferg=d500 wgt=1.0 par=n
2    si1 S 2 3 4 5 6 7 8 9 10 11 12 13 14 15 16 17 18 19
3         ...
4         488 489 490 491 492 493 494 495 496 497 498 499
5    sp1 3.4554e-02 3.1679e-03 3.4342e-03 3.7141e-03 4.0218e-03 4.3460e-03
6         ...
7         8.4262e-04 7.5150e-04 6.3363e-04 5.0349e-04 3.3726e-04 1.1304e-04
8    si2 0.0000e+00 1.0000e-08
9    sp2 0 1
10   si3 1.0000e-08 1.0510e-08
11   sp3 0 1
12   ...
13   si499 5.7080e+02 6.0000e+02
14   sp499 0 1
15   ds500 S 501 502 503 504 505 506 507 508 509 510 511 512 513 514 515 516 517 518
16         ...
17         987 988 989 990 991 992 993 994 995 996 997 998
18   si501 L -2.6120e+00 3.1988e-16 -3.4500e+01 -2.6120e+00 3.1988e-16 -3.3500e+01
19         ...
20         -2.6120e+00 3.1988e-16 3.3500e+01 -2.6120e+00 3.1988e-16 3.4500e+01
21   sp501 2.4102e-08 1.1591e-08 8.7685e-09 3.2129e-09 4.8040e-10 6.0146e-10
22         ...
23   ...
24   si998 L -2.6120e+00 3.1988e-16 -3.4500e+01 -2.6120e+00 3.1988e-16 -3.3500e+01
25         ...
26         -2.6120e+00 3.1988e-16 3.3500e+01 -2.6120e+00 3.1988e-16 3.4500e+01
27   sp998 0.0000e+00 0.0000e+00 0.0000e+00 0.0000e+00 0.0000e+00 0.0000e+00
28         ...
29         0.0000e+00 0.0000e+00 0.0000e+00 0.0000e+00 0.0000e+00 0.0000e+00
```

sdef: MCNP card for fixed source
erg=d1: energy follows a distribution defined in *si*1
pos=ferg=d500: position follows a distribution defined in *ds*500 that depends on energy
wgt=1: weight value by default
par=n: neutron source

si'X': left and right edge of each energy bin
sp'X': probability of the *si'X'* card

si1 S: *'S'* indicates values in this card are distribution numbers. One number per energy bin [2-499]
sp1: Sum of the total flux for each energy bin

ds500 S: Analog to *si* card for dependent distributions. One per energy bin [501-998]

si'X' L: *'L'* indicates values in this card are discrete. Each consecutive 3 numbers correspond to (x,y,z) coordinates
sp'X': value of flux per each (x,y,z) coordinate

Figure D.10: Layout of MCNP6.2 SDEF card using results from FMESH4 tally with 498 energy bins and compatible with ADVANTG3.2